The Effects of SARS-CoV-2 ORF7b on Mitochondrial Metabolism

by

Lucas Mina

A thesis submitted in partial fulfillment of the requirements for the degree of

Master of Science

Department of Cell Biology
University of Alberta

ABSTRACT

The endoplasmic reticulum (ER) mitochondria-associated membrane (MAM), or the contact site between the ER and mitochondria, serves a control station for mitochondrial metabolism. Here, chaperones and enzymes control the Ca^{2+} flux between the two organelles, thereby altering energy production via mitochondrial oxidative phosphorylation. For example, the ER-localized thioredoxin-related transmembrane protein 1 (TMX1) interacts with sarco/endoplasmic reticulum Ca^{2+} ATPase 2b (SERCA2b) to decrease its activity. This function means that dysregulation of MAM proteins can easily disrupt energy flux, leading to increased reactive oxygen species (ROS) production and oxidative stress. In fact, dysfunctional MAMs have been observed in a variety of diseases, including viral infections. Of interest to us is the severe acute respiratory syndrome coronavirus 2 (SARS-CoV-2), wherein various SARS-CoV-2 proteins are known to interact with MAM proteins. In this thesis, we have characterized the interactions between the SARS-CoV-2 accessory protein ORF7b and MAM proteins. We have found that ORF7b disrupted interactions between SERCA2b and its regulators, calnexin and TMX1. Concordant with this, we observed a shift in Ca^{2+} equilibrium towards the mitochondria, and consequently, an increase in mitochondrial oxygen consumption and ROS production. ORF7b can therefore influence mitochondrial metabolism by targeting the MAMs.

ACKNOWLEDGMENTS

Firstly, I would like to express my sincerest gratitude to my supervisor, Dr. Thomas Simmen. Thank you for giving me the opportunity to take on a master's project in your lab. Your invaluable guidance over the years has shaped me into the researcher that I am today. I would like to thank you for encouraging me to explore new research topics and laboratory techniques, as well as for supporting my extracurricular activities. Next, I would like to thank the members of my supervisory committee, Dr. Richard Wozniak and Dr. Bradley Kerr. Your feedback during my committee meetings were fundamental in keeping my project in the right direction. I would also like to thank my external examiner, Dr. Howard Young, for giving me insightful feedback on this thesis.

I would like to thank the members of the Simmen Lab, past and present. To Carolina, Sol, and Tomas, thank you for introducing me to research work and making my first years of research a wonderful experience. To Arthur, Chen, Kei, Megan, and Samuel, thank you for being my support system in the lab over the last two years. Despite the challenges of doing graduate school during a pandemic, your presence in the lab has made this experience a memorable one. I could not imagine coming into the lab every day without having you to keep me company. And to all the graduate students and faculty members of Cell Biology, thank you for welcoming me into the department. It was a pleasure getting to know each and every one of you.

Finally, I would like to thank my parents, my sisters, my friends, and Nadia for supporting me through every stage of my graduate studies. Your company and words of encouragement have kept me afloat over the last two years. I would not have been able to survive graduate school if it were not for you, and I will be forever grateful.

TABLE OF CONTENTS

LIST OF TABLES

LIST OF FIGURES

LIST OF ABBREVIATIONS

ATP	Adenosine triphosphate
ADP	Adenosine diphosphate
BAP31	B cell receptor-associated protein 31
Bcl-2	B-cell lymphoma 2
Drp1	Dynamin-related protein 1
ER	Endoplasmic reticulum
Ero1α	ER oxidoreductase 1α
ETC	Electron transport chain
FAD$^+$	Flavin adenine dinucleotide
Fis1	Mitochondrial fission 1 protein
Grp75	Glucose-regulated protein 75
GTP	Guanosine triphosphate
HCMV	Human cytomegalovirus
HCV	Hepatitis C virus
HIV-1	Human immunodeficiency virus 1
IFN	Interferon
IL	Interleukin
IMM	Inner mitochondrial membrane
IP$_3$R	Inositol 1,4,5-triphosphate receptor
MAM	Mitochondria-associated membrane
MAVS	Mitochondrial antiviral signalling protein
MCU	Mitochondrial calcium uniporter
Mfn1	Mitofusin 1
Mfn2	Mitofusin 2
mPTP	Mitochondrial permeability transition pore
NAD$^+$	Nicotinamide adenine dinucleotide
NFAT	Nuclear factor of activated T-cells

NLRP3	NOD-like receptor family pyrin domain containing 3
NS/NSP	Nonstructural protein
OMM	Outer mitochondrial membrane
Opa1	Optic atrophy 1
ORF7b	Open reading frame 7b
OST	Oligosaccharyl transferase
PACS-2	Phosphofurin acidic cluster sorting 2
PDI	Protein disulfide isomerase
PE	Phosphatidylethanolamine
PKB	Protein kinase B
PLN	Phospholamban
PTPIP51	Protein tyrosine phosphatase interacting protein-51
PS	Phosphatidylserine
RIG-1	Retinoic acid-inducible gene I
ROS	Reactive oxygen species
SARS-CoV-2	Severe acute respiratory syndrome coronavirus 2
SERCA	Sarco/endoplasmic reticulum Ca^{2+} ATPase
Sig-1R	Sigma-1 receptor
SR	Signal recognition particle receptor
SRP	Signal recognition particle
STING	Stimulator of interferon genes
TCA	Tricarboxylic acid
TMX1	Thioredoxin-related transmembrane protein 1
TOMM40	Translocase of the outer mitochondrial membrane 40
TRAM	Translocating chain-associating membrane protein
VAPB	Vesicle-associated membrane protein-associated protein B
VDAC	Voltage-dependent anion channel
vMIA	Viral mitochondria-localized inhibitor of apoptosis

Vpr   Viral protein R

Vpu   Viral protein U

CHAPTER 1: Introduction

1. INTRODUCTION

1.1. Endoplasmic reticulum

1.1.1. Overview

Eukaryotic cells are comprised of membrane-bound organelles which carry out specialized roles that are necessary for the cell to function. The endoplasmic reticulum (ER) is the largest organelle within the cell, and is a major site for protein synthesis, folding, and transport; calcium storage; and lipid and steroid synthesis (Schwarz & Blower, 2016). The ER is a continuous phospholipid membrane system that consists of the nuclear envelope, which surrounds the nucleus; and the peripheral ER, which comprises of interconnected tubules and sheets that extend throughout the cytosol (Voeltz et al., 2002). Although the ER is a single membrane system with a continuous luminal space, it consists of different domains that arise from the distribution of certain proteins which perform diverse and specialized functions for the cell. For example, the rough ER is enriched with ribosomes and signal recognition particle (SRP) receptors (SRs), serving as the site for protein synthesis. On the other hand, smooth ER, which lacks ribosomes, facilitate the synthesis of lipid, phospholipids, and steroids (Goetz & Nabi, 2006), whereas transitional ER is enriched with coat protein complex II proteins which are responsible for packaging proteins for transport to the Golgi complex and subsequent secretion (Shindiapina & Barlowe, 2010). In addition, the ER is known to form membrane contacts with other organelles and the plasma membrane. At these contact sites, various protein complexes work together to carry out specialized functions, including membrane binding, molecule transfer, and organelle dynamics. In this thesis, we will explore the mitochondria-associated membrane (MAM), the region of the ER that forms membrane contacts with the mitochondria.

1.1.2. Protein synthesis

The rough ER serves as a major site for the synthesis of proteins, in particular membrane proteins and proteins targeted to the secretory pathway (Jan et al., 2014). Within eukaryotic cells, protein targeting to the ER is often cotranslational. In other words, protein translocation and insertion into the ER membrane are coupled to protein synthesis. This process requires the binding of the ribosome-nascent chain complex (RNC) to the cytosolic face of the ER membrane (giving rise to rough ER) (Mothes et al., 1994). Coupling of protein synthesis with ER membrane targeting

and insertion is important to prevent proteins, particularly hydrophobic membrane proteins, from premature folding or aggregation within the cytosol.

The synthesis of membrane or secretory proteins begins in the cytosol, where the RNC is recognized and bound by the SRP via a hydrophobic signal sequence within the N-terminus of the nascent polypeptide chain (Walter et al., 1981). The mammalian SRP can be divided into two domains: the S-domain and the Alu-domain. The S-domain of the SRP contains the universally conserved SRP54 protein, which is responsible for binding the signal sequence, whereas as the Alu-domain is responsible for pausing translation elongation as soon as the signal sequence emerges from the ribosome (Akopian et al., 2013). The resulting mRNA/RNC/SRP complex is then targeted to the ER membrane via the SR (Gilmore et al., 1982; Meyer et al., 1982), which is an integral membrane protein found on the rough ER (Hortsch & Meyer, 1985). Upon binding of the SRP to the SR, the nascent polypeptide, at the expense of guanosine triphosphate (GTP), is transferred to the translocon. The translocon is a multi-protein complex comprised of the central heterotrimeric Sec61 αβγ complex, which forms an ER-membrane-spanning pore through which the emerging polypeptide can enter the ER lumen (Akopian et al., 2013; Johnson & van Waes, 1999; Rapoport, 2007), as well as the translocating chain-associating membrane protein (TRAM), which is required for the efficient translocation of proteins across the ER membrane (Görlich et al., 1992; Krieg et al., 1989).

If the protein is destined for the secretory pathway or the ER lumen, then the protein will be completely translocated across the ER membrane, during which a signal peptidase cleaves the signal sequence, permitting the protein to freely enter the ER lumen (Auclair et al., 2012; Evans et al., 1986). However, if instead the nascent polypeptide is destined to be an integral membrane protein, which typically contains at least one region of hydrophobic residues within the polypeptide chain, translocation of the protein across the ER membrane will pause, and the protein will be laterally shifted across the ER membrane, where it will remain (Heinrich et al., 2000).

1.1.2.1 Integral membrane proteins

Typical proteins that are subject to SRP-dependent cotranslational targeting to ER are integral membrane proteins. In most cases, these proteins contain one or more non-cleavable, hydrophobic sequences, also known as signal anchors (Berndt et al., 2009; Mercier et al., 2017), which make these proteins prone to aggregation in the aqueous environment of the cytosol and

thus require cotranslational insertion into hydrophobic ER membrane. Signal anchor sequences are positioned internally within the polypeptide chain and serve a dual function. First, signal anchors can act as the signal for SRP-dependent targeting to the ER. Second, signal anchors act as transmembrane anchors which keep the protein membrane-bound. Thus, they are generally longer than cleaved signal sequences, consisting of around 18-25 mostly hydrophobic amino acids, given that they must span the lipid bilayer (Goder & Spiess, 2001).

Depending on the final topology assumed by the protein, three types of single-spanning transmembrane proteins can be distinguished. Type I transmembrane proteins are initially targeted to the ER by a cleavable signal sequence, and then anchored to the membrane by a signal anchor. In Type II transmembrane proteins, a signal anchor is responsible for both ER membrane targeting and anchoring. Type II transmembrane proteins induce the translocation of their C-terminal end across the membrane, assuming a final topology with a luminal C-terminus and a cytosolic N-terminus. The opposite is the case for Type III transmembrane proteins, which translocate their N-terminal end across the ER membrane, giving rise to a cytosolic C-terminus and a luminal N-terminus (Goder & Spiess, 2001). Through cross-linking studies, TRAM was shown to be in contact with transmembrane segments during translocation and is required for efficient insertion of proteins in the ER membrane (Do et al., 1996). More recently, the conserved ER membrane protein complex (EMC) has been found to cooperate with the translocon to ensure accurate insertion and topology of membrane proteins (Chitwood et al., 2018; O'Keefe et al., 2021).

The most established determinant of orientation and protein topology is the distribution of charged residues in the extramembrane domains flanking the signal anchor of transmembrane proteins. Termed as the 'positive-inside rule,' this rule postulates that positively charged residues, such as lysine and arginine, are more likely to be found on the cytoplasmic side of transmembrane segments. This was first shown for bacterial proteins, where positively charged residues were found to be statistically more abundant in cytoplasmic loops than in periplasmic loops (von Heijne, 1986; von Heijne, 1989). Although it remains unclear how positively charged residues determine protein topology, it has been suggested that interactions between positive charges of the protein with negatively charged lipids on the cytosolic membrane surface could favour the retention of positively charged extramembrane domains in the cytosol (Bogdanov et al., 2014; van Klompenburg, 1997).

1.1.3. Protein folding

Within the ER, newly synthesized proteins must undergo proper protein modification and folding, a process mediated by ER molecular chaperones and folding enzymes. For instance, upon entering the ER, proteins can be modified by Asn-linked glycosylation (N-glycosylation), which is a critical step for the folding, stability, and function of glycoproteins (Helenius & Aebi, 2004). This modification is catalyzed by oligosaccharyltransferase (OST), which transfers preassembled glycans to Asn on the nascent chain via the consensus acceptor site (Asn-X-Ser/Thr; X being any amino acid except Pro) (Breuer et al., 2001; Gavel & Heijne, 1990).

Molecular chaperones are proteins that assist other proteins in assuming their native conformation, but are not part of the final structure (Ellis & van der Vies, 1991). Classical chaperones, which include the heat shock proteins, are found in almost all cellular organelles and bind directly to the polypeptide chain of misfolded or aggregation-prone proteins. On the other hand, carbohydrate-binding chaperones are specific to the ER and involve interactions with glycan modifications. Calnexin, an ER transmembrane protein, and its soluble homologue, calreticulin, are two well-established examples (Bergeron et al., 1994; Saito, 1999). These chaperones possess a carbohydrate-binding domain that binds N-monoglucosylated peptides following the trimming of their glycan by glucosidases I and II (Ware et al., 1995). Such a function is important for the stabilization of glycoprotein folding events in order to prevent protein aggregation (Hebert et al., 1996; Vassilakos et al., 1998), as well as for the retention of non-native glycoproteins in the ER for proper refolding (Rajagopalan et al., 1994).

In addition to molecular chaperones, the ER is home to folding enzymes which catalyze oxidation-reduction and isomerization reactions that are essential for protein folding. Importantly, the protein disulfide isomerase (PDI) family of oxidoreductases facilitates proper protein folding by catalyzing the formation, isomerization, or reduction of disulfide bonds via their luminal Cys-X-X-Cys reductase active site, thus conferring structural stability for proteins (Galligan & Petersen, 2012). Notable members of the PDI family include ERp57, which associates with unfolded glycoproteins recognized by calnexin and calreticulin to catalyze the formation of disulfide bonds (Oliver et al., 1997; Zapun et al., 1998); and thioredoxin-related transmembrane protein 1 (TMX1), which is involved in the quality control of major histocompatibility complex class 1 molecules (Section 1.3.4.4).

1.1.4. Calcium storage

In addition to facilitating protein synthesis and folding, the ER also serves as a storage site for calcium (Ca^{2+}). Within the cell, the typical concentration of free Ca^{2+} within the ER ranges from 100 to 800 μM, whereas intracellular Ca^{2+} concentrations in the cytosol are much lower at around 100 nM (Berridge et al., 2000; Burdakov et al., 2005). Ca^{2+} is a signalling molecule used to drive a variety of intracellular processes and regulate homeostasis. Most notably, Ca^{2+} is involved in protein folding and stability. As mentioned previously, the ER is responsible for the folding and maturation of membrane proteins and secretory proteins. This process is mediated by ER-resident chaperones, many of which, including calnexin and calreticulin, require Ca^{2+} as a cofactor for optimal chaperone activity, and are characterized by a high capacity to bind Ca^{2+} (Corbett et al., 1999; Lodish et al., 1992; Michalak et al., 2002; Vassilakos et al., 1998; Ware et al., 1995). Thus, depletion of Ca^{2+} can alter the protein folding process in the ER, resulting in a condition known as ER stress (Carreras-Sureda et al., 2018). ER stress activates the unfolded protein response, which is a signaling pathway that activates transcriptional responses aimed to reduce protein misfolding and restore ER homeostasis (Walter & Ron, 2011). Importantly, disturbances in ER Ca^{2+} levels have been tied to multiple diseases, including neurological disorders, cancer, and viral infections (Mekahli et al., 2011; M. Wang & Kaufman, 2016).

In addition to functioning within the ER, Ca^{2+} plays an important role within other organelles. For instance, Ca^{2+} in the mitochondria can promote oxidative phosphorylation or even cell death (Section 1.2.2). Furthermore, increases in cytosolic Ca^{2+} as a result of ER Ca^{2+} exit may result in the activation of the nuclear factor of activated T-cells (NFAT) pathway, which is involved in immune responses against viral infections (Farrow et al., 2011; J. Zhang et al., 2016). Ca^{2+} achieves this by activating the phosphatase calcineurin, which dephosphorylates and induces the movement of the cytoplasmic components of NFAT transcription complexes into the nucleus (Crabtree & Olson, 2002). Thus, in order for Ca^{2+}-dependent intracellular signalling pathways to work, spatial Ca^{2+} levels must be tightly controlled. For instance, Ca^{2+} levels in the ER are maintained in part by the activity of ER-localized chaperones. In addition to directly binding Ca^{2+}, ER chaperones are also known to physically associate with ER Ca^{2+} pumps and channels to regulate their activities, further influencing the levels of Ca^{2+} within the ER (Section 1.3.4.4).

High ER Ca^{2+} levels are also maintained by ER membrane pumps and channels that mediate the flux of Ca^{2+} between the ER and the cytosol. For example, sarco/endoplasmic

reticulum Ca^{2+} ATPases (SERCAs) are responsible for the refilling of ER Ca^{2+} (Section 1.3.4.2). SERCAs mediate the hydrolysis of ATP required to actively pump Ca^{2+} against its concentration gradient into the ER. In contrast, channels like ryanodine receptors and inositol 1,4,5-triphosphate receptors (IP_3R) are responsible for the release of ER Ca^{2+} when cytosolic Ca^{2+} levels are low (Clapham, 2007). However, if ER Ca^{2+} levels are rapidly diminished through IP_3R-mediated Ca^{2+} release, a mechanism known as store-operated Ca^{2+} entry is activated (Putney, 1986). Here, stromal interaction molecule 1 migrates along the ER membrane towards ER-plasma membrane contact sites, where it binds to Orai1 on the plasma membrane, forming channels that allow influx of extracellular Ca^{2+} into the ER, restoring ER Ca^{2+} levels (Feske et al., 2006; McNally et al., 2013; Prakriya et al., 2006; Roos et al., 2005).

In summary, ER Ca^{2+} homeostasis is maintained by a complex network of proteins that maintain ER Ca^{2+} levels and mediate Ca^{2+} release and uptake. Alterations to cellular Ca^{2+} balance can have the potential to disturb ER homeostasis and induce ER stress.

1.2. Mitochondria

1.2.1. Overview

The mitochondrion is a double-membrane-bound organelle that is present in most eukaryotic cells, and plays a dominant role for the production of energy for the cell. Like the ER, mitochondria are divided into several domains that carry out specialized roles. For example, the outer mitochondrial membrane (OMM), which encloses the mitochondria, is enriched with integral membrane proteins called porins. A prominent type of porin is the voltage-dependent anion channel (VDAC), which serves as the primary transporter of ions, metabolites, and nucleotides between the cytosol and mitochondria (Shoshan-Barmatz et al., 2010). The inner mitochondrial membrane (IMM) houses the components of the electron transport chain (ETC) and ATP synthase, which are involved in oxidative phosphorylation and ATP generation (Busch, 2020). Furthermore, the IMM is compartmentalized into dynamic folds called cristae, which expand the surface area of the IMM, thus increasing the capacity of the mitochondria to produce ATP (Paumard et al., 2002). The OMM and the IMM are separated by the aqueous intermembrane space, which houses the machinery for oxidative protein folding (Edwards et al., 2021). Finally, the matrix is the space enclosed by the IMM, and houses the majority of the total protein content of the mitochondria.

These proteins include the enzymes involved in the breakdown of pyruvate and fatty acids and enzymes of the tricarboxylic acid (TCA) cycle (Denton, 2009).

1.2.2. Mitochondrial metabolism

A prominent role for mitochondria is the production of energy for the cell. In eukaryotic cells, the mitochondria serve as the primary location for the production of adenosine triphosphate (ATP), which is an energy-carrying molecule that is consumed in various processes, including ion transport, protein phosphorylation, and chemical synthesis (Bertram et al., 2006). ATP production begins in the cytoplasm, where glucose is converted to pyruvate via glycolysis. Pyruvate then enters the mitochondria matrix, where it acts as a substrate for the TCA cycle. At this step, Ca^{2+} plays an important role by activating the enzymes of the TCA cycle, including pyruvate dehydrogenase, oxoglutarate dehydrogenase, and isocitrate dehydrogenase (Denton & McCormack, 1993; Traaseth et al., 2004). These dehydrogenases mediate the transfer of electrons from substrates to co-enzymes, including nicotinamide adenine dinucleotide (NAD^+) and flavin adenine dinucleotide (FAD), producing NADH and $FADH_2$. These electron carriers are then fed into the ETC, where the electrons from NADH and $FADH_2$ are transferred to electron acceptors, such as O_2 (Guo et al., 2017). The electron flow along the ETC is coupled with the transfer of protons from the matrix into the intermembrane space, generating an electrochemical proton gradient across the IMM. The energy accumulated as a result this proton gradient is then used to drive the last stage of metabolism, oxidative phosphorylation, wherein the ATP synthase phosphorylates adenosine diphosphate (ADP) to produce ATP.

The ETC, which is found on the IMM, is comprised of Complexes I-IV and electron transporters, including cytochrome c (Guo et al., 2017). A key member of the ETC is Complex IV, also known as cytochrome c oxidase. During the final step of the ETC, Complex IV transfers the electrons from the ETC to the final electron acceptor, O_2, to generate H_2O. However, the transfer of electrons along the ETC is not 100% efficient. Under physiological conditions, up to 2% of the electrons that are transferred along the ETC leak out of the ETC and bind to O_2, generating reactive oxygen species (ROS) (R. Zhao et al., 2019). ROS are signaling molecules that important for various cell processes, including cell proliferation and cell fate determination, and are involved in the modification of different kinds of proteins, including kinases, caspases, and ion channels (de Giusti et al., 2013). However, excessive ROS levels can lead to a condition of oxidative stress and

be detrimental to the cell. At high levels, ROS can cause lipid peroxidation, DNA damage, mitochondrial damage, and even apoptosis (Orrenius et al., 2007).

1.2.2.1. Apoptosis

Mitochondria also play a key role in the activation of apoptosis, or programmed cell death. Apoptosis starts with the permeabilization of the OMM (Crompton, 1999). Various apoptotic stimuli, such as excessive mitochondrial Ca^{2+} and ROS levels, can induce the opening of the mitochondrial permeability transition pore (mPTP) (Assaly et al., 2012; Beutner et al., 2017; Halestrap, 2004; Haworth & Hunter, 1979). The opening of the mPTP results in the loss of the proton gradient generated by the ETC, resulting in the uncoupling of oxidative phosphorylation. mPTP opening also allows H_2O to enter the mitochondrial matrix, which results in mitochondrial swelling and subsequent rupturing of the OMM, leading to the release of mitochondrial proteins, including cytochrome c (Crompton, 1999). In the cytosol, cytochrome c, together with the apoptosis protease activating factor, activates the caspase cascade, ultimately leading to cell death (Kinnally et al., 2011; Riedl et al., 2005; J. C. Yang & Cortopassi, 1998; Zou et al., 1999).

Given that the ETC is a major source of ROS and that elevated levels of ROS can be a trigger for apoptosis, compromised integrity of the ETC can contribute to excessive ROS production and cell death induction (Hwang et al., 2014). All in all, the proper functioning of the ETC and enzymes in the mitochondria is crucial to maintaining proper intracellular levels of ATP and ROS, which ultimately influence cell fate.

1.2.3. Mitochondrial membrane dynamics

Mitochondria are highly dynamic organelles that are modified via cycles of fusion and fission events. Collectively known as mitochondrial membrane dynamics, these events regulate mitochondrial morphology in response to cellular conditions. Mitochondrial membrane dynamics are regulated by a group of dynamin-related GTPases. Mitofusin-1 (Mfn1) and -2 (Mfn2) and optic atrophy 1 (Opa1) proteins make up the machinery for mitochondrial fusion, which comprises of the fusion of the OMM and fusion of the IMM (Eura, 2003; Olichon et al., 2002). Fusion of the OMM is regulated by Mfn1 and Mfn2, which are inserted in the OMM and form homo- and heterotypic complexes with each other at the expense of GTP, tethering the OMM of adjacent mitochondria. On the other hand, fusion of the IMM is regulated by Opa1, which is located on the

IMM and forms homotypic oligomeric complexes to connect distinct IMMs. In addition, Opa1 has been shown to be required for maintaining cristae structure and mitochondrial activity (Patten et al., 2014). Altogether, these events lead to the formation of elongated mitochondria, which is important for the merging of mitochondria fragments, thus promoting the transfer of proteins and metabolites across the mitochondrial network (Archer, 2013). Consistent with their role in mitochondria fusion, loss of Mfn1, Mfn2, and Opa1 can result in abnormal mitochondrial network, loss of mitochondrial integrity, and increased sensitivity to apoptotic stimuli (Chen et al., 2003; Cipolat et al., 2004; Han et al., 2020; Y. Yang et al., 2018).

Mitochondria can also break down into smaller fragments through mitochondrial fission, which is an essential process for clearing damaged parts of mitochondria (Tiku et al., 2020). Here, the cytosolic GTPase dynamin-related protein 1 (Drp1) plays an important role. Under conditions of mitochondrial fission, such as oxidative stress (K. Wang et al., 2015) or cell division (Horbay & Bilyy, 2016), Drp1 is recruited from the cytosol to the mitochondria through Drp1 receptors which are enriched on the OMM (R. Liu & Chan, 2015; Osellame et al., 2016). At the OMM, Drp1 forms an oligomeric structure that wraps around the mitochondrial scission site, and, at the expense of GTP, Drp1 undergoes a conformational change which results in OMM constriction, resulting in fragmented mitochondria. In line with this function of Drp1, loss of Drp1 has been tied to mitochondrial hyperfusion and compromised cell proliferation (Qian et al., 2012). Altogether, the regulation of mitochondrial membrane dynamics is important for maintaining normal mitochondrial network and function.

1.3. Mitochondria-associated membranes

1.3.1. Overview

Despite carrying out independent biological functions, the ER and the mitochondria are not independent structures. Over the past few decades, research has demonstrated that regions of the ER are physically connected to the mitochondria, forming junctions known as mitochondria-associated membranes (MAMs). The existence of this unique ER subdomain was biochemically demonstrated by J.E. Vance, who described a protocol to isolate ER membranes that co-fractionated with mitochondria from rat liver (Vance, 1990). In this protocol, crude mitochondria fractions were subjected to centrifugation on a Percoll gradient, resulting in the isolation of MAMs from pure mitochondria (Vance, 1990).

Since its discovery in 1990, MAMs have emerged as a fundamental platform for various cellular processes, including Ca^{2+} homeostasis, mitochondrial function, immune responses, lipid synthesis and transport, and autophagy (Giorgi et al., 2015). Such events rely on the exchange of biomolecules across the ER-mitochondria interface. For this reason, several regulatory proteins reside in the MAMs to ensure accurate inter-organelle communication between the ER and mitochondria (Figure 1). In fact, in-depth mass spectrometry analysis has identified more than 1000 proteins that localize to the MAMs (Sala-Vila et al., 2016). This report will explore in detail the proteins that are involved in the regulation of two important hallmarks of MAM function: Ca^{2+} homeostasis and mitochondrial metabolism.
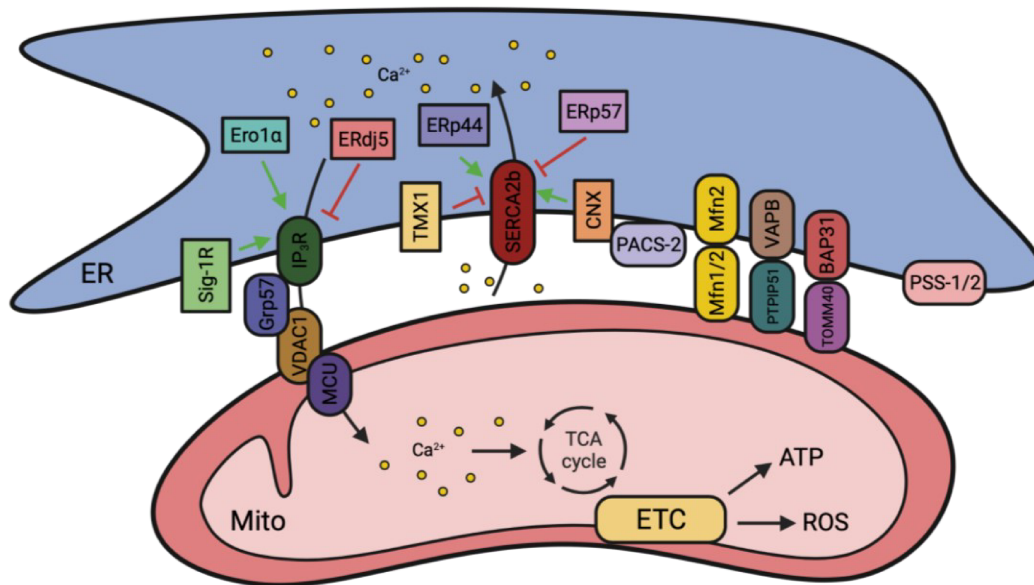
Figure 1. Protein composition of MAMs. The MAM is an important site for various cellular processes, including Ca^{2+} homeostasis, mitochondrial function, and lipid synthesis. The MAM is a hub for ER chaperones and oxidoreductases, such as calnexin (CNX) and TMX1, which regulate the activity of Ca^{2+} handling proteins, including SERCA2b and IP_3R. Ca^{2+} transferred to the mitochondria promotes mitochondrial metabolism by activating the enzymes of the TCA cycle. Lipid synthesis involves PS synthase-1 (PSS-1) and PSS-2. The integrity of MAMs is maintained by protein tethers, including Grp75, Mfn1, and Mfn2. For details, read text. Created with BioRender.com

1.3.2. Lipid metabolism and transport

By the early 1990s, MAMs have been found to play a role for the synthesis of phospholipids (Vance, 1990), which are molecules that can form lipid bilayers and therefore are fundamental components of biological membranes. The role of MAMs in lipid synthesis was revealed when Vance (1990) described the presence of phospholipid synthetic activity for phosphatidylserine (PS), phosphatidylethanolamine (PE), and phosphatidylcholine in MAM fractions (Vance, 1990). Since this discovery, subsequent studies have revealed that the machinery involved in the formation of phospholipids is found at the MAMs, including PS synthase-1 and -2, which are highly enriched in the MAMs compared to the bulk ER (Stone & Vance, 2000). Furthermore, it has been found that around 10% of MAM proteins from mouse liver are involved in the metabolism of lipids, including cholesterol, fatty acids, steroids (Sala-Vila et al., 2016).

MAMs have also emerged as an important site for lipid trafficking. Lipid composition of membranes varies across different organelles, and this distribution is made possible by intracellular lipid trafficking mechanisms, wherein lipids are transported from the site of synthesis, typically ER membranes, to their destination membranes, such as the mitochondria. For example, PE is highly enriched in the IMM, where it promotes cristae curvature and plays a role for mitochondrial function and cell survival (Steenbergen et al., 2005; Zborowski et al., 1983). PE is synthesized in the mitochondria from the decarboxylation of PS (Borkenhagen et al., 1961). However, in order for this to occur, PS must be imported from the ER, where it is synthesized by PS synthase-1 and -2 (Stone & Vance, 2000), to the IMM, where PS decarboxylase is located (Zborowski et al., 1983). Thus, MAMs play a crucial role by forming membrane contacts whereby the ER membrane and the OMM become closely juxtaposed, thus allowing the import of newly-synthesized PS into the mitochondria (Voelker, 1993).

In addition to mediating lipid synthesis and transport, MAMs also serve as a site for lipid-protein interactions that play important roles in executing cellular processes. For example, ceramides, a type of lipid molecule found within cellular membranes, physically interact with and anchor sigma-1 receptor (Sig-1R) at the MAMs (Hayashi & Fujimoto, 2010). At the MAMs, Sig-1R stabilizes IP$_3$R, therefore promoting Ca^{2+} flux from the ER to the mitochondria (Hayashi & Su, 2007) (Section 1.3.4.1). In mouse brain, GM1-ganglioside, a type of glycosphingolipid, was found to physically associate with phosphorylated IP$_3$R in MAMs and influence Ca^{2+}-mediated apoptosis (Sano et al., 2009).

1.3.3. Protein tethering

The structure of MAMs is not constant. Instead, it changes dynamically depending on the cell status. Under normal conditions, up to 20% of the mitochondria network within HeLa cells are in close apposition with the ER (Giacomello & Pellegrini, 2016; Rizzuto et al., 1998). Electron tomography studies have revealed that the width of the gap between the ER and mitochondria is around 25 nm at the rough ER and 10 nm at the smooth ER (Csordás et al., 2006). Such findings are consistent with the idea that ER-mitochondria contact sites are maintained by proteins that act as tethers that bring the two organelles together. For example, Mfn2, which is involved in mitochondrial fusion, also mediates the coupling of the mitochondria to the ER (de Brito & Scorrano, 2008; Dorn, 2020). Whereas Mfn1 is found only on the OMM, Mfn2 is inserted in the both the OMM and ER membrane. Therefore, ER-localized Mfn2 can interact with mitochondria-localized Mfn2 or Mfn1 to form tethers between the two organelles. Another protein involved in maintaining MAM integrity is the phosphofurin acidic cluster sorting 2 (PACS-2) protein. PACS-2 is involved in apoptosis, but is also known to increase ER-mitochondria coupling and communication (Betz et al., 2013; Simmen et al., 2005).

In addition to the individual MAM protein described above, protein complexes also play an important part in maintaining ER-mitochondria contact sites. A well-established complex is one comprised of VDAC1, IP$_3$R, and glucose-regulated protein 75 (Grp75) (Szabadkai et al., 2006). VDAC1, an isoform of VDAC, is found on the OMM, whereas IP$_3$R is found on the ER membrane. At the MAMs, these two channels are bound by the cytosolic chaperone Grp75, forming tethers between the ER and the mitochondria (Szabadkai et al., 2006). The IP$_3$R/Grp75/VDAC1 complex also plays an important role in Ca^{2+} transfer across the ER-mitochondria interface (Section 1.3.4). Another example is the tether formed by the integral ER membrane protein, vesicle-associated membrane protein-associated protein B (VAPB), and the OMM protein tyrosine phosphatase interacting protein-51 (PTPIP51), which also mediates Ca^{2+} transfer from the ER to mitochondria (de Vos et al., 2012). Notably, perturbations in ER-mitochondria contacts and signaling as a result of disruptions to VAPB/PTPIP51 tethers have been linked to neurodegenerative diseases (Paillusson et al., 2017; Stoica et al., 2014, 2016). More recently, the B cell receptor-associated protein 31 (BAP31) has been shown to interact with translocase of the OMM 40 (TOMM40) at the MAMs (Namba, 2019). BAP31 is an ER transmembrane protein that plays an important role in cell death (Section 1.3.5), whereas TOMM40 is required for the movement of proteins into the

mitochondria (M. Yang et al., 2020). Altogether, the integrity of MAMs is maintained by a variety of proteins that act as bridges between the ER and mitochondria.

1.3.4. Calcium homeostasis

Ca^{2+} is a signaling molecule that acts as a driving force for mitochondrial metabolism. As mentioned previously, the ER serves as the main store for intracellular Ca^{2+}, and releases Ca^{2+} through IP_3R, which is the ER Ca^{2+} channel enriched at the MAMs (Wieckowski et al., 2009). Owing to the presence of MAM protein tethers, such as the IP_3R/Grp75/VDAC1 complex, the ER and mitochondria have a spatial relationship with each other that allows Ca^{2+} released from the ER to be transported into the mitochondria. Ca^{2+} enters the mitochondria matrix via VDAC1 on the OMM and the mitochondrial calcium uniporter (MCU) on the IMM. Although Ca^{2+} can freely pass through VDAC1, MCU has a weak affinity for Ca^{2+} (Romero-Garcia & Prado-Garcia, 2019; N. Wang et al., 2021). Thus, the physical contacts formed by IP_3R/Grp75/VDAC1 complex is important to overcome the low affinity of MCU for Ca^{2+}, increasing the efficiency of Ca^{2+} entry into the mitochondria.

In the matrix, Ca^{2+} can play a variety of roles. As mentioned previously, Ca^{2+} activates the enzymes of the TCA cycle. The TCA cycle provides the needed substrates for the ETC, thus promoting the production of ATP. Therefore, if the concentration of Ca^{2+} within the mitochondria is too low, this can lead to cellular energy metabolic disorders. On the other hand, excessive mitochondrial Ca^{2+} can lead to the permeabilization of mitochondrial membranes and subsequent cell death (Section 1.2.2.1). In addition, mitochondrial Ca^{2+} can bind to cardiolipin on the IMM to promote the disintegration of Complex II of the ETC. This can lead to increased ROS production, which is a trigger for apoptosis (Hwang et al., 2014). Overall, Ca^{2+} can promote mitochondrial metabolism but also induce cell death. Ultimately, which event occurs depends on the flux of Ca^{2+} from the ER into the mitochondria, highlighting the importance of MAMs for cell fate.

1.3.4.1. Control of Ca^{2+} flux by MAM regulatory proteins

In addition to the Ca^{2+} channels described above, MAMs are enriched with regulatory proteins that are involved in maintaining ER-mitochondrial Ca^{2+} flux. These include proteins that regulate the activity of IP_3R. For example, the mammalian target of rapamycin complex 2 can accumulate in MAMs in response to various growth factors and phosphorylate protein kinase B

(PKB), elevating its activity. Activated PKB then phosphorylates IP$_3$R, inhibiting its activity, decreasing ER Ca^{2+} release, and preventing mitochondrial Ca^{2+} overload (Betz et al., 2013; Szado et al., 2008). In contrast, the tumor suppressor promyelocytic leukemia protein can antagonize the activity of PKB by elevating the activity of protein phosphatase 2A, thus promoting Ca^{2+} transfer to the mitochondria and enhancing the sensitivity of cells to apoptotic cues (Giorgi et al., 2010). Another example is ER oxidoreductase 1α (Ero1α), which is able to activate IP$_3$R-mediated Ca^{2+} release from the ER, through oxidation of IP$_3$R or binding to the IP$_3$R inhibitor ER oxidoreductase ERp44, thus promoting Ca^{2+} flux towards the mitochondria (Anelli et al., 2012; Gilady et al., 2010).

Additionally, Sig-1R, which is an ER transmembrane chaperone, stabilizes IP$_3$R to maintain Ca^{2+} transfer towards the mitochondria (Hayashi & Su, 2007). Upon conditions of mitochondrial stress, Sig-1R binds to IP$_3$R, thus reducing the degradation of IP$_3$R and promoting mitochondrial Ca^{2+} uptake (Hayashi & Su, 2007). Accordingly, upon deletion of Sig-1R, mitochondrial ATP production decreases (Pal et al., 2012). Finally, anti-apoptotic membranes of the B-cell lymphoma 2 (Bcl-2) family of proteins, including Bcl-2 and Bcl-XL, can directly bind to IP$_3$R and inhibit its activity; they can also bind to VDAC1 to decrease Ca^{2+} transfer to the mitochondria, preventing Ca^{2+} overload and apoptosis (Arbel & Shoshan-Barmatz, 2010; Monaco et al., 2012).

1.3.4.2. Sarco/endoplasmic reticulum Ca^{2+} ATPase

The sarco/endoplasmic reticulum Ca^{2+} ATPase (SERCA) is a P-type ATPase found in the sarcoplasmic reticulum within cardiac and skeletal muscle and in the ER within other cell types. P-type ATPases are integral membrane pumps that perform the transport of various ions and lipids across cellular membranes, coupled with the hydrolysis of ATP to ADP (Olesen et al., 2007; Palmgren & Nissen, 2011). According to the Post-Albers model, P-type ATPases convert between two conformations: an E1 state and an E2 state. In E1, the ion-binding site of the pump faces one side of the membrane and has high affinity for the primary metal ion, whereas in E2, the ion-binding site faces the other side of the membrane and has low affinity for the ion (X. C. Zhang & Zhang, 2019). In the case of SERCA, two Ca^{2+} ions are transported from the cytosol to the S/ER lumen, coupled with the transport of three protons from the S/ER lumen to the cytosol and the

hydrolysis of ATP (Meis & Vianna, 1979; Periasamy & Kalyanasundaram, 2007; Toyoshima et al., 2000).

The SERCA family is comprised of three genes: SERCA1, SERCA2, and SERCA3, which encode for different isoforms that arise from splicing variations (Wuytack et al., 2002). Notably, the SERCA2 gene encodes for the cardiac-specific and ubiquitous isoforms of SERCA: SERCA2a, which is restricted to cardiac, skeletal, and smooth muscles; and SERCA2b, which is the ubiquitous isoform expressed in all cell types (Lytton et al., 1989, 1992; Vangheluwe et al., 2005). Generally speaking, SERCA isoforms are highly conserved and share a similar structure, which consists of transmembrane domain, composed of 10 transmembrane helices, and three cytoplasmic domains: the nucleotide binding domain, the actuator domain, and the phosphorylation domain (Toyoshima et al., 2000). However, an exception to this is the SERCA2b isoform, which contains an 11th transmembrane helix that creates a luminal C-terminus for SERCA2b. Owing to this 11th transmembrane helix, SERCA2b has been found to have a higher affinity for Ca^{2+} and sensitivity to the ER environment compared to other SERCA isoforms (Gorski et al., 2012; Vandecaetsbeek et al., 2009).

1.3.4.3. Regulation of SERCA by phospholamban

Historically, phospholamban (PLN) has been identified as a regulator of SERCA activity. PLN is a 52-amino acid integral membrane protein expressed in cardiac muscle and slow-twitch skeletal muscles, where it acts as an inhibitor of SERCA to modulate Ca^{2+}-dependent contractility (Luo et al., 1994; MacLennan & Kranias, 2003; Santana et al., 1997; Simmerman et al., 1986). The inhibition of SERCA activity by PLN is allosteric in nature, with the inhibitory transmembrane region of PLN located at a binding site distinct from the putative Ca^{2+} entry site and ATP binding site of SERCA (Akin et al., 2013). Furthermore, SERCA inhibition by PLN is a dynamic event, and depends in part on the phosphorylation state of PLN, with unphosphorylated PLN being the active form. For example, under β-adrenergic stimulation, which represents the 'flight-or-fight' reaction and is associated with increased cardiac output, cyclic AMP-dependent protein kinase A phosphorylates Ser-16 on the cytosolic N-terminus region of PLN. This inactivates PLN and reverses the inhibition of SERCA, leading to augmented cardiac contractility (Kranias & Solaro, 1982; Kuschel et al., 1999). Given that PLN is predominantly expressed in cardiac and smooth

muscle, its main target is the SERCA2a isoform. However, PLN is also known to inhibit other isoforms of SERCA, including SERCA2b (Verboomen et al., 1992).

1.3.4.4. Redox regulation of SERCA2b

Over the last few decades, our understanding of the mechanisms behind SERCA regulation have expanded. In particular, the activity of ubiquitously expressed isoform SERCA2b has been shown to highly depend on its redox state. More specifically, the activity is SERCA2b is negatively regulated by the oxidation of two cysteines in the luminal Loop 4 of SERCA2b. In the resting state of SERCA2b, under the high ER Ca^{2+} levels, calreticulin interacts with the luminal C-terminal sequence of SERCA2b, which contains a consensus site for N-linked glycosylation that has been shown to be required for its interaction with calreticulin (Gunteski-Hamblin et al., 1988; John et al., 1998). Calreticulin recruits the ER oxidoreductase ERp57 to Loop 4 of SERCA2b to mediate the formation of disulfide bonds, reducing the activity of SERCA2b (Camacho & Lechleiter, 1995; Y. Li & Camacho, 2004). On the other hand, when ER Ca^{2+} levels go below 50 μM, ERp57 dissociates from SERCA2b, restoring the function of SERCA2b (Y. Li & Camacho, 2004). Furthermore, various studies on cardiac muscle have reported that prooxidative modification of SERCA on a cytosolic cysteine contributes to decreased SERCA activity, thus impairing cardiac muscle relaxation (Knyushko et al., 2005; Qin et al., 2013; Thompson et al., 2014).

As the main pump responsible for refilling of Ca^{2+} in the ER, SERCA2b can also aggregate in the MAMs (Ellgaard et al., 2018; Lynes et al., 2013). Therefore, it is no surprise that various proteins that localize in the MAMs can regulate the redox state of SERCA2b and affect the uptake of Ca^{2+} into the ER, thereby influencing transfer of Ca^{2+} across the ER-mitochondria interface and mitochondrial activity. For example, when incorporated in the MAMs, the cytosolic tumor suppressor protein p53 can decrease the oxidation of SERCA2b, thus promoting its activity and increasing ER Ca^{2+} levels. As a result, the flux of Ca^{2+} from the ER to the mitochondria increases, promoting apoptosis (Giorgi et al., 2015). Additionally, upon low ER Ca^{2+} levels, the ER reductase ERdj5 can reduce luminal disulfide-bonded cysteines of SERCA2b, thus activating SERCA2b and promoting import of Ca^{2+} into the ER (Ushioda et al., 2016).

In contrast, members of the PDI family have been implicated in the oxidation and inactivation of SERCA2b. As ER-resident oxidoreductases, PDI members facilitate proper protein folding by catalyzing the formation or breakage of disulfide bonds. A well-established member is

the TMX1 (Matsuo et al., 2001), which is involved in the quality control of major histocompatibility complex class 1 molecules and clearance of folding-defective peptides within the ER (Guerra et al., 2018; Matsuo et al., 2009). TMX1 is a Type I transmembrane protein that localizes to the ER membrane and interacts preferentially with transmembrane polypeptides (Guerra et al., 2018; Matsuo et al., 2004; Pisoni et al., 2015). Furthermore, the cytosolic domain of TMX1 contains a palmitoylation motif necessary for its targeting to the MAMs (Lynes et al., 2012). At the MAMs, TMX1 promotes the oxidation of SERCA2b cysteines to decrease SERCA2b activity and import of Ca^{2+} into the ER, thus directing Ca^{2+} flux towards the mitochondria (Raturi et al., 2016). Although SERCA2b activity is typically associated with mitochondrial activity, as demonstrated by the increase in oxidative phosphorylation upon inhibition of the SERCA2b inhibitor Bcl-2 (Dremina et al., 2004; Lagadinou et al., 2013), this is not always the case. For example, depletion of TMX1 can lead to active SERCA2b and increased retention of Ca^{2+} within the ER, thus reducing the transfer of Ca^{2+} from the ER to the mitochondria and limiting mitochondrial metabolism (Raturi et al., 2016; X. Zhang et al., 2019). Furthermore, cells lacking TMX1 show a lower degree of tight associations between the ER and mitochondria (Raturi et al., 2016), which is a factor for Ca^{2+} flux between the ER and mitochondria (Csordás et al., 2006).

Another well-established example of SERCA2b redox regulation is one that involves the ER Ca^{2+}-binding chaperone calnexin. Calnexin is a Type I transmembrane protein (Bergeron et al., 1994; Michalak et al., 1992; Wada et al., 1991) which assists in glycoprotein folding and quality control. Calnexin performs this function by colocalizing with the translocon (Lakkaraju et al., 2012) and binding to newly synthesized, monoglucosylated, N-linked glycoproteins. However, a significant portion of calnexin also targets the MAMs in a palmitoylation-dependent manner (Lynes et al., 2012, 2013). At the MAMs, calnexin interacts with the C-terminus of SERCA2b (Lynes et al., 2013; Roderick et al., 2000) and maintains the redox state of SERCA2b, thus stimulating its activity and promoting oxidative phosphorylation. Notably, it has been found that the effect of TMX1 on SERCA2b was partially antagonized by calnexin (Raturi et al., 2016). Upon depletion of calnexin, SERCA2b activity is reduced, resulting in decreased levels of ER Ca^{2+}, less Ca^{2+} transfer to the mitochondria, and limited mitochondrial metabolism (Gutiérrez et al., 2020).

1.3.5. Cell death

Given the prominent role of MAMs in maintaining cell homeostasis, it is no surprise that MAMs can also have a role for cell death events. Death signals mediated by MAMs include the transfer of Ca^{2+} between the ER and mitochondria. For instance, excess transfer of Ca^{2+} to the mitochondria can lead to oxidative stress and induce the opening of mPTPs, leading to the swelling of the matrix and subsequent apoptosis (Kinnally et al., 2011).

MAM-mediated death signals also involve protein-protein interactions and translocation of proteins. For example, the MAM-localized mitochondrial fission 1 protein (Fis1)/BAP31 complex plays an important role in transmitting apoptotic signals between the ER and mitochondria (N. Wang et al., 2021). Under non-stressed conditions, BAP31 is bound to calnexin. However, during apoptosis induction or cell stress, calnexin dissociates from BAP31 and moves away from the MAMs (Delom et al., 2007; Lynes et al., 2013), allowing BAP31 to increase its interaction with Fis1. Fis1 then cleaves BAP31 into p20-BAP31, which can initiate downstream signaling pathways that induce apoptosis, including the activation of caspases and the promotion of Ca^{2+} transfer from the ER to the mitochondria (Iwasawa et al., 2011; N. Wang et al., 2021).

1.3.6. Antiviral signalling

In addition to their roles in Ca^{2+} signalling and regulation of mitochondrial activity, MAMs have emerged as an important site for immune-viral responses (Figure 2). An important player for the MAM-mediated antiviral response is the mitochondrial antiviral signalling protein (MAVS), which localizes on the OMM at ER-mitochondria contact sites (Horner et al., 2011). Upon infection by RNA viruses, viral RNA is recognized by the cytosolic pathogen recognition receptor retinoic acid-inducible gene I (RIG-I) protein. RIG-I is then targeted to the MAMs where it binds MAVS (Horner et al., 2011). This interaction activates the downstream antiviral signalling pathways, resulting in the production and subsequent release of proinflammatory cytokines, such as interferon-I (IFN-I) and IFN-III, from infected tissue (Bender et al., 2015; Seth et al., 2005). In addition, the MAM-enriched stimulator of interferon genes (STING) can bind MAVS upon viral infection, thus increasing the response against viral infections (Ishikawa & Barber, 2008; Smith, 2021).

Given the prominent role of MAMs in regulating various cell processes, including antiviral responses, it is not surprising that numerous viral proteins target this structure. In fact, disruption

of contacts between the ER and mitochondria is a common strategy for many viruses during infection. One well-characterized example is the human cytomegalovirus (HCMV) viral mitochondria-localized inhibitor of apoptosis (vMIA) protein. While vMIA is initially synthesized at the ER, it eventually retargets to the MAMs, where it can interact with Sig-1R, thus destabilizing IP$_3$R and influencing Ca^{2+} transfer (Bozidis et al., 2010; Missiroli et al., 2018; Williamson et al., 2011; Williamson & Colberg-Poley, 2010). Furthermore, vMIA affects mitochondrial morphology by promoting mitochondrial fragmentation during viral infection (Kaarbø et al., 2011; McCormick et al., 2003). As a result, the number of MAMs is reduced, thereby decreasing the interaction between MAVS and STING and limiting the downstream antiviral signaling against HCMV. Other examples are the hepatitis C virus (HCV) nonstructural proteins 3 (NS3) and 4A (NS4A), which are known to cleave MAVS, leading to the suppression of antiviral responses (Bender et al., 2015; Horner et al., 2012). The human immunodeficiency virus 1 (HIV-1) viral protein R (Vpr) targets the MAMs and can have a strong cytotoxic effect on host cells. Vpr inserts into the membranes of the ER, OMM, and MAMs via a C-terminal transmembrane segment, and can disrupt the mitochondrial membrane potential ($\Delta\Psi_M$) and induce apoptosis (Huang et al., 2012). Additionally, it has been found that Vpr interacts with Drp1 and Mfn2. As a consequence of these interactions, Drp1 and Mfn2 are downregulated via a ubiquitin ligase complex, resulting in mitochondrial fragmentation (Huang et al., 2012).

Taken together, these studies highlight the important role of MAMs for antiviral responses, and how viral proteins target this structure and induce MAM dysfunction for their own benefit. In this thesis, we will explore the severe acute respiratory syndrome coronavirus 2, and its implication for MAM dysregulation.
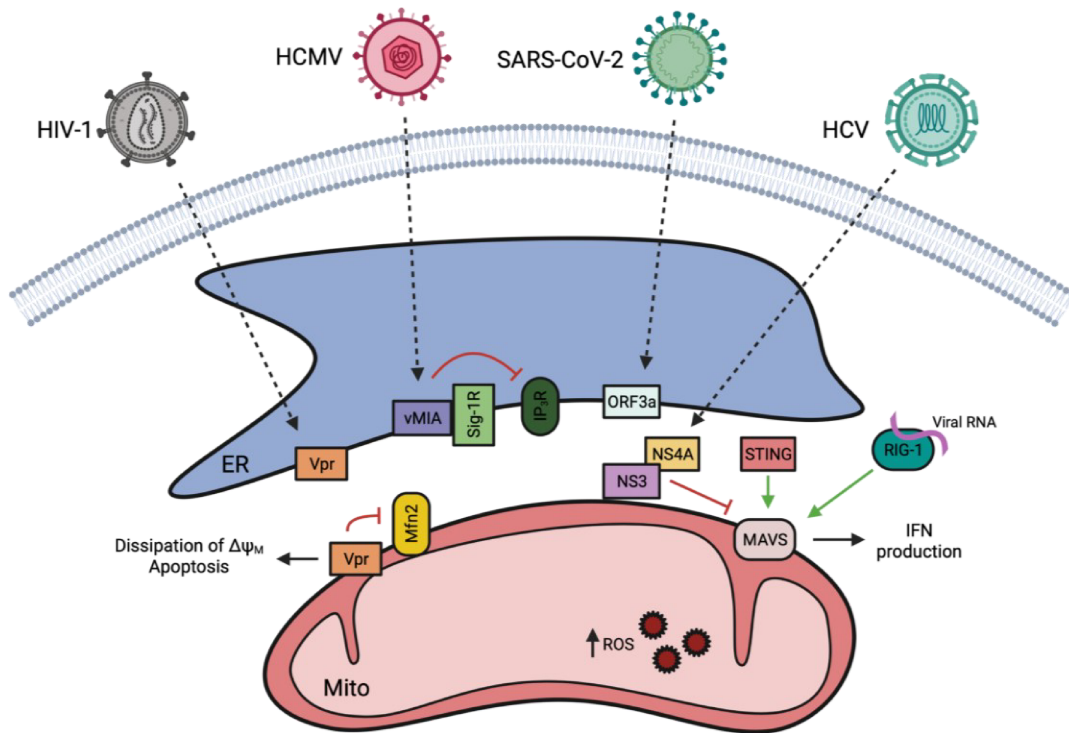
Figure 2. Antiviral signaling at the MAMs. Upon viral infection, RIG-1 binds to MAVS to promote IFN production. STING can also bind to MAVS at the MAMs to increase response against viral infections. HCV proteins NS3 and NS4A can cleave MAVS, leading to the suppression of antiviral responses. The HCMV protein vMIA targets the MAMs, where it interacts with Sig-1R, thus destabilizing IP$_3$R. HIV-1 Vpr targets the MAMs and interacts with and downregulates Mfn2, compromising mitochondrial integrity. SARS-CoV-2 ORF3a has been associated with the activation of proinflammatory responses and increased ROS production. For details, read text. Created with BioRender.com

1.4. Severe acute respiratory syndrome coronavirus 2

1.4.1. Overview

Severe acute respiratory syndrome coronavirus 2 (SARS-CoV-2) is the virus responsible for the coronavirus disease 2019 (COVID-19) within humans and other mammals (F. Wu et al., 2020). In order to infect host cells, SARS-CoV-2 requires the angiotensin-converting enzyme 2 receptor, which is highly expressed on the surface of many cell types, including capillary rich organs such as the lungs and kidneys, as well as the gut and the brain (Samavati & Uhal, 2020). Thus, SARS-CoV-2 can infect a wide variety of cell types, which means that COVID-19 infections can manifest in a variety of symptoms associated with different parts of the body, including systemic inflammation, which is characterized by elevated levels of pro-inflammatory cytokines in the blood (Buicu et al., 2021; Rodrigues et al., 2020).

Another hallmark of SARS-CoV-2 infections is mitochondrial dysfunction (Ajaz et al., 2021; Pliss et al., 2022). Given that mitochondria play an important role for cell survival and immune-viral responses, viruses are known to modulate mitochondrial function within host cells to their own benefit. SARS-CoV-2 is no exception; for instance, numerous studies have reported that that SARS-CoV-2 causes mitochondrial membrane depolarization, mPTP opening, and increased ROS production, thus contributing to mitochondrial damage and host cell death (Ramachandran et al., 2022; Shang et al., 2022).

1.4.2. Genomic structure

As a betacoronavirus, the SARS-CoV-2 virion contains positive-sense, single-stranded RNA (Cao et al., 2021). As one of the largest viral RNA genomes (around 30 kilobases), the SARS-CoV-2 genome encodes for 29 different proteins. Among these encoding proteins are the highly conserved structural proteins: spike (S), nucleocapsid (N), membrane (M), and envelope (E) proteins; and nonstructural proteins (NSP1-16). These proteins are necessary for entry and replication of the virus within the host cells: structural proteins make up the coronavirus virion and are key factors for infection of host cells, whereas nonstructural proteins are generated post-infection from an auto-proteolytic process and are necessary for replication and viral assembly processes (Naqvi et al., 2020).

In addition to the structural and nonstructural proteins, the SARS-CoV-2 genome also encodes for nine accessory proteins (Redondo et al., 2021). Generally, coronavirus accessory

proteins are dispensable for virus infiltration and replication. Unlike with structural and nonstructural proteins, accessory proteins display high variability across coronavirus members. Thus, the function of accessory proteins, especially that of newly emerged viruses, are not completely understood (V'kovski et al., 2021). However, research on SARS-CoV-2 has indicated that several accessory proteins encoded by the virus modulate host cellular processes and contribute to the virulence and pathogenesis of SARS-CoV-2. For example, the SARS-CoV-2 open reading frame 8 protein (ORF8) is known to mediate the downregulation of major histocompatibility complex class I molecules, thereby making SARS-CoV-2-infected cells less prone to lysis by T lymphocytes (Y. Zhang et al., 2021). In this thesis, we will explore a lesser understood SARS-CoV-2 accessory protein, ORF7b.

1.5. The SARS-CoV-2 accessory protein ORF7b

1.5.1. Overview

One of the accessory proteins encoded by the SARS-CoV-2 genome is ORF7b. ORF7b is a small protein composed of 43 amino acids, and shares around 85% identity and 97% sequence similarity with its SARS-CoV homolog (Redondo et al., 2021; Yoshimoto, 2020). The SARS-CoV homolog of ORF7b has been previously reported to be an integral membrane protein with a cytoplasmic C-terminus, suggesting that ORF7b is most likely a Type III transmembrane protein. (D. X. Liu et al., 2014; Schaecher et al., 2007). The putative transmembrane domain of ORF7b is necessary for the retention of this protein in the Golgi complex within infected cells (Schaecher et al., 2007, 2008). Additionally, ORF7b has been reported to be present in purified SARS-CoV virions, but are not necessary for viral replication (Pekosz et al., 2006; Schaecher et al., 2007). However, no subsequent studies have been conducted to further explore the functional properties of ORF7b.

As with its SARS-CoV homolog, the function of the SARS-CoV-2 ORF7b is largely unknown, but a recent study has shown that ORF7b activates the IFN signaling pathway and promotes expression of inflammatory cytokines, including IFN-β, interleukin (IL)-6, and tumor necrosis factor-α (TNF-α), thereby inducing cell death (R. Yang et al., 2021). Furthermore, SARS-CoV-2 viruses lacking the ORF7b gene produced smaller viral plaques compared to the wildtype virus in vitro (Silvas et al., 2021). This finding suggests that ORF7b may play a role for the virulence and viral fitness of SARS-CoV-2, albeit having a minor impact on the pathology and

disease outcomes of COVID-19, following studies on patients and animal models (Mazur-Panasiuk et al., 2021; Silvas et al., 2021).

1.5.2. ORF7b targets the ER and interacts with MAM proteins

Within the last two years, microscopy imaging experiments have been conducted to assess the localization and targeting sites of SARS-CoV-2 accessory proteins within cell models (Lee et al., 2020; Samavarchi-Tehrani et al., 2020). Confocal imaging of HEK 293 cells revealed that ORF7b showed organelle-specific localization patterns, as opposed to whole-cell expression patterns, suggesting that ORF7b interacts with host cell proteins of specific organelles (Lee et al., 2020). Additionally, immunofluorescence microscopy studies conducted by Samavarchi-Tehrani et al. (2020) revealed that ORF7b targeted the ER and Golgi complex specifically. Other SARS-CoV-2 proteins that exhibit a similar targeting pattern include S, M, ORF3a, and ORF6 (Samavarchi-Tehrani et al., 2020).

In addition, multiple viral protein-host protein interaction screens for SARS-CoV-2 have been conducted (Gordon et al., 2020; Lee et al., 2020; J. Li et al., 2021; Samavarchi-Tehrani et al., 2020; Stukalov et al., 2021; Y. Zhou et al., 2022). Through assays such as co-immunoprecipitation, mass spectrometry, and proximity labelling, these studies have revealed the host protein interactomes of SARS-CoV-2 proteins, including ORF7b. Interestingly, in addition to targeting the ER, ORF7b was found to interact with various MAM proteins, including Mfn2, MAVS, calnexin, and TMX1 (Stukalov et al., 2021). (A comprehensive list of the host cell interactome of ORF7b can be found on covid19interactome.org.) Given that MAMs play a major role in the regulation of mitochondrial function, we hypothesized that SARS-CoV-2 could disrupt mitochondrial metabolism by way of MAM protein interactions. So, to provide insight into the mechanisms that tie SARS-CoV-2 infections to mitochondrial dysregulation, my project aims to characterize ORF7b in the context of MAMs.

As mentioned earlier, the targeting of MAMs by viral proteins is not an uncommon phenomenon. Within the SARS-CoV-2 virus, a well-studied example is the accessory protein ORF3a. Like ORF7b, ORF3a is a transmembrane protein and forms a viroporin (Section 1.5.3) (Toft-Bertelsen et al., 2021; J. Zhang, Ejikemeuwa, et al., 2022). One study showed that the interacting proteins of the SARS-CoV-2 ORF3a interactome overlapped with the MAM proteome (Lee et al., 2020). Furthermore, a considerable change in the proteomic composition of the MAMs

occurred upon expression of ORF3a, implying that ORF3a influences ER-mitochondria contact sites (Lee et al., 2020). Although the mechanism behind these changes to MAM composition remains to be investigated, expression of ORF3a has been associated with the induction of cell death that is concurrent with the activation of proinflammatory responses and increased cellular oxidative stress (J. Zhang, Li, et al., 2022).

1.5.3. ORF7b forms a viroporin

A recent virus-host interactome found that ORF7b displayed self-association, suggesting that its oligomeric form may carry out important roles for SARS-CoV-2 infections (J. Li et al., 2021). Following this, another study identified ORF7b as one of the four SARS-CoV-2 genome-encoded viroporins (Toft-Berthelsen et al., 2021). Viroporins are small proteins that are encoded by a variety of viral genomes and target host cellular membranes (Nieva et al., 2012). Typically, viroporins contain at least one region capable of forming a transmembrane helix, and can assemble into oligomers within membranes, forming pores that alter membrane permeability and integrity (Gonzalez & Carrasco, 2003). While viroporins are generally not necessary for viral replication, they are known to participate in the assembly and release of virions from infected cells via host cell membrane remodeling. In fact, deletion of viroporin-encoding genes from the viral genome can significantly reduce the efficiency of viral propagation, highlighting the beneficial role of viroporins for viral infections (Gonzalez & Carrasco, 2003).

Another important aspect of viroporins is its ion channel function. For instance, viroporins have been in implicated in the regulation of intracellular Ca^{2+} levels during viral infection. Increases in intracellular Ca^{2+}, resulting from the entry of extracellular Ca^{2+} into the cell or Ca^{2+} leakage from intracellular stores, such as the ER, have been observed upon expression of various viroporins, including the rotavirus NSP4 (Hyser et al., 2010; Hyser & Estes, 2015) and picornavirus 2B viroporins (Ito et al., 2012; Triantafilou et al., 2013). As described earlier, perturbations in Ca^{2+} homeostasis can have consequences to cell fate. In fact, Ca^{2+}-induced apoptosis is an event that has been observed when viral proteins, including viroporins, are expressed in cells (Madan et al., 2008).

Given that viroporins play a role in viral propagation and cellular homeostasis, they have been desirable targets for the development of antiviral drugs. Many chemical compounds have been identified to disrupt the function of various viroporins. For example, amantadine is an

antagonist of the influenza A M2 viroporin, and prevents the release of the viral genetic material into the host cytoplasm, thereby inhibiting viral production (Watkins et al., 2020). In the case of ORF7b, a recent study has shown that its ion channel activity was blocked by emodin and xanthene (Toft-Bertelsen et al., 2021).

1.5.4. ORF7b resembles PLN

In line with the finding that ORF7b forms a viroporin, it has been recently suggested that ORF7b can assemble into a pentameric channel stabilized by leucine interactions, given that the predicted transmembrane region of ORF7b is enriched with evenly spaced leucine residues that resemble a leucine zipper motif (Fogeron et al., 2021; Nikolaev & Pervushin, 2009). Interestingly, this leucine zipper motif has also been identified in other regulatory proteins, including PLN (A. Y. Liu et al., 2022). This leucine zipper motif stabilizes the PLN homopentamer, which is the inactive form of PLN (Chu et al., 1998; Cornea et al., 1997; Simmerman et al., 1996). In light of the structure of ORF7b, it has been proposed that ORF7b could interfere with the function of PLN by interacting with PLN via the leucine zipper motif, thus disrupting SERCA regulation and Ca^{2+} transport (Fogeron et al., 2021). Given that intracellular Ca^{2+} plays a critical role for contractility of cardiac muscle, dysregulation of PLN could lead to heart arrhythmias (Verstraelen et al., 2021). In fact, heart arrhythmias are a common symptom of SARS-CoV-2 infections, thus highlighting the potential role of ORF7b in interfering with Ca^{2+} homeostasis in cardiac muscle. However, this has yet to be experimentally demonstrated.

1.6. Goals of this thesis

Given that the role of the SARS-CoV-2 accessory protein ORF7b has not yet been well elucidated, the goal of this thesis is to further our understanding of ORF7b. Since MAMs play a significant role in the regulation of mitochondrial metabolism, we aim to evaluate whether the MAM protein interactions of ORF7b have an effect on mitochondrial metabolism. Characterization of the potential effect of ORF7b on mitochondrial metabolism can provide insight on SARS-COV-2 infections and the mechanisms by which SARS-CoV-2 modulates mitochondrial functions.

CHAPTER 2: Materials and Methods

2. MATERIALS AND METHODS

2.1. Materials and reagents

Table 1. Chemicals and reagents

Chemical/reagent	Source
Acrylamide 30%	Bio-Rad
Ammonium persulfate (APS)	Bio-Rad
β-mercaptoethanol	BioShop
Bovine serum albumin (BSA)	Sigma
Bromophenol Blue	Bio-Rad
CHAPS	Sigma
Deoxycholic acid	Sigma
Dimethyl sulfoxide (DMSO)	Caledon
Egtazic acid (EGTA)	Sigma
Ethanol	Commercial Alcohols
Ethylenediaminetetraacetic acid (EDTA)	Sigma
Glycine	Thermo Fisher Scientific
HEPES	Sigma
Isopropanol	Thermo Fisher Scientific
Magnesium chloride	Thermo Fisher Scientific
Methanol	Fisher Chemicals
NP-40	Calbiochem
Saponin	Sigma
Skim milk powder	Carnation
Sodium bicarbonate (NaHCO$_3$)	EMD
Sodium carbonate (Na$_2$CO$_3$)	EMD
Sodium chloride (NaCl)	Thermo Fisher Scientific
Sodium dodecyl sulphate (SDS)	JT Baker
Sucrose	EMD
Tetramethyl ethylenediamine (TEMED)	EMD
Tris	Invitrogen
Triton X-100	Sigma

Table 2. Primary antibodies

Antibody	Source	Reference	Host	Clonality	Working dilution	Application
AMPK	Millipore	07-181	Rb	Polyclonal	1:1000	WB
p-AMPK	Millipore	07-681	Rb	Polyclonal	1:1000	WB
Biotin	Sigma	B3640	Gt	Polyclonal	1:1000	WB
Calnexin	BD Biosciences	610523	Ms	Monoclonal	1:2000	WB
Drp1	Abcam	ab56788	Ms	Monoclonal	1:3000	WB

Ero1α	Millipore	MABT376	Ms	Monoclonal	1:1000	WB
ERp57	Millipore	ABE1032	Rb	Polyclonal	1:200	IF
FLAG	Abcam	ab1257	Gt	Polyclonal	1:10000	WB
FLAG	Rockland	200-301-B13	Ms	Monoclonal	1:10000	WB
					1:200	IF
					2 μL	IP
HA	Cell Signaling	3724S	Rb	Monoclonal	1:5000	WB
HA	Biolegend	901501	Ms	Monoclonal	2 μL	IP
MCU	Sigma	HPA016480	Rb	Polyclonal	1:1000	WB
NOX4	Abcam	ab109225	Rb	Monoclonal	1:1000	WB
SERCA2b	Millipore	MAB2636	Ms	Monoclonal	1:1000	WB
TMX1	Invitrogen	MA5-26309	Ms	Monoclonal	1:1000	WB
TTC35	Invitrogen	PA5-54617	Rb	Polyclonal	1:1000	WB
γ-Tubulin	Invitrogen	MA1-850	Ms	Monoclonal	1:10000	WB

Table 3. Secondary antibodies

Antibody	Source	Reference	Host	Clonality	Working dilution	Application
Alexa Fluor 350 anti-Rabbit IgG	Invitrogen – Molecular Probes	A11046	Gt	Polyclonal	1:500	IF
Alexa Fluor 488 anti-Mouse IgG	Invitrogen – Molecular Probes	A11029	Gt	Polyclonal	1:1000	IF
Alexa Fluor 680 anti-Mouse IgG	Invitrogen – Molecular Probes	A21057	Gt	Polyclonal	1:10000	WB
Alexa Fluor 790 anti-Rabbit IgG	Invitrogen – Molecular Probes	A11369	Gt	Polyclonal	1:10000	WB
Alexa Fluor 680 anti-Goat IgG	Invitrogen – Molecular Probes	A21084	Dk	Polyclonal	1:10000	WB
Alexa Fluor 800 anti-Goat IgG	Invitrogen – Molecular Probes	A32930	Dk	Polyclonal	1:10000	WB

Abbreviations: WB: Western blot; IF: Immunofluorescence; IP: Immunoprecipitation; Rb: Rabbit; Ms: Mouse; Gt: Goat; Dk: Donkey

Table 4. Buffers and solutions

Buffer/solution	Composition
4X separating buffer	1.5 M Tris pH 8.8, 0.4% SDS
4X stacking buffer	0.5 M Tris pH 6.8, 0.4% SDS
Biotin-iodoacetamide (BIAM) reaction buffer	50 mM tris-HCl pH8, 50 mM NaCl, 5 mM EDTA, 1% Triton X-100, 0.1% IGEPAL CA-630
Carbonate transfer buffer	10 mM $NaHCO_3$, 3 mM Na_2CO_3, 20% methanol
CHAPS lysis buffer	10 mM Tris pH 7.4, 150 mM NaCl, 1 mM EDTA, 1% CHAPS
IF antibody solution	0.2% Saponin, 2% BSA, in PBS++
IF blocking solution	0.2% Saponin, 2% BSA, in PBS++
IF wash solution	0.2% Saponin, 0.2% BSA, in PBS++
m-RIPA lysis buffer	50 mM Tris, 150 mM NaCl, 1% NP-40, 0.5% deoxycholic acid, 0.1% SDS, 5mM $MgCl_2$
Mitochondria homogenization buffer	250 mM sucrose, 10 mM HEPES, pH 7.4, 1 mM EDTA, 1 mM EGTA
Sample loading buffer	60 mM tris pH 6.8, 2% SDS, 10% glycerol, 5% β-mercaptoethanol, 0.01% bromophenol blue
SDS-PAGE running buffer	25 mM tris, 200 mM glycine, 0.1% SDS
Tris buffered saline-Triton X-100 (TBS-T)	10mM Tris pH 8.0, 150 mM NaCl, 0.05% Triton X-100
WB antibody solution	10mM tris pH 8.0, 150 mM NaCl, 0.05% Triton X-100, 2% skim milk powder or BSA
WB blocking solution	10mM tris pH 8.0, 150 mM NaCl, 0.05% Triton X-100, 2% skim milk powder or BSA

Table 5. Plasmids

Plasmid	Tag	Vector	Source
ORF7b	C-terminal 3xFLAG	pcDNA3.1	Dr. Tom Hobman's Lab
SERCA2b	N-terminal 2xHA	pcDNA3.1	Precision Bio Laboratories
Ero1α	C-terminal Myc	pcDNA3.1	Dr. Robert Sitia's Lab

2.2. Methods

2.2.1. Cell culture

2.2.1.1. Maintenance of cells

Vero E6 cells were obtained from Dr. Tom Hobman's Lab, and HEK 293T cells were obtained from ATCC. Cells were cultured in Gibco Dulbecco's Modified Eagle Medium Nutrient Mixture F-12 (DMEM; 11320033, Invitrogen) supplemented with 10% fetal bovine serum (FBS; F1051, Sigma) at 37°C with 5% CO_2. Cells were passaged using 0.25% trypsin-EDTA (2520056,

Invitrogen), a maximum of 25 times after resuscitation. Stable cell lines were cultured in growth media supplemented with 1 mg/mL geneticin (10131027, Invitrogen). At least 3 days prior to experimentation, media was replaced with growth media without geneticin. Cell count was performed using the Countess II FL Automated Cell Counter (Life Technologies).

2.2.1.2. Transient transfection of cells

At least 24 h after seeding, cells were transfected with pcDNA3, ORF7b-FLAG, SERCA2b-HA, or Ero1α-Myc plasmids. Transfection was done using Lipofectamine 3000 (L3000015, Invitrogen) or Metafectene Pro (T040, Biontex), following the manufacturer's protocol. Transfection complexes were prepared in Opti-MEM Reduced Serum Medium (31985070, Invitrogen). Experiments were conducted 24-48 h after transfection, with at least 50% of the cells transfected.

2.2.1.3. Generation of stable cell lines

To generate ORF7b-expressing stable Vero E6 cell lines, cells were transfected with pcDNA3 or pcDNA3-ORF7b-FLAG using Lipofectamine 3000, as described previously. 48 h after transfection, cells were trypsinized and seeded thinly in 10-cm dishes with growth media containing 2 mg/mL geneticin to select for positive stable clones. Media was replaced every 3 days for approximately 2 weeks, until individuals cell colonies were visible. Individual colonies were selected and grown in 12-well plates. To verify ORF7b expression, cells were collected, lysed, and analyzed via Western blot using the FLAG antibody (Table 2).

2.2.1.4. Isolation of plasmid DNA

DH5α E. coli bacteria (Invitrogen) was used to amplify plasmid DNA. Briefly, 100 μL of bacteria was incubated with 1 μL of plasmid DNA on ice for 20 min. Bacteria was then heat-shocked in a 45°C water bath for 45 s and added to 1 mL of sterile Luria-Bertani (LB) broth (241420, BD Biosciences). Bacteria was pelleted down and resuspended in 100 μL of LB broth. Bacteria was then plated onto LB agar (244520, BD Biosciences) plates containing ampicillin (Sigma). The agar plates were incubated at 37°C overnight. The following day, colonies of bacteria containing the plasmid DNA were picked and grown in 50 mL of LB broth containing ampicillin, in a 220-rpm rotary shaker at 37°C overnight. The following day, the plasmid DNA was isolated

from the bacteria using the Plasmid Midiprep Kit (12143, QIAGEN), following the manufacturer's protocol. Plasmid DNA was resuspended in TE buffer (12090015, Invitrogen). DNA concentration was determined using the Nanodrop 2000C spectrophotometer (Thermo Scientific).

2.2.2. Preparation of whole cell lysates

To prepare whole cell lysates, cells were harvested via scraping with m-RIPA lysis buffer (Table 4) supplemented with 1X cOmplete EDTA free protease inhibitor (11873580001, Roche) and 1X PhosSTOP phosphatase inhibitor (4906845001, Roche), and kept on ice for 10 min. Lysates were vortexed and centrifuged at 12,000 rcf for 15 min at 4°C to remove nuclei and unbroken cells. Protein concentration of lysates was determined by Pierce Bicinchoninic Acid (BCA) Protein Assay Kit (23225, Thermo Fisher Scientific), following the manufacturer's protocol.

2.2.3. Immunoblotting

2.2.3.1. Sodium dodecyl sulfate-polyacrylamide gel electrophoresis

Prior to sodium dodecyl sulfate-polyacrylamide gel electrophoresis (SDS-PAGE), lysates were mixed with loading buffer (Table 4) and boiled for 5 min at 100°C. Equal amounts of protein per sample were loaded onto SDS-PAGE gels. Precision Plus Protein Dual Color Standards (1610374, Bio-Rad) was used as protein markers. The gels were electrophoresed in SDS-PAGE running buffer (Table 4) at 150 V for 60-80 min.

2.2.3.2. Western blot

After resolving the proteins via SDS-PAGE, the proteins were then transferred to nitrocellulose membranes (0.45-μM; 1620115, Bio-Rad) in carbonate transfer buffer (Table 4) at 400 mA for 2 h. Membranes were blocked in blocking solution (Table 4) for 1 h at 4°C and incubated with primary antibodies (Table 2). After incubation with primary antibodies, membranes were washed 3 times with tris buffered saline-Triton X-100 (TBS-T; Table 4) for 5 min each time, then incubated with secondary antibodies (Table 3). After incubation with secondary antibodies, membranes were washed 3 times with TBS-T. Proteins were detected using a LI-COR imaging system (Biosciences). Protein bands were analyzed and quantified using Image Lab (Bio-Rad).

2.2.4. Cell fractionation

2.2.4.1 Subcellular fractionation

ORF7b-expressing stable Vero E6 cells were grown to confluency in 10-cm plates prior to experimentation. Cells were collected with 600 µL mitochondria homogenization buffer (Table 4) supplemented with 1X cOmplete EDTA free protease inhibitor, per plate, and homogenized with a ball-bearing homogenizer (Isobiotec, ball clearance 14-µM). The resulting homogenates were centrifuged at 800 rcf for 10 min at 4°C to remove unbroken cells and nuclei. Post-nuclear supernatants were centrifuged at 12,000 rcf for 10 min at 4°C to yield heavy membrane (HM) fractions. The supernatants were then centrifuged at 60,000 rpm for 60 min at 4°C using a TLA 120.2 rotor (Beckman) to obtain light membrane (LM) fractions. The supernatants were then incubated in ice-cold 100% acetone (BDH1101, BDH Chemicals) overnight and centrifuged at 12,000 rcf for 10 min at 4°C to yield cytosolic fractions. All fractions were resuspended in m-RIPA lysis buffer. Fractions were loaded equal amounts in an 8-18% gradient SDS-PAGE gel and analyzed via Western blotting, as previously described.

2.2.4.2. Percoll gradient fractionation

Stable Vero E6 cells were grown to confluency in 15 20-cm dishes and harvested with 10 mL of mitochondria homogenization buffer supplemented with 1X cOmplete EDTA free protease inhibitor. The cells were centrifuged at 1,500 rpm for 5 min at 4°C using a JA-12 rotor (Beckman) and resuspended in 5 mL of mitochondria homogenization buffer. The cells were then homogenized as previously described. The resulting homogenates were centrifuged at 2,000 rpm for 10 min at 4°C to remove unbroken cells and nuclei. Post-nuclear supernatants were centrifuged at 8,500 rpm for 10 min at 4°C to yield crude mitochondria fractions. The supernatants were then centrifuged at 60,000 rcf for 60 min at 4°C using a TLA 120.2 rotor to obtain microsome fractions. The supernatants were then incubated in ice-cold 100% acetone overnight and centrifuged at 16,100 rcf for 20 min at 4°C to yield cytosolic fractions. The previously isolated crude mitochondria fractions were resuspended in 1 mL of mitochondria homogenization buffer and layered on top of 7.5 ml of 18% Percoll (diluted from 100% in mitochondria homogenization buffer; 17-0891-02, GE Healthcare) in a 10-mL ultra-clear polycarbonate Beckman tube. The tube was centrifuged at 33,300 rpm for 35 min at 4°C using a Ti-90 rotor (Beckman) to obtain the MAM and mitochondria fractions. To remove the Percoll, the MAM fractions were centrifuged at 60,000

rpm for 1 h at 4°C using a TLA 120.2 rotor, and the mitochondria fractions were centrifuged at 10,000 rcf for 10 min at 4°C. All fractions were resuspended in m-RIPA lysis buffer. Fractions were loaded equal amounts in an 8-18% gradient SDS-PAGE gel and analyzed via Western blotting, as previously described.

2.2.5. Carbonate extraction

HEK 293T cells were seeded in 5 10-cm dishes at a concentration of 5×10^6 cells per plate. The following day, the cells were transfected with ORF7b using Lipofectamine 3000, as previously described. 48 h after transfection, cells were collected with 400 μL mitochondria homogenization buffer supplemented with 1X cOmplete EDTA free protease inhibitor, per plate, and homogenized with a ball-bearing homogenizer. The resulting homogenates were pooled together and centrifuged at 1,200 rcf for 10 min at 4°C to remove unbroken cells and nuclei. Post-nuclear supernatants were split into two equal parts and centrifuged at 60,000 rpm for 60 min at 4°C using a TLA 120.2 rotor to obtain membrane pellets. One pellet was resuspended in 200 μL mitochondria homogenization buffer. The second pellet was resuspended in 200 μL sodium carbonate buffer (pH 11.5). Both pellets were kept on ice for 30 min. Then, the homogenates were centrifuged at 125,000 rcf for 30 min at 4°C using a TLA 120.2 rotor. The pellets were resuspended in 50 μL m-RIPA lysis buffer. To precipitate the solubilized proteins, 45 μL of trichloroacetic acid (TX1045, Millipore Sigma) was added to each supernatant and kept on ice for 30 min. The supernatants were centrifuged at 16,100 rcf for 10 min at 4°C. The pellets were washed with ice-cold 100% acetone twice, and resuspended in 50 μL m-RIPA lysis buffer. Fractions were loaded equal amounts in an 8-18% gradient SDS-PAGE gel and analyzed via Western blotting, as previously described.

2.2.6. PNGase F de-N-glycosylation

HEK 293T cells were seeded in 1 well of a 6-well plate per condition at a concentration of 1×10^6 cells per well. The following day, the cells were transfected with ORF7b or Ero1α using Lipofectamine 3000, as previously described. 48 h after transfection, cells collected and lysed with 100 μL 1X glycoprotein denaturing buffer (diluted from 10X in ddH$_2$O; B1704S, NE BioLabs) and sonicated. Lysates were then boiled for 5 min at 100°C. Lysates were then subjected to de-N-glycosylation using PNGase F (P0704L, NE BioLabs), following the manufacturer's protocol. After incubating the lysates in the reaction buffer for 1 h at 37°C, the lysates were diluted in loading

buffer and boiled for 5 min at 100°C. Samples were loaded equal amounts on an SDS-PAGE gel and analyzed via Western blotting, as previously described.

2.2.7. Co-immunoprecipitation

Per condition, 3.0 x 10^6 HEK 293T cells were seeded in 2 10-cm plates 3 days prior to experimentation. The following day, cells were transfected with ORF7b and/or SERCA2b using Lipofectamine 3000, following the manufacturer's protocol. On the day of the experiment, cells were washed with Dulbecco's phosphate-buffered saline containing Ca^{2+} and Mg^{2+} (PBS++; 14040133, Thermo Fisher Scientific) and incubated with 5 mL 2 mM dithiobis succinimidyl propionate (DSP; 22585, Thermo Fisher Scientific) in PBS++ for 30 min at room temperature, to maintain protein crosslinking. Then, the cells were quenched with 5 mL 10 mM ammonium chloride (A9434, Sigma) for 10 min. Cells were harvested in m-RIPA lysis buffer supplemented with 1X cOmplete EDTA free protease inhibitor and 1X PhosSTOP phosphatase inhibitor and kept on ice for 10 min. Lysates were vortexed and centrifuged at 12,000 rcf for 15 min at 4°C to remove nuclei and unbroken cells. Protein concentration of lysates was determined by Pierce BCA Protein Assay Kit. At least 100 μg of each lysate was stored at -80°C as the input samples. 1000-1500 μg of each lysate, adjusted to 500 μL of m-RIPA lysis buffer, was incubated with primary antibodies (Table 2) overnight at 4°C on a rotating shaker. The next day, Dynabeads Protein A magnetic beads (10002D, Invitrogen) were equilibrated 3 times in m-RIPA lysis buffer at 4°C for 5 min each time, and added to each sample and incubated for 1 h at 4°C on a rotating shaker. Protein A beads were washed 3 times in m-RIPA lysis buffer and boiled in sample loading buffer (Table 4) at 100°C for 5 min to obtain the bound samples. The input samples were diluted in sample loading buffer and boiled at 100°C for 5 min. Input and bound protein samples were resolved by SDS-PAGE and analyzed via Western blot, as previously described.

2.2.7.1. Protein redox state

Per condition, 4 x 10^5 HEK 293T cells were seeded in 3 wells of a 6-well plate and transfected with ORF7b and/or SERCA2b using Lipofectamine 3000, following the manufacturer's protocol. 48 h post transfection, prior to experimentation, cells were treated with 10 mM dithiothreitol (DTT; A22066A, Invitrogen) or 5 mM diamide (D3648, Sigma-Aldrich) for 10 min at 37°C, constituting the fully reduced and fully oxidized controls. Cells were washed with

PBS++ and lysed with 60 μL biotin-iodoacetamide (BIAM) reaction buffer (Table 4) containing 200 μM BIAM (21334, Thermo Fisher Scientific) and 1X cOmplete EDTA free protease inhibitor. Then, cell lysates were pooled and placed on a rocker for 10 min at 4°C. Lysates were then vortexed and centrifuged at 12,000 rcf for 10 min at 4°C to remove nuclei and unbroken cells. The supernatants were kept in the dark for 90 min at room temperature to allow for the biotinylation of reduced proteins. Bio-Spin columns (737-6221, Bio-Rad) were washed with CHAPS buffer (Table 4) three times and once with CHAPS buffer supplemented with 1X cOmplete EDTA free protease inhibitor. To remove the unreacted BIAM, each cell lysate was loaded into two columns and centrifuged at 1,000 rcf for 4 min at 4°C. 10 μL of each lysate was stored at -80°C as the input samples. Each cell lysate was incubated with primary antibodies (Table 2) overnight at 4°C on a rotating shaker. The next day, Dynabeads Protein A magnetic beads were equilibrated 3 times in CHAPS buffer at 4°C for 5 min each time, and added to each sample and incubated for 1 h at 4°C on a rotating shaker. Protein A beads were washed 3 times in CHAPS buffer and boiled in sample loading buffer containing 50 mM DTT at 75°C for 10 min to obtain the bound samples. The input samples were diluted in sample loading buffer containing 50 mM DTT and boiled at 100°C for 5 min. Input and bound protein samples were resolved by SDS-PAGE and analyzed via Western blot, as previously described.

2.2.8. Immunofluorescence microscopy

2.2.8.1. Preparation of slides

Vero E6 cells were seeded on ethanol-sterilized 12-mm glass coverslips (12-545-82, Fisherbrand) previously coated with poly-L-lysine (P4832, Sigma), and transfected the following day as previously described. Briefly, cells were fixed with 4% paraformaldehyde (PFA) solution in PBS++ (diluted from 16% PFA, 15710, Electron Microscopy Sciences) for 20 min at room temperature, and quenched with 50 mM ammonium chloride for 10 min at room temperature. Cells were then permeabilized with 1 mL of wash solution (Table 4) containing 0.1% Triton X-100 for 1 min and blocked with 1 mL of blocking solution (Table 4) for 15 min at room temperature. Cells were incubated with primary antibodies (Table 2) for 1 h at room temperature and rinsed with wash solution (Table 4). Cells were then incubated with secondary antibodies (Table 3) for 30 min. Coverslips were washed again and mounted using VECTASHIELD Vibrance Antifade Mounting Media (H1700, Vector Laboratories). Imaging was performed using an Axio Observer Z1 inverted

phase contrast fluorescence microscope (Zeiss) equipped with a 100X objective lens. Micrographs were analyzed using the AxioVision software (Zeiss).

2.2.8.2. Analysis of mitochondrial morphology

For analysis of mitochondrial network, cells were incubated with 100 nM MitoTracker (M7512, Thermo Fisher Scientific) for 30 min at 37°C, then processed for immunofluorescence microscopy as previously described. Additionally, cells were stained with DAPI (D9542, Sigma) for 5 min at room temperature prior to blocking. Micrographs were analyzed using Fiji. Mitochondrial morphology was evaluated using the parameters form factor (FF = 4π x area/perimeter^2) and aspect ratio (AR = major radius/minor radius).

2.2.9. Live-cell Ca^{2+} measurement

Wildtype or ORF7b-expressing stable Vero E6 cells were seeded on ethanol-sterilized, poly-L-lysine-coated, 12-mm glass coverslips and transfected the following day using Lipofectamine 3000, as previously described. At the time of imagine, cells were approximately 80% confluent. Live-cell imaging was done with an Olympus FV1000 laser-scanning confocal microscope equipped with a 20X objective lens (XLUMPLANFL, NA 1.0, Olympus). Images were acquired using the Olympus FluoView software and analyzed with the Time Series Analyzer v3.0 plugin on Fiji (NIH, USA).

2.2.9.1. ER Ca^{2+}

24 h after transfection with ER-RGECO (J. Wu et al., 2014), Vero E6 cells were transferred to the microscope chamber filled with Hank's Balanced Salt Solution (HBSS) containing Ca^{2+} and Mg^{2+} (HBSS++; 14025092, Thermo Fisher Scientific). Then, cells were perfused with HBSS++ at a flow rate of 5 mL/min for the first 30 s using a perfusion pump system (Watson-Marlow Alitea-AB, Sin-Can) to establish baseline fluorescence. Then, cells were perfused with HBSS (14175095, Thermo Fisher Scientific) supplemented with 1.75 µM MgCl$_2$ (MX0045-1, EM Science), 410 µM MgSO$_4$ (230391, Sigma-Aldrich), 100 µM EGTA (4100, OmniPur EMD), and 60 µM tert-butylhydroquinone (TBHQ; 97%, 112941, Sigma-Aldrich) for 14.5 min, to measure the clearance of Ca^{2+} from the ER. Images were taken every 3 s in the Alexa546 channel (excitation 559 nm/emission 575-675 nm).

2.2.9.2. Mitochondrial Ca^{2+}

24 after transfection with Mito-RGECO (J. Wu et al., 2014), Vero E6 cells were transferred to the microscope chamber filled with HBSS++. Then, cells were perfused with HBSS++ at a flow rate of 5 mL/min for the first 30 s using a perfusion pump system to establish baseline fluorescence. Then, cells were perfused with HBSS++ containing 10 µM carbonyl cyanide p-trifluoromethoxy phenylhydrazone (FCCP; 15218, Cayman) for 12.5 min, to induce mitochondrial Ca^{2+} release; or with HBSS++ containing 50 µM histamine (H7125, Sigma) for 4.5 min, to induce Ca^{2+} release from the ER and subsequent uptake into the mitochondria. Images were taken every 5 s for the FCCP group and every 1 s for the histamine group, in the Alexa546 channel (excitation 559 nm/emission 575-675 nm).

2.2.10. High-resolution respirometry

HEK 293T cells were seeded in 12-well plates and transfected the following day using Metafectene Pro, as previously described. Experiments were done 48 h after transfection. Prior to experimental analysis, the Oxygraph-2k machines (Oroboros Instruments, Innsbruck, Austria) were washed with 70% ethanol, 90% ethanol, and milliQ water, and calibrated by adding 2.3 mL of growth media to each chamber for 30-45 min until oxygen signals were stable.

Cells were lifted with trypsin and neutralized in fresh growth medium. Cells were spun down at 120 rcf for 5 min at room temperature and resuspended in 2.8 mL of growth media. Cell concentration was determined using the Countess II FL Automated Cell Counter. For respirometry analysis, 2 mL of intact cells were loaded into each chamber. Cellular respiration was recorded by measuring oxygen flux as a function of time, at 37 °C and with a stirrer speed of 750 rpm. First, routine respiration was measured in the presence of endogenous substrates. To measure leak respiration, 1 µL of 4 mg/mL oligomycin (141829, Abcam) was added to each chamber. The stepwise addition of 1 µL of 1 mM FCCP (C2920, Sigma-Aldrich) to each chamber was performed and maximal respiration was recorded. Finally, residual oxygen consumption was measured by adding 1 µL of 0.5 mM antimycin A to each chamber.

2.2.11. ATP measurement

HEK 293T cells were seeded in 12-well plates at a concentration of 250,000 cells per well. The next day, cells were transfected with ORF7b using Lipofectamine 3000, as previously described. 48 h after transfection, cells were resuspended in CHAPS buffer (Table 4) supplemented with 1X cOmplete EDTA free protease inhibitor. Cellular ATP content was determined using the ATP Determination kit (A22066, Molecular Probes) following the manufacturer's protocol. Luminescence was measured using a Synergy 4 plate reader (Bio Tek) at 560 nm. ATP levels were normalized to protein concentration, which was determined using BCA Protein Assay Kit, as previously described.

2.2.12. Reactive oxygen species measurement

ROS measurements were conducted using a BD LSRFortessa flow cytometer (BD Biosciences). Data analysis was performed using the BD FACSDiva software (BD Biosciences).

2.2.12.1 Mitochondrial ROS

Transfected HEK 293T and Vero E6 cells were grown to confluency in 12-well plates. On the day of the experiment, cells were incubated with 500 nM CellROX Orange (C10443, Molecular Probes) or with 1 µM MitoSOX (M36008, Molecular Probes) for 45 min at 37°C. Cells were lifted with trypsin and resuspended in growth media and centrifuged at 100 rcf for 5 min at room temperature. Cells were then resuspended in HBSS containing 0.5% BSA. CellROX Orange and MitoSOX fluorescence signals (excitation 510 nm/emission 580 nm) were measure for at least 10,000 individual cells per sample. As a positive control, cells were treated with 0.4 mM tert-butyl hydroperoxide (TBHP; C10493A, Invitrogen) 1 h prior to experiment.

2.2.12.2. Cytoplasmic ROS

Transfected HEK 393T cells were grown to confluency in 12-well plates. On the day of the experiment, cells were incubated with 1 µM CellROX Green (C10444, Molecular Probes) for 1 h at 37°C. Cells were lifted with trypsin and resuspended in growth media and centrifuged at 100 rcf for 5 min at room temperature. Cells were then resuspended in HBSS containing 0.5% BSA. CellROX Green fluorescence signal (excitation 545 nm/emission 565 nm) was measured for

at least 10,000 individual cells per sample. As a positive control, cells were treated with 0.4 mM TBHP 1 h prior to experiment.

2.2.13 Statistical analysis

Statistical analysis was done using Prism (GraphPad). For comparisons between groups, a student's t- test was used. Data is presented as mean, with error bars indicating the standard error of the mean. Statistical significance refers to * P < 0.05; ** P < 0.01; *** P < 0.001; **** P < 0.0001.

CHAPTER 3: Results

3. RESULTS

3.1. Preface

The experiments presented herein were conducted using two cell lines: HEK 293T and Vero E6. The HEK 293 cell line is an immortalized cell line established from embryonic kidney cells (Russell et al., 1977). Several subtypes have been obtained thereafter, including HEK 293T, which was established by the expression of a temperature-sensitive SV40 T-antigen mutant, which allows plasmids containing the SV40 origin of replication to replicate when transfected into the cells (DuBridge et al., 1987). Among human cell lines, HEK 293T is widely utilized due to its rapid growth rate and propensity for transfection. Given that our experiments rely on the transient transfection of ORF7b into our cell model, HEK 293T was an appropriate choice for this project.

The Vero cell line, on the other hand, was established from kidney epithelial cells extracted from an African green monkey (Yasumura & Kawakita, 1963). Since then, several subtypes, including Vero E6, have been derived. Like the HEK 293 cell line, the Vero cell line is an immortalized cell line. However, Vero cells are more adherent that HEK 293 cells, which make them suitable for experiments such as microscopy (Emeny & Morgan, 1979). In addition, Vero cells are widely used in virology research. Vero cells are IFN expression deficient, which means that they do not secrete IFNs during viral infection. Therefore, the antiviral defense mechanism of Vero cells is compromised (Emeny & Morgan, 1979). This means that Vero cells are susceptible to many viruses, including SARS-CoV-2 and other coronaviruses, and have become a popular choice within the field of virology, in particular for the development of vaccines against viral diseases (Kiesslich & Kamen, 2020). For these reasons, we decided to conduct some of our experiments using the Vero E6 cell line.

3.2. Results

3.2.1. ORF7b is an integral membrane protein

The sequence of the SARS-CoV homolog of ORF7b contains a putative transmembrane domain and a cytosolic C-terminus region, pointing towards a Type III transmembrane protein topology (D. X. Liu et al., 2014; Schaecher et al., 2007). Given the high sequence similarity between the ORF7b homologs (Redondo et al., 2021; Yoshimoto, 2020), we hypothesized that the SARS-CoV-2 ORF7b could have a similar structure. Indeed, bioinformatic analysis of the SARS-

CoV-2 ORF7b sequence using TOPCON (topcon.net) predicts a transmembrane region from residues 9-29, with a luminal N-terminus and a cytosolic C-terminus (Figure 3A). Such a topology is consistent with a Type III transmembrane protein. However, the topology of ORF7b has not yet been biochemically demonstrated. Thus, sodium carbonate extraction was performed on cell membrane homogenates to test whether ORF7b is an integral protein. This method relies on the alkaline pH which converts membrane vesicles into membrane sheets, and reduces non-covalent protein interactions, thereby releasing loosely attached peripheral membrane proteins without disrupting the integrity of lipid bilayer membranes (Fujiki et al., 1982; Kim et al., 2015). We detected ORF7b signal in the total membrane homogenates, and upon sodium carbonate treatment, ORF7b was retained in the pellet (P) fraction, similar to the integral ER membrane protein marker calnexin, while the peripheral ER membrane protein marker TTC35 was extracted into the soluble (S) fraction (Figure 3B). Thus, our data suggests that SARS-CoV-2 ORF7b, like its SARS-CoV homolog, is an integral membrane protein.

To further investigate the topology of ORF7b topology, we conducted a PNGase F de-N-glycosylation assay. This protocol utilizes PNGase F to remove N-linked oligosaccharides from glycoproteins. Such modifications can be observed as molecular weight shifts on a Western blot. Analysis of the ORF7b sequence showed that Asn-38 is part of a consensus site for a potential N-glycosylation (Figure 3A). If Ans-38 is in the ER lumen, it could be glycosylated, and treatment with PNGase F would result in its de-glycosylation, which would be observed as a downward shift in the molecular weight for ORF7b. Such is the case for Ero1α (Figure 3C), which is a glycosylated protein in the ER. However, if ORF7b assumes a Type III transmembrane topology, as indicated by TONCONS, then Asn-38 would be in the cytosol, and we would not expect it to be glycosylated. Thus, we would observe no molecular weight shift for ORF7b. As predicted, no apparent change was observed for the molecular weight of ORF7b after treatment with PNGase F, which is consistent with the idea that the C-terminus region of ORF7b is cytosolic.

Figure 3. ORF7b is an integral membrane protein. (A) Sequence analysis of ORF7b, generated using TOPCONS (topcons.net) (i: inside of the membrane/cytosolic, o: outside of the membrane/luminal, M: membrane region). Asn-38 is highlighted as a potential N-glycosylation site. **(B)** Total membrane homogenates from ORF7b-expressing HEK 293T cells were subjected to carbonate extraction and separated into pelleted (P) and soluble (S) membrane fractions, which were analyzed via Western blot for FLAG, calnexin, and TTC35. **(C)** HEK 293T cells were transfected with ORF7b-FLAG for 48 h prior to lysis. Lysates were subjected to de-N-glycosylation using PNGase F. Lysates were analyzed via Western blot for FLAG. The Ero1α group served as a positive control.

3.2.2. ORF7b targets the MAMs

Previous immunofluorescence microscopy studies have revealed that ORF7b targets the ER (Lee et al., 2020). Additionally, various SARS-CoV-2 viral protein-host protein interaction screens have shown that ORF7b interacts with MAM proteins (Samavarchi-Tehrani et al., 2020; Stukalov et al., 2021). Such an interaction would suggest that ORF7b localizes in the proximity of ER-mitochondria contact sites. Thus, to investigate the intracellular localization of ORF7b, we analyzed the distribution of this SARS-CoV-2 accessory protein in Vero E6 cells by immunofluorescence microscopy. As expected, ORF7b showed a dispersed reticular staining pattern that was similar to the distribution of the ER protein marker ERp57, consistent with the finding of previous studies that ORF7b localizes to the ER (Figure 4A). Additionally, we found that ORF7b staining overlapped with ER-mitochondria contact sites, indicated by areas where ERp57 staining was in close proximity with MitoTracker staining (enlarged, Figure 4A). We then complemented this analysis by subjecting total membrane homogenates of HEK 293T cells to differential centrifugation, which separates the membranes into heavy membranes (HM) fractions and light membrane (LM) fractions (Figure 4B). This assay showed that the majority of the ORF7b signal was found in the HM fraction, which contains the mitochondria, the rough ER, and the MAMs (Gilady et al., 2010; Myhill et al., 2008), further pointing towards a localization to the MAMs for ORF7b.

In order to ascertain the localization of ORF7b to the MAMs, we then analyzed the distribution of ORF7b on a Percoll gradient, which can isolate the MAMs from mitochondria (Gilady et al., 2010; Stone & Vance, 2000). Membranes isolated as crude mitochondria via differential centrifugation are resolved on a Percoll gradient, resulting in a pure mitochondria fraction that is enriched with the mitochondria protein marker MCU, and a MAM fraction that is enriched with established MAM protein markers Ero1α, calnexin, and TMX1 (Figure 5) (Gilady et al., 2010; Gutiérrez et al., 2020; Raturi et al., 2016). This fractionation showed that ORF7b was present in the MAMs, with virtually no ORF7b in the pure mitochondria fraction. This result is consistent with the fractionation data that showed that ORF7b is found in HM fractions obtained via differential centrifugation.

Since MAM-targeted viral proteins are known to alter MAM protein composition through protein-protein interactions, including SARS-CoV-2 ORF3a (Lee et al., 2020), we were interested in whether ORF7b affected the intracellular distribution of MAM proteins (Figure 5). In the control

(empty vector; EV) group, TMX1 was relatively more enriched in the MAM fraction in comparison to the microsome fraction. However, in the ORF7b group, the TMX1 signal in the MAM fraction was decreased. A similar observation was made for calnexin, albeit to a lesser degree, whereas the distribution pattern of Ero1α remained the same between the control and ORF7b groups. Altogether, our subcellular fractionation experiments showed that ORF7b is enriched in the MAMs and alters the distribution of some MAM proteins.
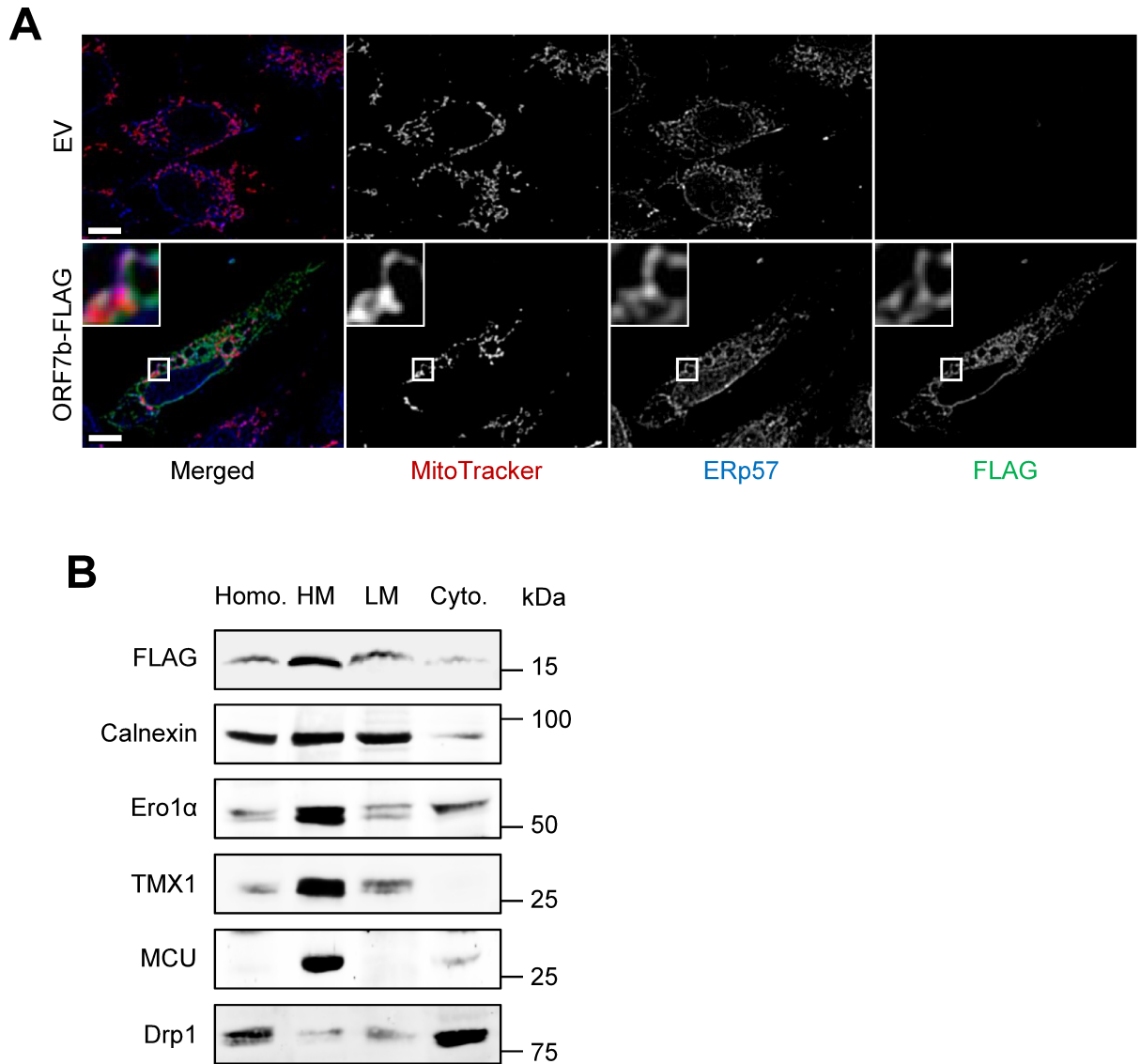
Figure 4. Intracellular localization of ORF7b. (A) Transfected Vero E6 cells were grown on 12-mm glass coverslips and processed for immunofluorescence microscopy. Cells were incubated with MitoTracker (mitochondria marker) and antibodies against ERp57 (ER marker) and FLAG (ORF7b marker). Scale bar = 10 μm. **(B)** Total membrane homogenates from ORF7b-transfected Vero E6 cells were fractionated into heavy membrane (HM), light membrane (LM), and cytosolic fractions, which were analyzed via Western blot for FLAG, calnexin, Ero1α, TMX1, MCU, and Drp1. EV: Empty vector.
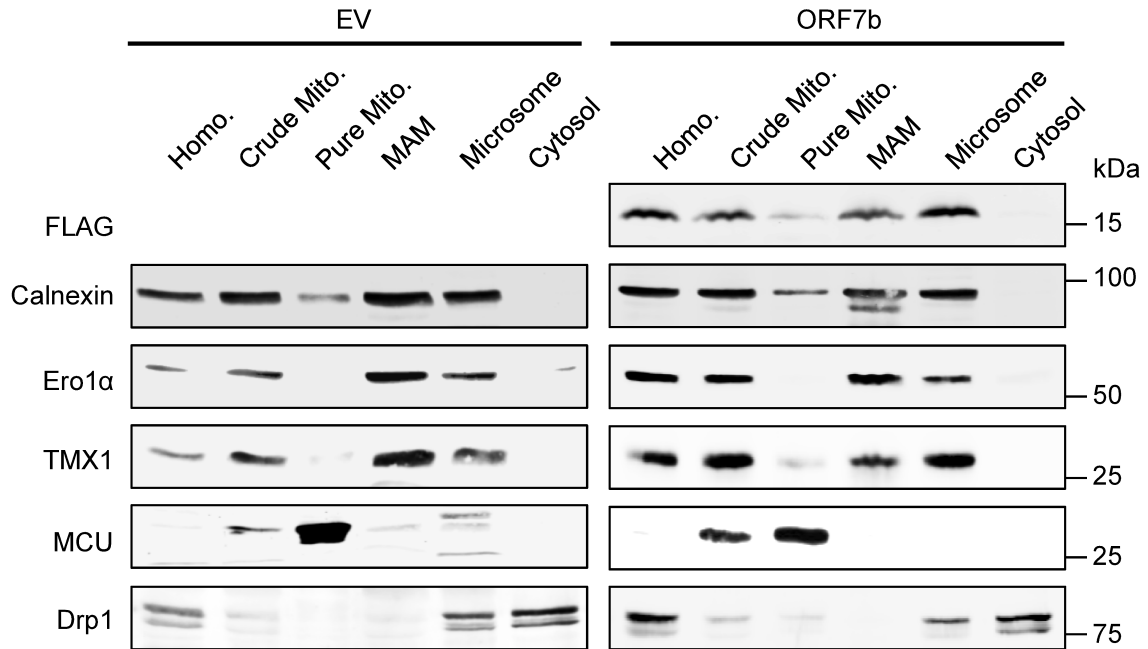
Figure 5. ORF7b cofractionates with the MAMs. Total membrane homogenates from control and ORF7b-transfected Vero E6 cells were fractionated into crude mitochondria, pure mitochondria, MAM, microsome, and cytosolic fractions using a Percoll gradient. Fractions were analyzed via Western blot for FLAG, calnexin, Ero1α, TMX1, MCU, and Drp1.

3.2.3. ORF7b disrupts MAM protein interactions

As previously mentioned, various SARS-CoV-2 viral protein-host protein interaction screens have revealed that ORF7b interacts with MAM proteins, including regulators of SERCA2b, calnexin and TMX1 (Gordon et al., 2020; Lee et al., 2020; Samavarchi-Tehrani et al., 2020; Stukalov et al., 2021). To verify the protein interactions of ORF7b with SERCA2b regulators, we conducted a co-immunoprecipitation assay. Briefly, HEK 293T cells were transfected with FLAG-tagged ORF7b. After 48 h, cells were lysed and subjected to immunoprecipitation using anti-FLAG antibodies (Figure 6A). This experiment showed that both calnexin and TMX1 co-immunoprecipitated with ORF7b, whereas in the control group, calnexin and TMX1 signals were absent. To further verify that these signals were not background bands or a result of non-specific antibody binding, we probed for the MAM-localized NOX4 protein, which is also known to mediate the activity of SERCA2b (Beretta et al., 2020; Tong et al., 2010). Unlike calnexin and TMX1, NOX4 was not detected in the IP sample of either control or ORF7b group. We also sought to determine whether ORF7b could interact with SERCA2b directly. Thus, we transfected our cells with FLAG-tagged ORF7b, as well as HA-tagged SERCA2b (since endogenous levels of SERCA2b are too low to detect). Interestingly, when we immunoprecipitated ORF7b, we detected a faint SERCA2b signal (Figure 6B). This finding suggests that ORF7b could also interact with SERCA2b, in addition its regulators.

Viral proteins have been known to interfere with protein-protein interactions within host cells. One example is vMIA, which localizes to the MAMs, where it can interact with Sig-1R, thus disrupting the interaction between Sig-1R and IP$_3$R and destabilizing IP$_3$R (Bozidis et al., 2010; Missiroli et al., 2018; Williamson & Colberg-Poley, 2010). Therefore, we hypothesized that a similar scenario could happen with ORF7b; given that ORF7b showed interaction with SERCA2b and its regulators, we sought to determine whether expression of ORF7b influenced interaction of these proteins with each other. Briefly, HEK 293T cells were transfected with FLAG-tagged ORF7b and HA-tagged SERCA2b. After 48 h, cells were lysed and subjected to immunoprecipitation using anti-HA antibodies (Figure 7A). As predicted, calnexin and TMX1 were pulled down in the control lysate, confirming that under normal conditions, SERCA2b interacted with these proteins. However, for ORF7b-expressing cells, there was a significant reduction in calnexin and TMX1 signals, suggesting that the interactions between SERCA2b and calnexin or TMX1 were disrupted upon ORF7b expression (Figure 7A, B). Interestingly, we also

detected a faint ORF7b band in the IP samples, further corroborating an interaction between SERCA2b and ORF7b. Altogether, our co-immunoprecipitation results show that ORF7b interacts with calnexin and TMX1, and this is concurrent with a reduction in interaction between these proteins and SERCA2b.

Given that calnexin and TMX1 mediate the redox state of SERCA2b (Gutiérrez et al., 2020; Raturi et al., 2016), our finding that ORF7b disrupted interactions between SERCA2b and calnexin and TMX1 prompted us to explore whether, as a result, the oxidation of SERCA2b was altered. Thus, we performed a biotinylated iodoacetamide (BIAM) labelling assay to determine SERCA2b redox state within control and ORF7b-expressing HEK 293T cells in the presence of a thiol-recognizing BIAM (Gutiérrez et al., 2020). This assay showed that SERCA2b was mostly reduced in control HEK 293T cells, based on SERCA2b-BIAM signals established from diamide and DTT treatments, which constitute the fully oxidized and reduced controls, respectively (Figure 7C). However, no apparent changes in SERCA2b-BIAM signal were observed for the ORF7b group, suggesting that expression of ORF7b does not have a major consequence on the redox state of SERCA2b (Figure 7C).
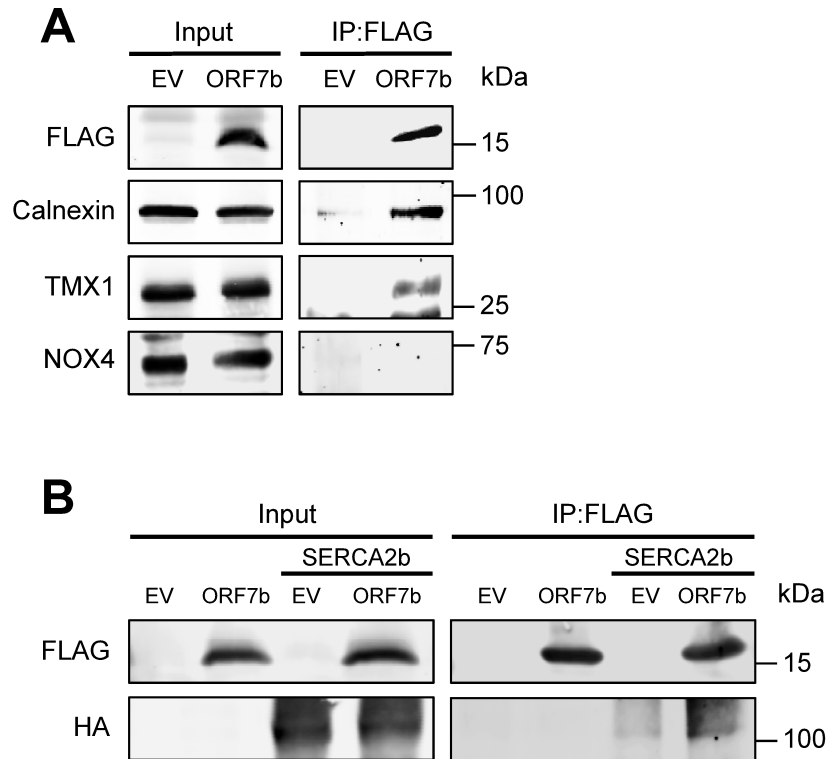
Figure 6. ORF7b interacts with MAM proteins. (A) HEK 293T cells were transfected with FLAG-tagged ORF7b for 48 h prior to lysis. Lysates were subjected to immunoprecipitation by anti-FLAG antibodies. Proteins were resolved via SDS-PAGE and immunoblotted against FLAG, TMX1, calnexin, and NOX4 (as a MAM protein negative control). **(B)** HEK 293T cells were transfected with FLAG-tagged ORF7b and HA-tagged SERCA2b for 48 h prior to lysis. Lysates were subjected to immunoprecipitation by anti-FLAG antibodies. Proteins were resolved via SDS-PAGE and immunoblotted against FLAG and HA.
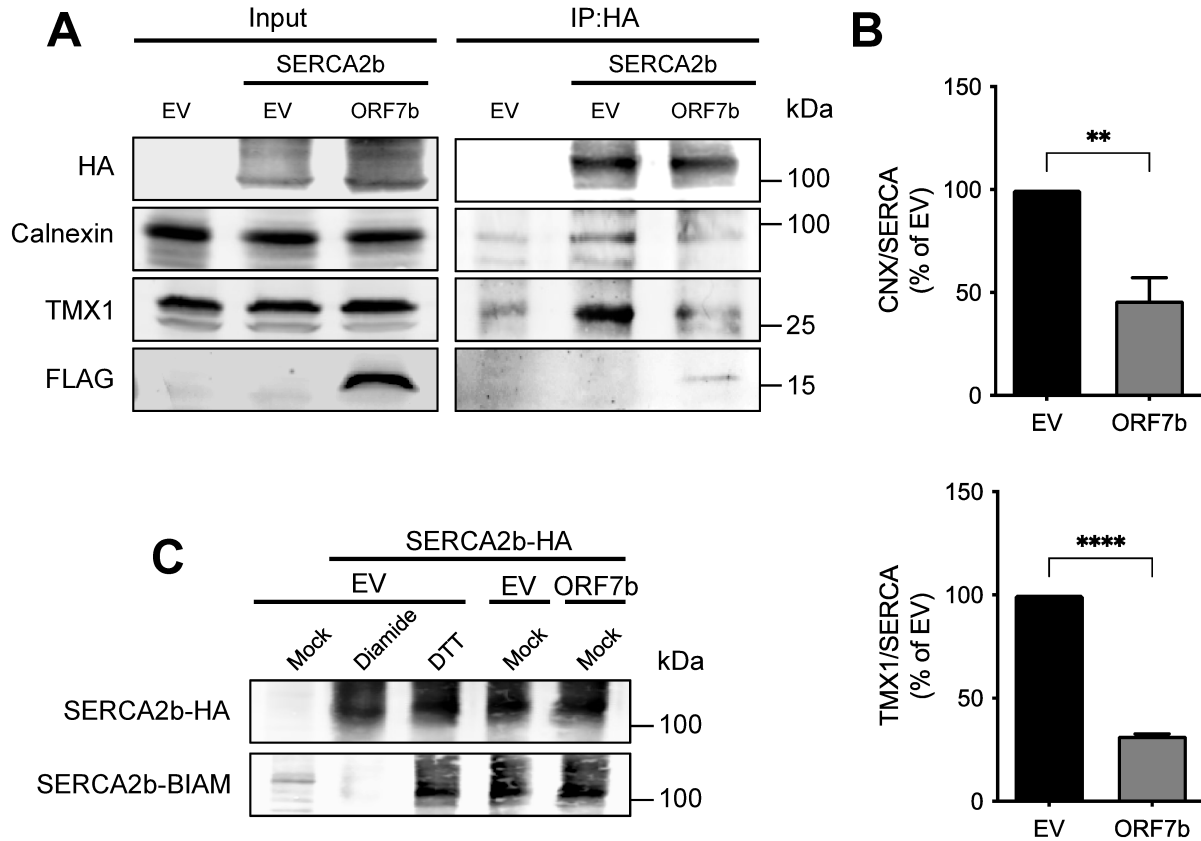
Figure 7. ORF7b disrupts MAM protein interactions. (A) HEK 293T cells were transfected with FLAG-tagged ORF7b and HA-tagged SERCA2b for 48 h prior to lysis. Lysates were subjected to immunoprecipitation by anti-HA antibodies. Proteins were resolved via SDS-PAGE and immunoblotted against HA, TMX1, calnexin, and FLAG. **(B)** Densitometric analysis of bands was performed using ImageJ. Data is presented as a mean of three replicates, with error bars indicating standard error of mean. ** $P < 0.01$, **** $P < 0.0001$. **(C)** Analysis of the oxidation state of SERCA2b was done using a biotinylated iodoacetamide (BIAM) switch assay. HEK 293T cells expressing FLAG-tagged ORF7b and HA-tagged SERCA2b were analyzed via Western blot for HA and BIAM signals. Diamide and DTT treatments constituted the fully oxidized and fully reduced control groups, respectively.

3.2.4. ORF7b alters Ca^{2+} levels

Our results thus far have indicated that ORF7b interacts with MAM proteins and disrupts interactions between SERCA2b and its regulators. Given that SERCA2b serves as the main pump responsible for Ca^{2+} refilling of the ER, we sought to explore whether ORF7b affected Ca^{2+} availability within the ER. We used the ER-targeted red fluorescent genetically encoded Ca^{2+} indicator for optical imaging (ER-RGECO) (Gutiérrez et al., 2020; J. Wu et al., 2014) to measure the total amount of Ca^{2+} in the ER within control and ORF7b-expressing Vero E6 cells, which were treated with the SERCA2b inhibitor TBHQ to prevent Ca^{2+} refilling of the ER, thereby depleting ER Ca^{2+} stores (Figure 8A). Our results show that the ER-RGECO signal in the ORF7b group was reduced by around 20% compared to the control group, indicating that ORF7b-expressing cells have less ER Ca^{2+} content (Figure 8A).

As mentioned earlier, MAMs provide the ER and mitochondria with a spatial relationship which permits Ca^{2+} transfer between the two organelles. Thus, levels of Ca^{2+} within these two organelles are highly related and can influence each other. To determine the relevance of our ER Ca^{2+} findings to mitochondrial Ca^{2+}, we used the mitochondria-targeted Ca^{2+} probe mito-RGECO (Gutiérrez et al., 2020; J. Wu et al., 2014) to measure the amount of Ca^{2+} in the mitochondria in control and ORF7b-expressing Vero E6 cells. Treatment with FCCP, which inhibits Ca^{2+} uptake to the mitochondria by depolarizing the mitochondrial membrane, did not show any significant differences in mitochondrial Ca^{2+} content between the control and ORF7b group (Figure 8B). However, IP$_3$R-mediated Ca^{2+} release from the ER and subsequent uptake into mitochondria upon treatment with histamine resulted in a 25% increase in Ca^{2+} transfer within ORF7b-expressing cells (Figure 8C). Altogether, our Ca^{2+} data suggests that ORF7b promotes mitochondrial Ca^{2+} uptake, concurrent with the finding that ORF7b-expressing cells have a reduced capacity to refill their ER Ca^{2+} stores via SERCA2b.
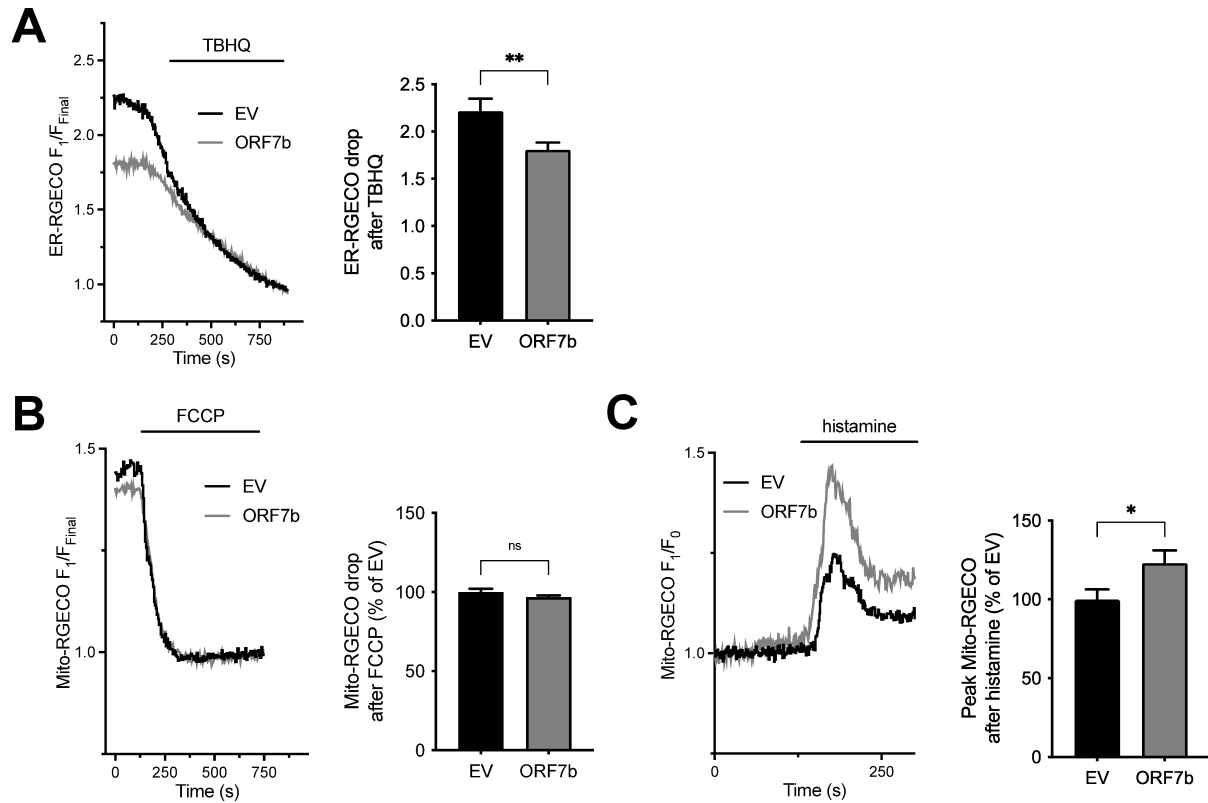
Figure 8. ORF7b alters Ca²⁺ levels. (A) Control and ORF7b-expressing Vero E6 cells were transfected with ER-RGECO and imaged by fluorescence microscopy to measure ER Ca^{2+}. 60 μM TBHQ was added to induce Ca^{2+} release from the ER. The drop in ER-RGECO fluorescent signal was recorded and quantified. **(B)** Control and ORF7b-expressing Vero E6 cells were transfected with Mito-RGECO and imaged by fluorescence microscopy to measure mitochondrial Ca^{2+}. 10 μM FCCP was added to induce Ca^{2+} release from the mitochondria. The drop in Mito-RGECO fluorescent signal was recorded and quantified. **(C)** Control and ORF7b-expressing Vero E6 cells were transfected with Mito-RGECO and imaged by fluorescence microscopy to measure mitochondrial Ca^{2+}. 50 μM histamine was added to induce Ca^{2+} release from the ER and subsequent uptake into the mitochondria. The peak in Mito-RGECO fluorescent signal was recorded and quantified. Data is presented as a mean of at least three replicates, with error bars indicating standard error of mean. * $P < 0.05$; ** $P < 0.01$.

3.2.5. ORF7b promotes mitochondrial activity

The finding that ORF7b promotes mitochondrial Ca^{2+} uptake would suggest that ORF7b could promote mitochondrial activity, since Ca^{2+} activates the enzymes of the TCA cycle, which generates the substrates needed for oxidative phosphorylation. Thus, we measured mitochondrial oxygen consumption within HEK 293T cells using high-resolution respirometry (Djafarzadeh & Jakob, 2017), given that oxygen is consumed via Complex IV of the ETC during oxidative phosphorylation. We found no difference in basal respiration and leak respiration between control and ORF7b-expressing cells. However, we found that ORF7b-expressing cells showed a significant increase in maximal oxygen consumption capacity compared to control cells (Figure 9A), which is often associated with increased substrate availability (Hill et al., 2012).

Given that both ATP and ROS production are tied to the activity of the ETC, we decided to measure mitochondrial ATP and ROS levels within ORF7b cells. We employed a luminescence-based assay to measure total cellular ATP levels, but did not detect a difference between control and ORF7b-expressing cells (Figure 9B). On the other hand, our experiments using fluorescent ROS-detecting reagents that target the mitochondria or the cytosol revealed that ORF7b-expressing cells had a two-fold increase in mitochondrial ROS, but similar amounts of cytosolic ROS compared to control cells (Figure 9C, D), which suggest that effects of ORF7b are directed to the mitochondria. Altogether, our results indicate that ORF7b promotes activity of the ETC within mitochondria.

Interestingly, we also observed an increase in the active form of AMPK, phosphorylated AMPK (p-AMPK) in ORF7b-expressing cells (Figure 9E). Given that AMPK is known to promote mitochondrial activity by inducing Ca^{2+} flux into the mitochondria through the activation of MCU (H. Zhao et al., 2019), our observation that levels of p-AMPK are increased within ORF7b-expressing cells is consistent with increased mitochondrial Ca^{2+} uptake and mitochondrial activity.
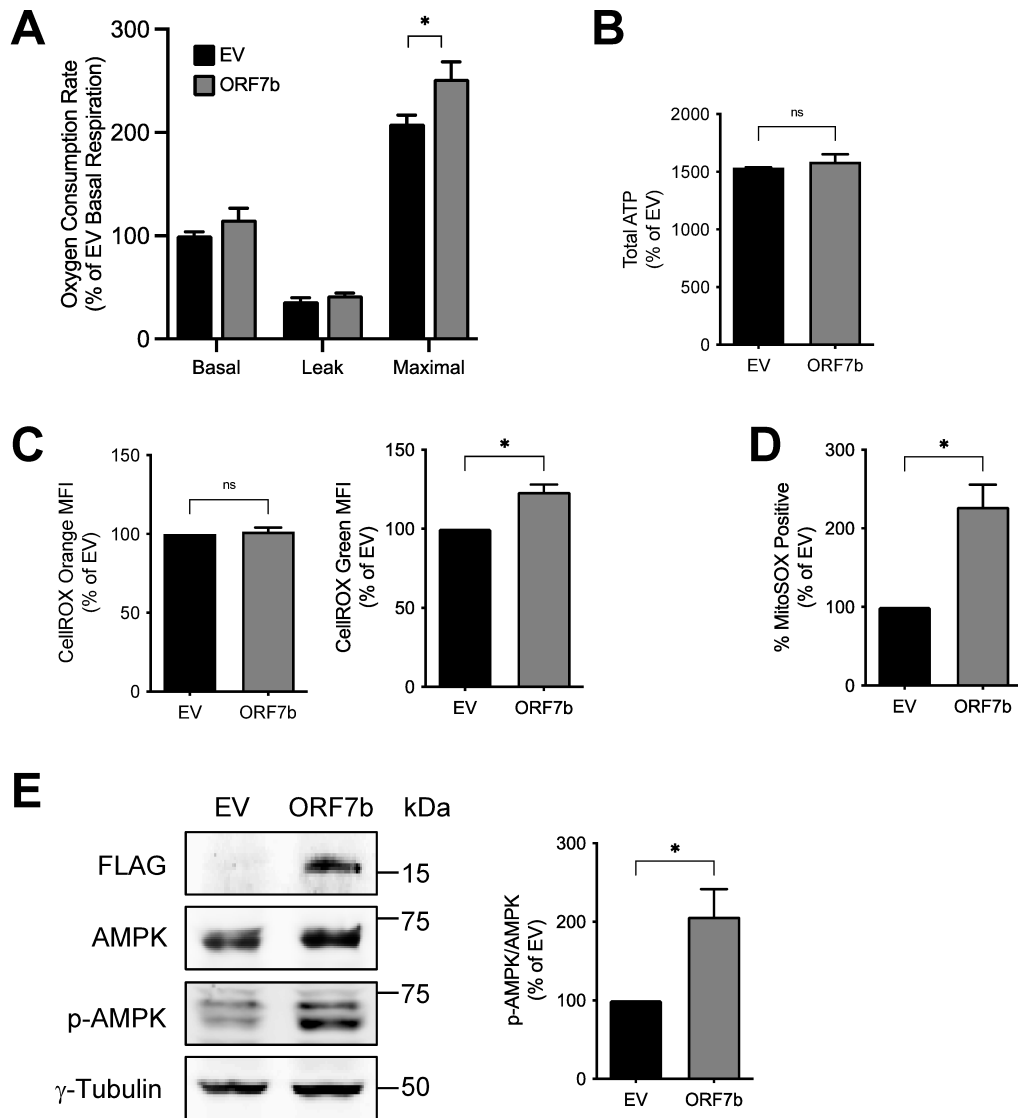
Figure 9. ORF7b promotes mitochondrial activity. (A) HEK 293T cells were transfected with ORF7b for 48 h prior to high-resolution respirometry analysis. Oxygen consumption rates were measured for basal, leak, and maximal respirations. **(B)** HEK 293T cells were transfected with ORF7b for 48 h prior to luminometry analysis. Total cellular ATP was measured as luminescence. **(C)** HEK 293T cells were transfected with ORF7b for 48 h prior to flow cytometry analysis. Cells were stained with the fluorescent ROS dye CellROX Green (mitochondrial ROS) or Orange (cytosolic ROS). ROS was measured as mean fluorescence intensity (MFI). **(D)** Vero E6 cells stably expressing ORF7b were plated in normal growth conditions 24 h prior to flow cytometry analysis. Cells were stained with the mitochondria-specific fluorescent ROS dye MitoSOX. Mitochondrial ROS was measured as % positive cells. **(E)** HEK 293T cells were transfected with ORF7b for 48 h prior to lysis. Lysates were analyzed via Western blot for FLAG, AMPK, p-AMPK, and γ-tubulin (as a loading control). Densitometric analysis of bands was performed using ImageJ. Data is presented as a mean of at least three replicates, with error bars indicating standard error of mean. * $P < 0.05$.

3.2.6. ORF7b alters mitochondrial morphology

The structural integrity of the mitochondria is greatly influenced by levels of Ca^{2+} and oxidative stress. For example, elevated levels of ROS resulting from excessive mitochondrial Ca^{2+} are recognized by redox sensors that activate downstream signaling pathways that stimulate proteins involved in mitochondrial fission, which often represents a step during apoptosis (Ježek et al. 2018). In addition, various studies have found that treatment of cells with the SERCA2b inhibitor thapsigargin led to an increase in intracellular Ca^{2+} levels, concomitant with an uptake of Ca^{2+} into mitochondria, which is associated with the increase in ROS formation and activation of the mitochondria fission machinery (Breckenridge et al., 2003; Hom et al., 2010; Hom et al., 2007). We were therefore interested in seeing whether changes to mitochondrial morphology occur within ORF7b-expressing cells, wherein we observed changes in levels of mitochondrial Ca^{2+} and ROS (Figure 10A). To do this, we analyzed mitochondrial network for two parameters, form factor and aspect ratio, which are related to mitochondrial branching and elongation, respectively (Harmuth et al. 2018). We found that, compared to the control, mitochondria within ORF7b-expressing cells had a reduced degree of both form factor and aspect ratio, which points towards a fragmented phenotype (Figure 10B). These results suggest that expression of ORF7b promotes mitochondrial fission, and is consisted with our finding that ORF7b promotes mitochondrial ROS production.
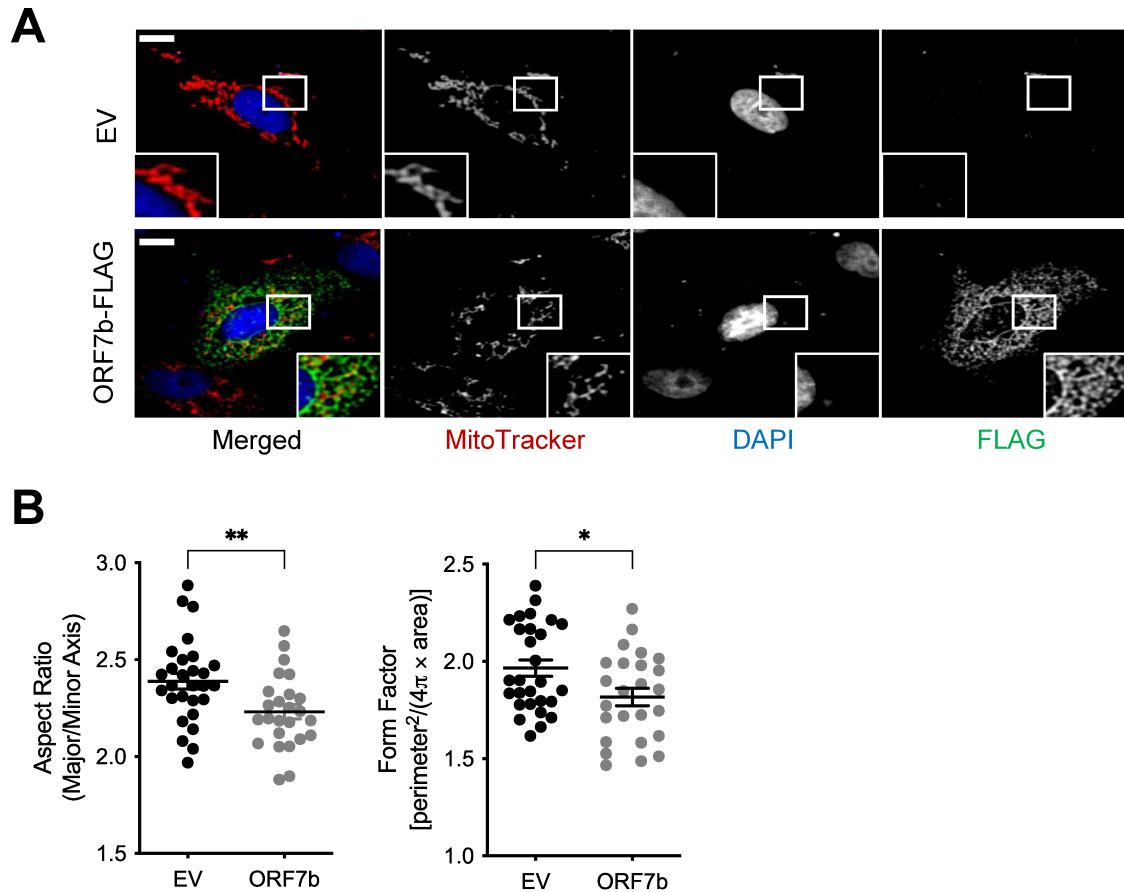
Figure 10. ORF7b promotes mitochondrial fragmentation. (A) Transfected Vero E6 cells were grown on 12-mm glass coverslips and processed for immunofluorescence microscopy. Cells were incubated with MitoTracker (mitochondria marker), DAPI (nuclear marker), and antibodies against FLAG (ORF7b marker). Scale bar = 10 μm. **(B)** MitoTracker staining was analyzed using Fiji for mean area, perimeter, and major and minor radii. Mitochondria branching and roundness were evaluated using the parameters form factor (FF = 4π x area/perimeter^2) and aspect ratio (AR = major radius/minor radius), respectively. * P < 0.05; ** P < 0.01.

CHAPTER 4: Discussion and Future Perspectives

4. DISCUSSION AND FUTURE PERSPECTIVES

4.1. Discussion and future work

4.1.1. ORF7b is an ER-targeted integral membrane protein

In this thesis, we analyzed the topology of the SARS-CoV-2 accessory protein ORF7b. Through biochemical assays, we were able to demonstrate that ORF7b is an integral membrane protein and that a potential N-glycosylation site on the C-terminus domain is not glycosylated (Figure 3B, C). Altogether, these findings could point towards a protein topology comprised of a transmembrane domain with cytosolic C-terminus and a luminal N-terminus, consistent with bioinformatic predictions that ORF7b assumes a Type III transmembrane protein topology. However, more sophisticated assays must be conducted to confirm the topology of ORF7b. Furthermore, we were able to assess the intracellular localization of ORF7b through immunofluorescence microscopy imaging and subcellular fractionation (Figure 4). Our results show that ORF7b localizes to the ER, consistent with previously reported observations that ORF7b targets the ER.

As mentioned earlier, various proteins encoded by the SARS-CoV-2 genome, including ORF7b, are found in the ER. Targeting of viral proteins to the endomembrane system (i.e., the ER and the Golgi complex) is not an uncommon event among enveloped RNA viruses, including SARS-CoV-2. Such viruses are known to hijack certain aspects of ER replication machinery to benefit their own replication and pathogenesis by ensuring the production of viral proteins (Ravindran et al., 2016; Sureda et al., 2020). First, viral replication proteins localize to the ER to mediate the severe restructuring of the ER membrane for the formation of membrane vesicles which serve as sites for the replication of viral RNA (Roingeard et al., 2022). Next, translated viral structural proteins, such as S, M, and E, in the case of SARS-CoV-2, translocate to the ER membrane and move through the ER-to-Golgi intermediate compartment (ERGIC), where they assemble with N-encapsulated, newly replicated viral genomic RNA to form new virions, which subsequently bud into the lumen of ERGIC. Finally, the virions and are released from the infected cell via exocytosis (Ravindran et al., 2016; V'kovski et al., 2021). Although viral accessory proteins are not required for viral replication, some viral accessory proteins that localize to the endomembrane system have been identified to impart a benefit for the formation and subsequent release of virions during infection. For instance, the viral protein U (Vpu), which is an ER

membrane-associated accessory protein encoded by HIV-1, promotes the release of newly synthesized HIV-1 virions from infected host cells. Vpu achieves this by binding and antagonizing Tetherin, which is a host restriction factor that inhibits the release of virions from host cells (Dubé et al., 2010). Whether ORF7b, which we have found to localize to the ER membrane, plays a role in the replication and budding of SARS-CoV-2 virions, remains to be investigated.

4.1.2. ORF7b disrupts interactions between SERCA2b and its regulators

Various protein screens have reported that ORF7b interacts with MAM-localized proteins, including calnexin and TMX1. Through our co-immunoprecipitation experiments, we were able to reproduce these findings (Figure 6). However, whether ORF7b targets the MAMs had not been previously investigated. In this thesis, we were able to demonstrate, through subcellular fractionation experiments, that ORF7b is indeed found in the MAMs (Figure 5).

Through subsequent co-immunoprecipitation experiments, we determined that ORF7b disrupted interactions between SERCA2b and its regulators, calnexin and TMX1 (Figure 7A, B). In line with this observation, we found that ORF7b-expressing cells had decreased ER Ca^{2+} stores (Figure 8A). Given that SERCA2b is responsible for the refilling of Ca^{2+} in the ER, decreased ER Ca^{2+} levels point toward a reduction in SERCA2b activity, as previously demonstrated by various studies (Gutiérrez et al., 2020; Raturi et al., 2016). In the hopes of shedding insight into the mechanisms tied to the regulation of SERCA2b activity by ORF7b, we conducted a BIAM labelling assay to investigate the oxidation state of SERCA2b in the presence of ORF7b. Despite observing reduced interaction between SERCA2b and its redox regulators upon ORF7b expression, we did not observe a change in the redox state of SERCA2b (Figure 7C). This result suggests that the oxidation of SERCA2b might not be the primary basis for altered SERCA2b activity. However, this experiment was performed only once, so statistical significance cannot yet be determined for these results.

What are other ways in which ORF7b could influence SERCA2b activity? One possibility is that ORF7b alters SERCA2b activity independent of its redox state or interactions with calnexin and TMX1. Given that we have found that ORF7b interacts directly with SERCA2b, we hypothesize that ORF7b could inhibit SERCA2b activity in a similar manner to PLN. As mentioned earlier, PLN binds SERCA via its inhibitory transmembrane domain. Since the putative transmembrane domain of ORF7b resembles that of PLN, we propose that the interaction between

ORF7b and SERCA2b could be enough to disrupt SERCA2b activity, thereby triggering the changes in ER Ca^{2+} that we have observed. One approach to investigate this is to directly measure the pump activity of SERCA2b within a proteoliposome system, in which SERCA2b and/or another protein of interest, such as ORF7b, is inserted into lipid membrane vesicles (Smeazzetto et al., 2017). In this setup, no other proteins are present, and would eliminate the influence of other proteins, such as calnexin and TMX1, on SERCA2b activity, which would otherwise be present in a cell model.

Another possible explanation for the changes in ER Ca^{2+} levels that we observed is that ORF7b could act independently of SERCA2b. As previously mentioned, ORF7b has been identified as a viroporin, which has been implicated in the regulation of intracellular Ca^{2+} levels through its ion channel function. Notably, Ca^{2+} leakage from the ER has been observed upon expression of viroporins, including the rotavirus NSP4 (Hyser et al., 2010; Hyser & Estes, 2015) and picornavirus 2B viroporins (Ito et al., 2012; Triantafilou et al., 2013). Whether ORF7b could potentially alter ER Ca^{2+} levels by way of its ion channel function remains to be investigated.

4.1.3. ORF7b promotes mitochondrial activity

An important function of MAMs is to control the flux of Ca^{2+} between the ER and mitochondria, which ultimately dictates mitochondrial activity. In line with our observation that ORF7b-expressing cells have a decreased ability to refill ER Ca^{2+} stores via SERCA2b, our data suggests that ORF7b could promote mitochondrial Ca^{2+} uptake (Figure 8C). Concordant with this finding, we observed increased oxygen consumption within ORF7b-expressing cells (Figure 9A). How does this role of ORF7b fit in our understanding of mitochondrial metabolism in the context of viral infections? Generally, viruses are known to alter mitochondrial metabolism in order to maintain an energy-sufficient environment for viral replication. The way by which viruses can induce changes in host cell metabolism depends on the type of virus. For instance, HCMV enhances mitochondrial metabolism by increasing mitochondrial biogenesis and respiration (Kaarbø et al., 2011). A related virus, the herpes simplex virus type 1, is known to increase mitochondrial metabolism via the induction of the TCA cycle (Vastag et al., 2011). Similarly, HCV upregulates TCA cycle enzymes to promote a regular supply of TCA cycle products (Diamond et al., 2010), which are needed to maintain ATP levels during infection. Infection with HCV is also known to promote mitochondrial fatty acid oxidation, which contributes to ATP

production (Diamond et al., 2010; Rasmussen et al., 2011). Thus, viruses target different aspects of mitochondrial metabolism in order to facilitate an optimal condition for viral infections; SARS-CoV-2 is no exception. For instance, a recent study found that the SARS-CoV-2 accessory protein ORF3c induces a shift from glucose to fatty acid oxidation and enhances oxidative phosphorylation (Mozzi et al., 2022). In this thesis, we provide evidence that suggests that the SARS-CoV-2 accessory protein ORF7b promotes mitochondrial metabolism by promoting mitochondrial Ca^{2+} uptake.

4.1.4. ORF7b induces a condition of oxidative stress

Our observation that ORF7b-expressing cells have increased levels of mitochondrial ROS compared to control cells (Figure 9C, D), point towards a condition of oxidative stress upon ORF7b expression. As previously mentioned, aberrant mitochondrial ROS production can directly impact cell fate and lead to apoptosis. When it comes to viral infections, the physiological roles of apoptosis are complex. On one hand, apoptosis can be an efficient antiviral defense mechanism since it eliminates infected cells. In contrast, viral-induced apoptosis in host cells would contribute to the pathogenicity of the virus (Benedict et al., 2002). In view of this, viruses are known to hijack intracellular signaling pathways to benefit their own survival by either suppressing host cell death to enable their replication inside infected cells, or promoting host cell death to obtain nutrients and disseminate further (Tiku et al., 2020).

In many cases, viruses have developed ways to inhibit or delay apoptosis in order to foster an environment suitable viral replication, especially during the early stages of infection. For example, the HCV NS5A protein is known to activate signal transducer and activator of transcription 3 (STAT-3) and nuclear factor κ B (NF-κB) survival pathways (Gong et al., 2001). However, apoptosis can still be activated during infection at a later point via immune activation, cellular damage caused by the virus, or specific viral proteins (Gatti et al., 2020). For example, the influenza A PB1-F2 protein targets the mitochondrial intermembrane space, where it disrupts mitochondrial dynamics and membrane potential, thereby inducing cell death (Zamarin et al., 2005). Within SARS-CoV-2, the accessory protein ORF3a was found to induce apoptosis by activating caspase-8, which cleaves Bid to tBid and induces the release of cytochrome c (Ren et al., 2020). In addition, a recent study found that SARS-CoV-2 ORF7b promoted apoptosis by inducing the expression of TNF-α (R. Yang et al., 2021).

Although we did not directly test for cell death induction in this study, we did, however, observe various hallmarks of apoptosis. For example, we found that ORF7b-expressing cells exhibited highly fragmented mitochondria (Figure 10), which, as mentioned earlier, often represents a step during apoptosis (Ježek et al., 2018). In addition, despite measuring increased oxygen consumption, which drives ATP production, we did not observe an increase in cellular ATP levels within ORF7b-expressing cells (Figure 9B). Given that apoptosis is an energy-consuming process, owing to a number of ATP-dependent steps, including caspase activation and chromatin condensation (Ferrari et al., 1998; Kass et al., 1996; Miyoshi et al., 2006), the lack of increased ATP levels within ORF7b-expressing cells wherein we observed increased oxygen consumption could indicate that ATP is being consumed at a higher rate within these cells in order to drive apoptosis.

In addition, we observed changes in protein distribution upon ORF7b expression that point towards a condition of apoptosis, namely the reduction of calnexin signal in MAM fractions (Figure 5). According to previous literature, under conditions of apoptosis or cell stress, calnexin dissociates from BAP31 and moves away from the MAMs (Delom et al., 2007). This allows BAP31 to increase its interaction with Fis1, which cleaves BAP31 to the pro-apoptotic p20-BAP31 (Iwasawa et al., 2011). Whether p20-BAP31 is present in ORF7b-expressing cells has yet to be investigated.

Further corroborating a condition of apoptosis upon ORF7b expression is the presence of a calnexin signal of lower molecular weight in the MAM fraction for the ORF7b group that is consistent with the partial cleavage of calnexin (Figure 5). Under apoptotic conditions, including infection with influenza virus, calnexin can be cleaved in its cytosolic domain tail by caspases, including caspase-3 and caspase-7, resulting in a cleaved product that is around 3 kDa smaller than the full-length calnexin (Takizawa, 2004). We hypothesize that the same thing happens upon ORF7b expression. Furthermore, caspase-3 is known to be activated by caspase-8, which is enriched at the OMM at ER-mitochondria contact sites (Chandra et al., 2004; Lakkaraju & van der Goot, 2013), which might explain why the cleaved calnexin signal is only observed in the MAM fraction. However, further experiments must be conducted to elucidate the mechanism behind calnexin cleavage upon ORF7b expression.

4.1.5. Could ORF7b trigger inflammation?

An important player in the innate immune response against pathogenic infections is the inflammasome (Zheng et al., 2020). Upon sensing viral infections, inflammasomes will trigger the innate immune response to eliminate the virus (Lupfer et al., 2015). However, dysregulation of inflammasome activity could lead to a state of severe inflammation, as the case if for acute inflammatory diseases. Increasing evidence shows that induction of inflammasome and dysregulation of the innate immune response can occur within SARS-CoV-2 infections, leading to augmented inflammatory responses that contribute to the clinical presentation of patients with COVID-19 (Rodrigues et al., 2020; Toldo et al., 2021; Vardhana & Wolchok, 2020).

Inflammasomes are named according to different sensing proteins: NLRP1, NLRP3, NLRC4, and AIM2 (Broz & Dixit, 2016). Among them, the NLRP3 (which stands for NOD-like receptor family pyrin domain containing 3) inflammasome is expressed in most cell types and serve important functions during RNA viral infections (X. Wang et al., 2014). In fact, it has been shown that NLRP3 inflammasomes are activated in blood cells during SARS-CoV-2 infections and are active in COVID-19 patients (Rodrigues et al., 2020; Toldo et al., 2021). The NLRP3 inflammasome is composed of NLRP3, the adaptor protein apoptosis-associated speck-like protein containing a caspase-recruitment domain (ASC), and pro-caspase-1 (Effendi & Nagano, 2021). In general, NLRP3 inflammasome activation upon viral infection requires a priming signal and an activation signal. The binding of viral membrane components to pattern recognition receptors on the host cell surface initiates the priming signal, leading to the activation of NF-κB. NF-κB then upregulates the expression of NLRP3, as well as proinflammatory cytokines pro-IL-1β and pro-IL-18, which remain inactive in the cytosol until stimulated by the second signal. The second signal, induced by a wide range of stimuli, including K^+ efflux, Ca^{2+} influx, and mitochondrial ROS, is required to promote NLRP3 inflammasome complex assembly and activation (He et al., 2016). Once the inflammasome complex is assembled, pro-caspase-1 is auto-processed to active caspase-1, which cleaves pro-IL-1β and pro-IL-18 to their active forms, IL-1β and IL-18. Eventually, these cytokines are released from the infected cell to trigger inflammation.

A link between inflammation and MAMs was first made upon the observation that ROS promoted the activation of NLRP3 inflammasomes. Upon elevated levels of ROS from damaged mitochondria, NLRP3 relocates to the MAMs and assembles into the inflammasome (R. Zhou et al., 2011). Thus, in light of the finding that ORF7b promotes mitochondrial ROS production

(Figure 9C, D), it would be interesting to investigate whether ORF7b could induce NLRP3 inflammasome activation, which has been reported in SARS-CoV-2 infections. Further endorsing ORF7b as a potential trigger for NLRP3 inflammasome formation is the fact that viroporins can induce NLRP3 inflammasome activity (Farag et al., 2020). Viroporin-induced NLRP3 inflammasome activation could be due to changes in Ca^{2+} homeostasis. For example, the HCV P7 and picornavirus 2B viroporins stimulate Ca^{2+} flux from the ER into the cytosol, providing the activation signal for NLRP3 inflammasome formation (Ito et al., 2012). Additionally, viroporins that are known to influence ROS production, such as the influenza A M2 viroporin, have also been implicated in NLRP3 inflammasome activation (Farag et al., 2020; R. Wang et al., 2019). On this basis, further investigation on the consequences of ORF7b on mitochondrial dysregulation and inflammatory responses must be conducted to further our understanding of the role of ORF7b for SARS-CoV-2 infections.

4.2. Conclusions

In this thesis, we gained a better understanding of the role of the SARS-CoV-2 accessory protein ORF7b (Figure 11). Herein, we were able to demonstrate that ORF7b is an integral membrane protein that targets the ER. More specifically, ORF7b localizes to the MAMs and interacts with various MAM-localized proteins, including SERCA2b and its regulators, namely calnexin and TMX1. We also show that upon ORF7b expression, interactions between SERCA2b and its regulators were diminished. Concordant with this, we observed a decrease in ER Ca^{2+} levels, which point towards an inhibition of SERCA2b activity upon ORF7b expression. However, given that there are many possibilities which would result in this phenotype, as outlined previously, further studies must be conducted to elucidate the mechanism by which ORF7b alters ER Ca^{2+} levels.

Furthermore, we were able to demonstrate the effects of ORF7b expression on mitochondrial metabolism. Our finding that ORF7b promotes mitochondrial metabolism and oxidative stress are consistent with the idea that SARS-CoV-2 can hijack mitochondrial function and manipulate the metabolic pathways of host cells. That being said, the consequences of these changes to mitochondrial metabolism triggered by ORF7b have yet to be investigated. Indeed, further studies must be conducted to fully understand the function of ORF7b as an important protein for SARS-CoV-2 infections.
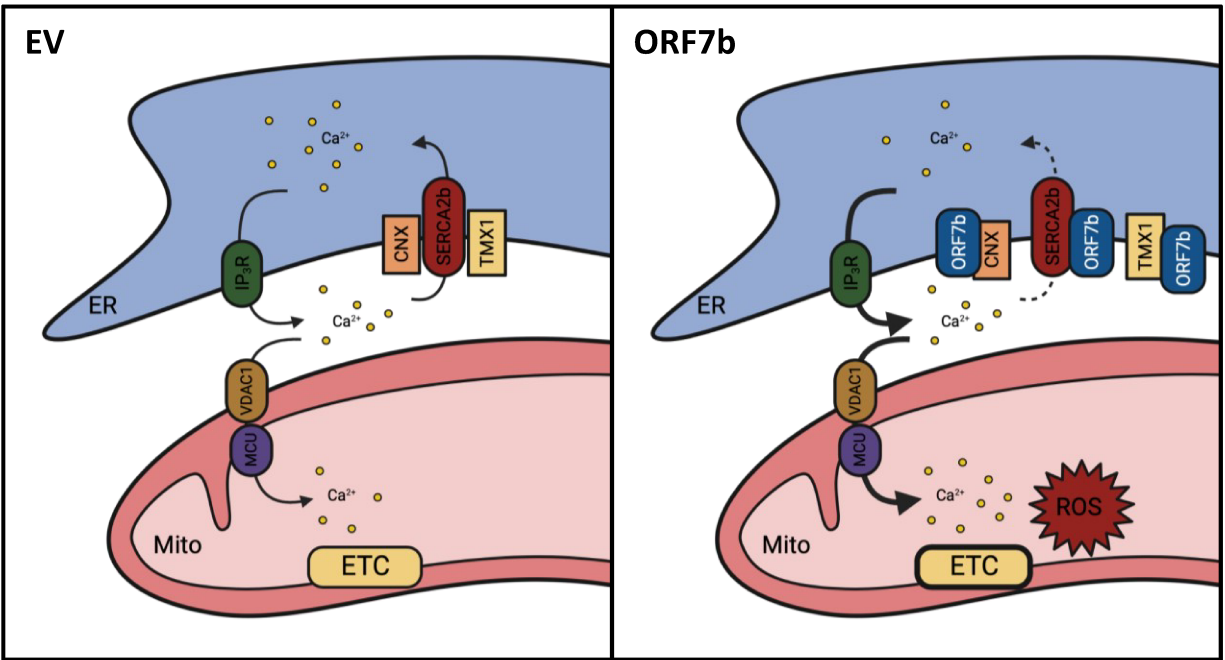
Figure 11. The role of ORF7b for ER-mitochondria Ca²⁺ homeostasis and mitochondrial metabolism. ORF7b targets the MAMs and reduces protein interactions between SERCA2b and its regulators, calnexin (CNX) and TMX1. Expression of ORF7b also promotes Ca²⁺ flux towards the mitochondria. Concordant with this, ORF7b-expressing cells exhibited higher mitochondrial metabolic activity, by way of increased oxygen consumption and ROS production. Created with BioRender.com

REFERENCES

REFERENCES

Ajaz, S., McPhail, M. J., Singh, K. K., Mujib, S., Trovato, F. M., Napoli, S., & Agarwal, K. (2021). Mitochondrial metabolic manipulation by SARS-CoV-2 in peripheral blood mononuclear cells of patients with COVID-19. *American Journal of Physiology-Cell Physiology*, *320*(1), C57–C65. https://doi.org/10.1152/ajpcell.00426.2020

Akin, B. L., Hurley, T. D., Chen, Z., & Jones, L. R. (2013). The Structural Basis for Phospholamban Inhibition of the Calcium Pump in Sarcoplasmic Reticulum. *Journal of Biological Chemistry*, *288*(42), 30181–30191. https://doi.org/10.1074/jbc.M113.501585

Akopian, D., Shen, K., Zhang, X., & Shan, S. (2013). Signal Recognition Particle: An Essential Protein-Targeting Machine. *Annual Review of Biochemistry*, *82*(1), 693–721. https://doi.org/10.1146/annurev-biochem-072711-164732

Anelli, T., Bergamelli, L., Margittai, E., Rimessi, A., Fagioli, C., Malgaroli, A., Pinton, P., Ripamonti, M., Rizzuto, R., & Sitia, R. (2012). Ero1α Regulates Ca $^{2+}$ Fluxes at the Endoplasmic Reticulum–Mitochondria Interface (MAM). *Antioxidants & Redox Signaling*, *16*(10), 1077–1087. https://doi.org/10.1089/ars.2011.4004

Arbel, N., & Shoshan-Barmatz, V. (2010). Voltage-dependent Anion Channel 1-based Peptides Interact with Bcl-2 to Prevent Antiapoptotic Activity. *Journal of Biological Chemistry*, *285*(9), 6053–6062. https://doi.org/10.1074/jbc.M109.082990

Archer, S. L. (2013). Mitochondrial Dynamics — Mitochondrial Fission and Fusion in Human Diseases. *New England Journal of Medicine*, *369*(23), 2236–2251. https://doi.org/10.1056/NEJMra1215233

Assaly, R., de Tassigny, A. d'Anglemont, Paradis, S., Jacquin, S., Berdeaux, A., & Morin, D. (2012). Oxidative stress, mitochondrial permeability transition pore opening and cell death during hypoxia–reoxygenation in adult cardiomyocytes. *European Journal of Pharmacology*, *675*(1–3), 6–14. https://doi.org/10.1016/j.ejphar.2011.11.036

Auclair, S. M., Bhanu, M. K., & Kendall, D. A. (2012). Signal peptidase I: Cleaving the way to mature proteins. *Protein Science*, *21*(1), 13–25. https://doi.org/10.1002/pro.757

Bender, S., Reuter, A., Eberle, F., Einhorn, E., Binder, M., & Bartenschlager, R. (2015). Activation of Type I and III Interferon Response by Mitochondrial and Peroxisomal MAVS and Inhibition by Hepatitis C Virus. *PLOS Pathogens*, *11*(11), e1005264. https://doi.org/10.1371/journal.ppat.1005264

Benedict, C. A., Norris, P. S., & Ware, C. F. (2002). To kill or be killed: viral evasion of apoptosis. *Nature Immunology*, *3*(11), 1013–1018. https://doi.org/10.1038/ni1102-1013

Beretta, M., Santos, C. X., Molenaar, C., Hafstad, A. D., Miller, C. C., Revazian, A., Betteridge, K., Schröder, K., Streckfuß-Bömeke, K., Doroshow, J. H., Fleck, R. A., Su, T., Belousov, V. v, Parsons, M., & Shah, A. M. (2020). Nox4 regulates InsP $_3$ receptor-dependent Ca $^{2+}$ release into mitochondria to promote cell survival. *The EMBO Journal*, *39*(19). https://doi.org/10.15252/embj.2019103530

Bergeron, J. J. M., Brenner, M. B., Thomas, D. Y., & Williams, D. B. (1994). Calnexin: a membrane-bound chaperone of the endoplasmic reticulum. *Trends in Biochemical Sciences*, *19*(3), 124–128. https://doi.org/10.1016/0968-0004(94)90205-4

Berndt, U., Oellerer, S., Zhang, Y., Johnson, A. E., & Rospert, S. (2009). A signal-anchor sequence stimulates signal recognition particle binding to ribosomes from inside the exit tunnel. *Proceedings of the National Academy of Sciences*, *106*(5), 1398–1403. https://doi.org/10.1073/pnas.0808584106

Berridge, M. J., Lipp, P., & Bootman, M. D. (2000). The versatility and universality of calcium signalling. *Nature Reviews Molecular Cell Biology*, *1*(1), 11–21. https://doi.org/10.1038/35036035

Bertram, R., Gram Pedersen, M., Luciani, D. S., & Sherman, A. (2006). A simplified model for mitochondrial ATP production. *Journal of Theoretical Biology*, *243*(4), 575–586. https://doi.org/10.1016/j.jtbi.2006.07.019

Betz, C., Stracka, D., Prescianotto-Baschong, C., Frieden, M., Demaurex, N., & Hall, M. N. (2013). mTOR complex 2-Akt signaling at mitochondria-associated endoplasmic reticulum membranes (MAM) regulates mitochondrial physiology. *Proceedings of the National Academy of Sciences*, *110*(31), 12526–12534. https://doi.org/10.1073/pnas.1302455110

Beutner, G., Alanzalon, R. E., & Porter, G. A. (2017). Cyclophilin D regulates the dynamic assembly of mitochondrial ATP synthase into synthasomes. *Scientific Reports*, *7*(1), 14488. https://doi.org/10.1038/s41598-017-14795-x

Bogdanov, M., Dowhan, W., & Vitrac, H. (2014). Lipids and topological rules governing membrane protein assembly. *Biochimica et Biophysica Acta (BBA) - Molecular Cell Research*, *1843*(8), 1475–1488. https://doi.org/10.1016/j.bbamcr.2013.12.007

Borkenhagen, L. F., Kennedy, E. P., & Fielding, L. (1961). Enzymatic Formation and Decarboxylation of Phosphatidylserine. *Journal of Biological Chemistry*, *236*(6), PC28–PC30. https://doi.org/10.1016/S0021-9258(19)63319-3

Bozidis, P., Williamson, C. D., Wong, D. S., & Colberg-Poley, A. M. (2010). Trafficking of UL37 Proteins into Mitochondrion-Associated Membranes during Permissive Human Cytomegalovirus Infection. *Journal of Virology*, *84*(15), 7898–7903. https://doi.org/10.1128/jvi.00885-10

Breckenridge, D. G., Stojanovic, M., Marcellus, R. C., & Shore, G. C. (2003). Caspase cleavage product of BAP31 induces mitochondrial fission through endoplasmic reticulum calcium signals, enhancing cytochrome c release to the cytosol. *Journal of Cell Biology*, *160*(7), 1115–1127. https://doi.org/10.1083/jcb.200212059

Breuer, W., Klein, R. A., Hardt, B., Bartoschek, A., & Bause, E. (2001). Oligosaccharyltransferase is highly specific for the hydroxy amino acid in Asn-Xaa-Thr/Ser. *FEBS Letters*, *501*(2–3), 106–110. https://doi.org/10.1016/S0014-5793(01)02641-2

Broz, P., & Dixit, V. M. (2016). Inflammasomes: mechanism of assembly, regulation and signalling. *Nature Reviews Immunology*, *16*(7), 407–420. https://doi.org/10.1038/nri.2016.58

Buicu, A.-L., Cernea, S., Benedek, I., Buicu, C.-F., & Benedek, T. (2021). Systemic Inflammation and COVID-19 Mortality in Patients with Major Noncommunicable Diseases: Chronic Coronary Syndromes, Diabetes and Obesity. *Journal of Clinical Medicine*, *10*(8), 1545. https://doi.org/10.3390/jcm10081545

Burdakov, D., Petersen, O. H., & Verkhratsky, A. (2005). Intraluminal calcium as a primary regulator of endoplasmic reticulum function. *Cell Calcium*, *38*(3–4), 303–310. https://doi.org/10.1016/j.ceca.2005.06.010

Busch, K. B. (2020). Inner mitochondrial membrane compartmentalization: Dynamics across scales. *The International Journal of Biochemistry & Cell Biology*, *120*, 105694. https://doi.org/10.1016/j.biocel.2020.105694

Camacho, P., & Lechleiter, J. D. (1995). Calreticulin inhibits repetitive intracellular Ca2+ waves. *Cell*, *82*(5), 765–771. https://doi.org/10.1016/0092-8674(95)90473-5

Cao, C., Cai, Z., Xiao, X., Rao, J., Chen, J., Hu, N., Yang, M., Xing, X., Wang, Y., Li, M., Zhou, B., Wang, X., Wang, J., & Xue, Y. (2021). The architecture of the SARS-CoV-2 RNA

genome inside virion. *Nature Communications*, *12*(1). https://doi.org/10.1038/s41467-021-22785-x

Carreras-Sureda, A., Pihán, P., & Hetz, C. (2018). Calcium signaling at the endoplasmic reticulum: fine-tuning stress responses. *Cell Calcium*, *70*, 24–31. https://doi.org/10.1016/j.ceca.2017.08.004

Chandra, D., Choy, G., Deng, X., Bhatia, B., Daniel, P., & Tang, D. G. (2004). Association of Active Caspase 8 with the Mitochondrial Membrane during Apoptosis: Potential Roles in Cleaving BAP31 and Caspase 3 and Mediating Mitochondrion-Endoplasmic Reticulum Cross Talk in Etoposide-Induced Cell Death. *Molecular and Cellular Biology*, *24*(15), 6592–6607. https://doi.org/10.1128/MCB.24.15.6592-6607.2004

Chen, H., Detmer, S. A., Ewald, A. J., Griffin, E. E., Fraser, S. E., & Chan, D. C. (2003). Mitofusins Mfn1 and Mfn2 coordinately regulate mitochondrial fusion and are essential for embryonic development. *Journal of Cell Biology*, *160*(2), 189–200. https://doi.org/10.1083/jcb.200211046

Chitwood, P. J., Juszkiewicz, S., Guna, A., Shao, S., & Hegde, R. S. (2018). EMC Is Required to Initiate Accurate Membrane Protein Topogenesis. *Cell*, *175*(6), 1507-1519.e16. https://doi.org/10.1016/j.cell.2018.10.009

Chu, G., Li, L., Sato, Y., Harrer, J. M., Kadambi, V. J., Hoit, B. D., Bers, D. M., & Kranias, E. G. (1998). Pentameric Assembly of Phospholamban Facilitates Inhibition of Cardiac Function in Vivo. *Journal of Biological Chemistry*, *273*(50), 33674–33680. https://doi.org/10.1074/jbc.273.50.33674

Cipolat, S., de Brito, O. M., Dal Zilio, B., & Scorrano, L. (2004). OPA1 requires mitofusin 1 to promote mitochondrial fusion. *Proceedings of the National Academy of Sciences*, *101*(45), 15927–15932. https://doi.org/10.1073/pnas.0407043101

Clapham, D. E. (2007). Calcium Signaling. *Cell*, *131*(6), 1047–1058. https://doi.org/10.1016/j.cell.2007.11.028

Corbett, E. F., Oikawa, K., Francois, P., Tessier, D. C., Kay, C., Bergeron, J. J. M., Thomas, D. Y., Krause, K.-H., & Michalak, M. (1999). Ca2+ Regulation of Interactions between Endoplasmic Reticulum Chaperones. *Journal of Biological Chemistry*, *274*(10), 6203–6211. https://doi.org/10.1074/jbc.274.10.6203

Cornea, R. L., Jones, L. R., Autry, J. M., & Thomas, D. D. (1997). Mutation and Phosphorylation Change the Oligomeric Structure of Phospholamban in Lipid Bilayers. *Biochemistry*, *36*(10), 2960–2967. https://doi.org/10.1021/bi961955q

Crabtree, G. R., & Olson, E. N. (2002). NFAT Signaling. *Cell*, *109*(2), S67–S79. https://doi.org/10.1016/S0092-8674(02)00699-2

Crompton, M. (1999). The mitochondrial permeability transition pore and its role in cell death. *The Biochemical Journal*, *341 (Pt 2)*, 233–249.

Csordás, G., Renken, C., Várnai, P., Walter, L., Weaver, D., Buttle, K. F., Balla, T., Mannella, C. A., & Hajnóczky, G. (2006). Structural and functional features and significance of the physical linkage between ER and mitochondria. *Journal of Cell Biology*, *174*(7), 915–921. https://doi.org/10.1083/jcb.200604016

de Brito, O. M., & Scorrano, L. (2008). Mitofusin 2 tethers endoplasmic reticulum to mitochondria. *Nature*, *456*(7222), 605–610. https://doi.org/10.1038/nature07534

de Giusti, V. C., Caldiz, C. I., Ennis, I. E., Pérez, N. G., Cingolani, H. E., & Aiello, E. A. (2013). Mitochondrial reactive oxygen species (ROS) as signaling molecules of intracellular

pathways triggered by the cardiac renin-angiotensin II-aldosterone system (RAAS). *Frontiers in Physiology*, *4*. https://doi.org/10.3389/fphys.2013.00126

de Vos, K. J., Mórotz, G. M., Stoica, R., Tudor, E. L., Lau, K.-F., Ackerley, S., Warley, A., Shaw, C. E., & Miller, C. C. J. (2012). VAPB interacts with the mitochondrial protein PTPIP51 to regulate calcium homeostasis. *Human Molecular Genetics*, *21*(6), 1299–1311. https://doi.org/10.1093/hmg/ddr559

Delom, F., Fessart, D., & Chevet, E. (2007). Regulation of calnexin sub-cellular localization modulates endoplasmic reticulum stress-induced apoptosis in MCF-7 cells. *Apoptosis*, *12*(2), 293–305. https://doi.org/10.1007/s10495-006-0625-4

Denton, R. M. (2009). Regulation of mitochondrial dehydrogenases by calcium ions. *Biochimica et Biophysica Acta (BBA) - Bioenergetics*, *1787*(11), 1309–1316. https://doi.org/10.1016/j.bbabio.2009.01.005

Denton, R. M., & McCormack, J. G. (1993). Calcium and the Regulation of Intramitochondrial Dehydrogenases. In *Mitochondrial Dysfunction* (pp. 390–403). Elsevier. https://doi.org/10.1016/B978-0-12-461205-1.50039-4

Diamond, D. L., Syder, A. J., Jacobs, J. M., Sorensen, C. M., Walters, K.-A., Proll, S. C., McDermott, J. E., Gritsenko, M. A., Zhang, Q., Zhao, R., Metz, T. O., Camp, D. G., Waters, K. M., Smith, R. D., Rice, C. M., & Katze, M. G. (2010). Temporal Proteome and Lipidome Profiles Reveal Hepatitis C Virus-Associated Reprogramming of Hepatocellular Metabolism and Bioenergetics. *PLoS Pathogens*, *6*(1), e1000719. https://doi.org/10.1371/journal.ppat.1000719

Djafarzadeh, S., & Jakob, S. M. (2017). High-resolution Respirometry to Assess Mitochondrial Function in Permeabilized and Intact Cells. *Journal of Visualized Experiments*, *120*. https://doi.org/10.3791/54985

Do, H., Falcone, D., Lin, J., Andrews, D. W., & Johnson, A. E. (1996). The Cotranslational Integration of Membrane Proteins into the Phospholipid Bilayer Is a Multistep Process. *Cell*, *85*(3), 369–378. https://doi.org/10.1016/S0092-8674(00)81115-0

Dorn, G. W. (2020). Mitofusins as mitochondrial anchors and tethers. *Journal of Molecular and Cellular Cardiology*, *142*, 146–153. https://doi.org/10.1016/j.yjmcc.2020.04.016

Dremina, E. S., Sharov, V. S., Kumar, K., Zaidi, A., Michaelis, E. K., & Schöneich, C. (2004). Anti-apoptotic protein Bcl-2 interacts with and destabilizes the sarcoplasmic/endoplasmic reticulum Ca2+-ATPase (SERCA). *The Biochemical Journal*, *383*(Pt 2), 361–370. https://doi.org/10.1042/BJ20040187

Dubé, M., Bego, M. G., Paquay, C., & Cohen, É. A. (2010). Modulation of HIV-1-host interaction: role of the Vpu accessory protein. *Retrovirology*, *7*(1), 114. https://doi.org/10.1186/1742-4690-7-114

DuBridge, R. B., Tang, P., Hsia, H. C., Leong, P. M., Miller, J. H., & Calos, M. P. (1987). Analysis of mutation in human cells by using an Epstein-Barr virus shuttle system. *Molecular and Cellular Biology*, *7*(1), 379–387. https://doi.org/10.1128/MCB.7.1.379

Edwards, R., Eaglesfield, R., & Tokatlidis, K. (2021). The mitochondrial intermembrane space: the most constricted mitochondrial sub-compartment with the largest variety of protein import pathways. *Open Biology*, *11*(3), rsob.210002. https://doi.org/10.1098/rsob.210002

Effendi, W. I., & Nagano, T. (2021). The Crucial Role of NLRP3 Inflammasome in Viral Infection-Associated Fibrosing Interstitial Lung Diseases. *International Journal of Molecular Sciences*, *22*(19), 10447. https://doi.org/10.3390/ijms221910447

Ellgaard, L., Sevier, C. S., & Bulleid, N. J. (2018). How Are Proteins Reduced in the Endoplasmic Reticulum? *Trends in Biochemical Sciences*, *43*(1), 32–43. https://doi.org/10.1016/j.tibs.2017.10.006

Ellis, R. J., & van der Vies, S. M. (1991). MOLECULAR CHAPERONES. *Annual Review of Biochemistry*, *60*(1), 321–347. https://doi.org/10.1146/annurev.bi.60.070191.001541

Emeny, J. M., & Morgan, M. J. (1979). Regulation of the Interferon System: Evidence that Vero Cells have a Genetic Defect in Interferon Production. *Journal of General Virology*, *43*(1), 247–252. https://doi.org/10.1099/0022-1317-43-1-247

Eura, Y. (2003). Two Mitofusin Proteins, Mammalian Homologues of FZO, with Distinct Functions Are Both Required for Mitochondrial Fusion. *Journal of Biochemistry*, *134*(3), 333–344. https://doi.org/10.1093/jb/mvg150

Evans, E. A., Gilmore, R., & Blobel, G. (1986). Purification of microsomal signal peptidase as a complex. *Proceedings of the National Academy of Sciences*, *83*(3), 581–585. https://doi.org/10.1073/pnas.83.3.581

Farag, N. S., Breitinger, U., Breitinger, H. G., & el Azizi, M. A. (2020). Viroporins and inflammasomes: A key to understand virus-induced inflammation. *The International Journal of Biochemistry & Cell Biology*, *122*, 105738. https://doi.org/10.1016/j.biocel.2020.105738

Farrow, M. A., Kim, E.-Y., Wolinsky, S. M., & Sheehy, A. M. (2011). NFAT and IRF Proteins Regulate Transcription of the Anti-HIV Gene, APOBEC3G. *Journal of Biological Chemistry*, *286*(4), 2567–2577. https://doi.org/10.1074/jbc.M110.154377

Ferrari, D., Stepczynska, A., Los, M., Wesselborg, S., & Schulze-Osthoff, K. (1998). Differential Regulation and ATP Requirement for Caspase-8 and Caspase-3 Activation during CD95- and Anticancer Drug–induced Apoptosis. *Journal of Experimental Medicine*, *188*(5), 979–984. https://doi.org/10.1084/jem.188.5.979

Feske, S., Gwack, Y., Prakriya, M., Srikanth, S., Puppel, S.-H., Tanasa, B., Hogan, P. G., Lewis, R. S., Daly, M., & Rao, A. (2006). A mutation in Orai1 causes immune deficiency by abrogating CRAC channel function. *Nature*, *441*(7090), 179–185. https://doi.org/10.1038/nature04702

Fogeron, M.-L., Montserret, R., Zehnder, J., Nguyen, M.-H., Dujardin, M., Brigandat, L., Cole, L., Ninot-Pedrosa, M., Lecoq, L., & Böckmann, A. (2021). SARS-CoV-2 ORF7b: is a bat virus protein homologue a major cause of COVID-19 symptoms? *BioRxiv*. https://doi.org/10.1101/2021.02.05.428650

Fujiki, Y., Fowler, S., Shio, H., Hubbard, A. L., & Lazarow, P. B. (1982). Polypeptide and phospholipid composition of the membrane of rat liver peroxisomes: comparison with endoplasmic reticulum and mitochondrial membranes. *Journal of Cell Biology*, *93*(1), 103–110. https://doi.org/10.1083/jcb.93.1.103

Galligan, J. J., & Petersen, D. R. (2012). The human protein disulfide isomerase gene family. *Human Genomics*, *6*(1), 6. https://doi.org/10.1186/1479-7364-6-6

Gatti, P., Ilamathi, H. S., Todkar, K., & Germain, M. (2020). Mitochondria Targeted Viral Replication and Survival Strategies—Prospective on SARS-CoV-2. *Frontiers in Pharmacology*, *11*. https://doi.org/10.3389/fphar.2020.578599

Gavel, Y., & Heijne, G. von. (1990). Sequence differences between glycosylated and non-glycosylated Asn-X-Thr/Ser acceptor sites: implications for protein engineering. *"Protein Engineering, Design and Selection,"* *3*(5), 433–442. https://doi.org/10.1093/protein/3.5.433

Giacomello, M., & Pellegrini, L. (2016). The coming of age of the mitochondria–ER contact: a matter of thickness. *Cell Death & Differentiation*, *23*(9), 1417–1427. https://doi.org/10.1038/cdd.2016.52

Gilady, S. Y., Bui, M., Lynes, E. M., Benson, M. D., Watts, R., Vance, J. E., & Simmen, T. (2010). Ero1α requires oxidizing and normoxic conditions to localize to the mitochondria-associated membrane (MAM). *Cell Stress and Chaperones*, *15*(5), 619–629. https://doi.org/10.1007/s12192-010-0174-1

Gilmore, R., Blobel, G., & Walter, P. (1982). Protein translocation across the endoplasmic reticulum. I. Detection in the microsomal membrane of a receptor for the signal recognition particle. *Journal of Cell Biology*, *95*(2), 463–469. https://doi.org/10.1083/jcb.95.2.463

Giorgi, C., Bonora, M., Sorrentino, G., Missiroli, S., Poletti, F., Suski, J. M., Galindo Ramirez, F., Rizzuto, R., di Virgilio, F., Zito, E., Pandolfi, P. P., Wieckowski, M. R., Mammano, F., del Sal, G., & Pinton, P. (2015). p53 at the endoplasmic reticulum regulates apoptosis in a Ca $^{2+}$ -dependent manner. *Proceedings of the National Academy of Sciences*, *112*(6), 1779–1784. https://doi.org/10.1073/pnas.1410723112

Giorgi, C., Ito, K., Lin, H.-K., Santangelo, C., Wieckowski, M. R., Lebiedzinska, M., Bononi, A., Bonora, M., Duszynski, J., Bernardi, R., Rizzuto, R., Tacchetti, C., Pinton, P., & Pandolfi, P. P. (2010). PML Regulates Apoptosis at Endoplasmic Reticulum by Modulating Calcium Release. *Science*, *330*(6008), 1247–1251. https://doi.org/10.1126/science.1189157

Giorgi, C., Missiroli, S., Patergnani, S., Duszynski, J., Wieckowski, M. R., & Pinton, P. (2015). Mitochondria-Associated Membranes: Composition, Molecular Mechanisms, and Physiopathological Implications. *Antioxidants & Redox Signaling*, *22*(12), 995–1019. https://doi.org/10.1089/ars.2014.6223

Goder, V., & Spiess, M. (2001). Topogenesis of membrane proteins: determinants and dynamics. *FEBS Letters*, *504*(3), 87–93. https://doi.org/10.1016/S0014-5793(01)02712-0

Goetz, J. G., & Nabi, I. R. (2006). Interaction of the smooth endoplasmic reticulum and mitochondria. *Biochemical Society Transactions*, *34*(3), 370–373. https://doi.org/10.1042/BST0340370

Gong, G., Waris, G., Tanveer, R., & Siddiqui, A. (2001). Human hepatitis C virus NS5A protein alters intracellular calcium levels, induces oxidative stress, and activates STAT-3 and NF-κB. *Proceedings of the National Academy of Sciences*, *98*(17), 9599–9604. https://doi.org/10.1073/pnas.171311298

Gonzalez, M. E., & Carrasco, L. (2003). Viroporins. *FEBS Letters*, *552*(1), 28–34. https://doi.org/10.1016/S0014-5793(03)00780-4

Gordon, D. E., Jang, G. M., Bouhaddou, M., Xu, J., Obernier, K., White, K. M., O'Meara, M. J., Rezelj, V. v., Guo, J. Z., Swaney, D. L., Tummino, T. A., Hüttenhain, R., Kaake, R. M., Richards, A. L., Tutuncuoglu, B., Foussard, H., Batra, J., Haas, K., Modak, M., … Krogan, N. J. (2020). A SARS-CoV-2 protein interaction map reveals targets for drug repurposing. *Nature*, *583*(7816), 459–468. https://doi.org/10.1038/s41586-020-2286-9

Görlich, D., Hartmann, E., Prehn, S., & Rapoport, T. A. (1992). A protein of the endoplasmic reticulum involved early in polypeptide translocation. *Nature*, *357*(6373), 47–52. https://doi.org/10.1038/357047a0

Gorski, P. A., Trieber, C. A., Larivière, E., Schuermans, M., Wuytack, F., Young, H. S., & Vangheluwe, P. (2012). Transmembrane Helix 11 Is a Genuine Regulator of the Endoplasmic Reticulum Ca2+ Pump and Acts as a Functional Parallel of β-Subunit on α-Na+,K+-ATPase.

Journal of Biological Chemistry, *287*(24), 19876–19885. https://doi.org/10.1074/jbc.M111.335620

Guerra, C., Brambilla Pisoni, G., Soldà, T., & Molinari, M. (2018). The reductase TMX1 contributes to ERAD by preferentially acting on membrane-associated folding-defective polypeptides. *Biochemical and Biophysical Research Communications*, *503*(2), 938–943. https://doi.org/10.1016/j.bbrc.2018.06.099

Gunteski-Hamblin, A. M., Greeb, J., & Shull, G. E. (1988). A novel Ca2+ pump expressed in brain, kidney, and stomach is encoded by an alternative transcript of the slow-twitch muscle sarcoplasmic reticulum Ca-ATPase gene. Identification of cDNAs encoding Ca2+ and other cation-transporting ATPases using an oligonucleotide probe derived from the ATP-binding site. *The Journal of Biological Chemistry*, *263*(29), 15032–15040.

Guo, R., Zong, S., Wu, M., Gu, J., & Yang, M. (2017). Architecture of Human Mitochondrial Respiratory Megacomplex I2III2IV2. *Cell*, *170*(6), 1247-1257.e12. https://doi.org/10.1016/j.cell.2017.07.050

Gutiérrez, T., Qi, H., Yap, M. C., Tahbaz, N., Milburn, L. A., Lucchinetti, E., Lou, P.-H., Zaugg, M., Lapointe, P. G., Mercier, P., Overduin, M., Bischof, H., Burgstaller, S., Malli, R., Ballanyi, K., Shuai, J., & Simmen, T. (2020). The ER chaperone calnexin controls mitochondrial positioning and respiration. In *Sci. Signal* (Vol. 13). http://stke.sciencemag.org/

Halestrap, A. (2004). Mitochondrial permeability transition pore opening during myocardial reperfusion—a target for cardioprotection. *Cardiovascular Research*, *61*(3), 372–385. https://doi.org/10.1016/S0008-6363(03)00533-9

Han, S., Nandy, P., Austria, Q., Siedlak, S. L., Torres, S., Fujioka, H., Wang, W., & Zhu, X. (2020). Mfn2 Ablation in the Adult Mouse Hippocampus and Cortex Causes Neuronal Death. *Cells*, *9*(1), 116. https://doi.org/10.3390/cells9010116

Haworth, R. A., & Hunter, D. R. (1979). The Ca2+-induced membrane transition in mitochondria. *Archives of Biochemistry and Biophysics*, *195*(2), 460–467. https://doi.org/10.1016/0003-9861(79)90372-2

Hayashi, T., & Fujimoto, M. (2010). Detergent-Resistant Microdomains Determine the Localization of σ-1 Receptors to the Endoplasmic Reticulum-Mitochondria Junction. *Molecular Pharmacology*, *77*(4), 517–528. https://doi.org/10.1124/mol.109.062539

Hayashi, T., & Su, T.-P. (2007). Sigma-1 Receptor Chaperones at the ER- Mitochondrion Interface Regulate Ca2+ Signaling and Cell Survival. *Cell*, *131*(3), 596–610. https://doi.org/10.1016/j.cell.2007.08.036

He, Y., Hara, H., & Núñez, G. (2016). Mechanism and Regulation of NLRP3 Inflammasome Activation. *Trends in Biochemical Sciences*, *41*(12), 1012–1021. https://doi.org/10.1016/j.tibs.2016.09.002

Hebert, D. N., Foellmer, B., & Helenius, A. (1996). Calnexin and calreticulin promote folding, delay oligomerization and suppress degradation of influenza hemagglutinin in microsomes. *The EMBO Journal*, *15*(12), 2961–2968.

Heinrich, S. U., Mothes, W., Brunner, J., & Rapoport, T. A. (2000). The Sec61p Complex Mediates the Integration of a Membrane Protein by Allowing Lipid Partitioning of the Transmembrane Domain. *Cell*, *102*(2), 233–244. https://doi.org/10.1016/S0092-8674(00)00028-3

Helenius, A., & Aebi, M. (2004). Roles of N-Linked Glycans in the Endoplasmic Reticulum. *Annual Review of Biochemistry*, *73*(1), 1019–1049. https://doi.org/10.1146/annurev.biochem.73.011303.073752

Hill, B. G., Benavides, G. A., Lancaster, J. R., Ballinger, S., Dell'Italia, L., Zhang, J., & Darley-Usmar, V. M. (2012). Integration of cellular bioenergetics with mitochondrial quality control and autophagy. *Bchm*, *393*(12), 1485–1512. https://doi.org/10.1515/hsz-2012-0198

Hom, J. R., Gewandter, J. S., Michael, L., Sheu, S.-S., & Yoon, Y. (2007). Thapsigargin induces biphasic fragmentation of mitochondria through calcium-mediated mitochondrial fission and apoptosis. *Journal of Cellular Physiology*, *212*(2), 498–508. https://doi.org/10.1002/jcp.21051

Hom, J., Yu, T., Yoon, Y., Porter, G., & Sheu, S.-S. (2010). Regulation of mitochondrial fission by intracellular Ca2+ in rat ventricular myocytes. *Biochimica et Biophysica Acta (BBA) - Bioenergetics*, *1797*(6–7), 913–921. https://doi.org/10.1016/j.bbabio.2010.03.018

Horbay, R., & Bilyy, R. (2016). Mitochondrial dynamics during cell cycling. *Apoptosis*, *21*(12), 1327–1335. https://doi.org/10.1007/s10495-016-1295-5

Horner, S. M., Liu, H. M., Park, H. S., Briley, J., & Gale, M. (2011). Mitochondrial-associated endoplasmic reticulum membranes (MAM) form innate immune synapses and are targeted by hepatitis C virus. *Proceedings of the National Academy of Sciences*, *108*(35), 14590–14595. https://doi.org/10.1073/pnas.1110133108

Horner, S. M., Park, H. S., & Gale, M. (2012). Control of Innate Immune Signaling and Membrane Targeting by the Hepatitis C Virus NS3/4A Protease Are Governed by the NS3 Helix α 0. *Journal of Virology*, *86*(6), 3112–3120. https://doi.org/10.1128/JVI.06727-11

Hortsch, M., & Meyer, D. I. (1985). Immunochemical analysis of rough and smooth microsomes from rat liver. Segregation of docking protein in rough membranes. *European Journal of Biochemistry*, *150*(3), 559–564. https://doi.org/10.1111/j.1432-1033.1985.tb09057.x

Huang, C.-Y., Chiang, S.-F., Lin, T.-Y., Chiou, S.-H., & Chow, K.-C. (2012). HIV-1 Vpr Triggers Mitochondrial Destruction by Impairing Mfn2-Mediated ER-Mitochondria Interaction. *PLoS ONE*, *7*(3), e33657. https://doi.org/10.1371/journal.pone.0033657

Hwang, M.-S., Schwall, C. T., Pazarentzos, E., Datler, C., Alder, N. N., & Grimm, S. (2014). Mitochondrial Ca2+ influx targets cardiolipin to disintegrate respiratory chain complex II for cell death induction. *Cell Death & Differentiation*, *21*(11), 1733–1745. https://doi.org/10.1038/cdd.2014.84

Hyser, J. M., Collinson-Pautz, M. R., Utama, B., & Estes, M. K. (2010). Rotavirus disrupts calcium homeostasis by NSP4 viroporin activity. *MBio*, *1*(5). https://doi.org/10.1128/mBio.00265-10

Hyser, J. M., & Estes, M. K. (2015). Pathophysiological Consequences of Calcium-Conducting Viroporins. In *Annual Review of Virology* (Vol. 2, pp. 473–496). Annual Reviews Inc. https://doi.org/10.1146/annurev-virology-100114-054846

Ishikawa, H., & Barber, G. N. (2008). STING is an endoplasmic reticulum adaptor that facilitates innate immune signalling. *Nature*, *455*(7213), 674–678. https://doi.org/10.1038/nature07317

Ito, M., Yanagi, Y., & Ichinohe, T. (2012). Encephalomyocarditis Virus Viroporin 2B Activates NLRP3 Inflammasome. *PLoS Pathogens*, *8*(8). https://doi.org/10.1371/journal.ppat.1002857

Iwasawa, R., Mahul-Mellier, A.-L., Datler, C., Pazarentzos, E., & Grimm, S. (2011). Fis1 and Bap31 bridge the mitochondria-ER interface to establish a platform for apoptosis induction. *The EMBO Journal*, *30*(3), 556–568. https://doi.org/10.1038/emboj.2010.346

Jan, C. H., Williams, C. C., & Weissman, J. S. (2014). Principles of ER cotranslational translocation revealed by proximity-specific ribosome profiling. *Science*, *346*(6210). https://doi.org/10.1126/science.1257521

Ježek, J., Cooper, K. F., & Strich, R. (2018). Reactive oxygen species and mitochondrial dynamics: The yin and yang of mitochondrial dysfunction and cancer progression. In *Antioxidants* (Vol. 7, Issue 1). MDPI. https://doi.org/10.3390/antiox7010013

John, L. M., Lechleiter, J. D., & Camacho, P. (1998). Differential Modulation of SERCA2 Isoforms by Calreticulin. *Journal of Cell Biology*, *142*(4), 963–973. https://doi.org/10.1083/jcb.142.4.963

Johnson, A. E., & van Waes, M. A. (1999). The Translocon: A Dynamic Gateway at the ER Membrane. *Annual Review of Cell and Developmental Biology*, *15*(1), 799–842. https://doi.org/10.1146/annurev.cellbio.15.1.799

Kaarbø, M., Ager-Wick, E., Osenbroch, P. Ø., Kilander, A., Skinnes, R., Müller, F., & Eide, L. (2011a). Human cytomegalovirus infection increases mitochondrial biogenesis. *Mitochondrion*, *11*(6), 935–945. https://doi.org/10.1016/j.mito.2011.08.008

Kaarbø, M., Ager-Wick, E., Osenbroch, P. Ø., Kilander, A., Skinnes, R., Müller, F., & Eide, L. (2011b). Human cytomegalovirus infection increases mitochondrial biogenesis. *Mitochondrion*, *11*(6), 935–945. https://doi.org/10.1016/j.mito.2011.08.008

Kass, G. E., Eriksson, J. E., Weis, M., Orrenius, S., & Chow, S. C. (1996). Chromatin condensation during apoptosis requires ATP. *The Biochemical Journal*, *318 (Pt 3)*, 749–752. https://doi.org/10.1042/bj3180749

Kiesslich, S., & Kamen, A. A. (2020). Vero cell upstream bioprocess development for the production of viral vectors and vaccines. *Biotechnology Advances*, *44*, 107608. https://doi.org/10.1016/j.biotechadv.2020.107608

Kim, H., Botelho, S. C., Park, K., & Kim, H. (2015). Use of carbonate extraction in analyzing moderately hydrophobic transmembrane proteins in the mitochondrial inner membrane. *Protein Science*, *24*(12), 2063–2069. https://doi.org/10.1002/pro.2817

Kinnally, K. W., Peixoto, P. M., Ryu, S.-Y., & Dejean, L. M. (2011). Is mPTP the gatekeeper for necrosis, apoptosis, or both? *Biochimica et Biophysica Acta (BBA) - Molecular Cell Research*, *1813*(4), 616–622. https://doi.org/10.1016/j.bbamcr.2010.09.013

Knyushko, T. v., Sharov, V. S., Williams, T. D., Schöneich, C., & Bigelow, D. J. (2005). 3-Nitrotyrosine Modification of SERCA2a in the Aging Heart: A Distinct Signature of the Cellular Redox Environment. *Biochemistry*, *44*(39), 13071–13081. https://doi.org/10.1021/bi051226n

Kranias, E. G., & Solaro, R. J. (1982). Phosphorylation of troponin I and phospholamban during catecholamine stimulation of rabbit heart. *Nature*, *298*(5870), 182–184. https://doi.org/10.1038/298182a0

Krieg, U. C., Johnson, A. E., & Walter, P. (1989). Protein translocation across the endoplasmic reticulum membrane: identification by photocross-linking of a 39-kD integral membrane glycoprotein as part of a putative translocation tunnel. *Journal of Cell Biology*, *109*(5), 2033–2043. https://doi.org/10.1083/jcb.109.5.2033

Kuschel, M., Karczewski, P., Hempel, P., Schlegel, W.-P., Krause, E.-G., & Bartel, S. (1999). Ser16 prevails over Thr17 phospholamban phosphorylation in the β-adrenergic regulation of cardiac relaxation. *American Journal of Physiology-Heart and Circulatory Physiology*, *276*(5), H1625–H1633. https://doi.org/10.1152/ajpheart.1999.276.5.H1625

Lagadinou, E. D., Sach, A., Callahan, K., Rossi, R. M., Neering, S. J., Minhajuddin, M., Ashton, J. M., Pei, S., Grose, V., O'Dwyer, K. M., Liesveld, J. L., Brookes, P. S., Becker, M. W., & Jordan, C. T. (2013). BCL-2 Inhibition Targets Oxidative Phosphorylation and Selectively Eradicates Quiescent Human Leukemia Stem Cells. *Cell Stem Cell*, *12*(3), 329–341. https://doi.org/10.1016/j.stem.2012.12.013

Lakkaraju, A. K., Abrami, L., Lemmin, T., Blaskovic, S., Kunz, B., Kihara, A., Dal Peraro, M., & van der Goot, F. G. (2012). Palmitoylated calnexin is a key component of the ribosome-translocon complex. *The EMBO Journal*, *31*(7), 1823–1835. https://doi.org/10.1038/emboj.2012.15

Lakkaraju, A. K. K., & van der Goot, F. G. (2013). Calnexin Controls the STAT3-Mediated Transcriptional Response to EGF. *Molecular Cell*, *51*(3), 386–396. https://doi.org/10.1016/j.molcel.2013.07.009

Lee, Y.-B., Jung, M., Kim, J., Kang, M.-G., Kwak, C., Mun, J.-Y., Kim, J.-S., & Rhee, H.-W. (2020). Endomembrane Systems are Reorganized by ORF3a and Membrane (M) of SARS-CoV-2. *SSRN Electronic Journal*. https://doi.org/10.2139/ssrn.3742314

Li, J., Guo, M., Tian, X., Wang, X., Yang, X., Wu, P., Liu, C., Xiao, Z., Qu, Y., Yin, Y., Wang, C., Zhang, Y., Zhu, Z., Liu, Z., Peng, C., Zhu, T., & Liang, Q. (2021). Virus-Host Interactome and Proteomic Survey Reveal Potential Virulence Factors Influencing SARS-CoV-2 Pathogenesis. *Med*, *2*(1), 99-112.e7. https://doi.org/10.1016/j.medj.2020.07.002

Li, Y., & Camacho, P. (2004a). Ca2+-dependent redox modulation of SERCA 2b by ERp57. *Journal of Cell Biology*, *164*(1), 35–46. https://doi.org/10.1083/jcb.200307010

Li, Y., & Camacho, P. (2004b). Ca2+-dependent redox modulation of SERCA 2b by ERp57. *Journal of Cell Biology*, *164*(1), 35–46. https://doi.org/10.1083/jcb.200307010

Liu, A. Y., Aguayo-Ortiz, R., Guerrero-Serna, G., Wang, N., Blin, M. G., Goldstein, D. R., & Michel Espinoza-Fonseca, L. (2022). Homologous cardiac calcium pump regulators phospholamban and sarcolipin adopt distinct oligomeric states in the membrane. *Computational and Structural Biotechnology Journal*, *20*, 380–384. https://doi.org/10.1016/j.csbj.2021.12.031

Liu, D. X., Fung, T. S., Chong, K. K. L., Shukla, A., & Hilgenfeld, R. (2014). Accessory proteins of SARS-CoV and other coronaviruses. In *Antiviral Research* (Vol. 109, Issue 1, pp. 97–109). Elsevier. https://doi.org/10.1016/j.antiviral.2014.06.013

Liu, R., & Chan, D. C. (2015). The mitochondrial fission receptor Mff selectively recruits oligomerized Drp1. *Molecular Biology of the Cell*, *26*(24), 4466–4477. https://doi.org/10.1091/mbc.E15-08-0591

Lodish, H. F., Kong, N., & Wikström, L. (1992). Calcium is required for folding of newly made subunits of the asialoglycoprotein receptor within the endoplasmic reticulum. *Journal of Biological Chemistry*, *267*(18), 12753–12760. https://doi.org/10.1016/S0021-9258(18)42340-X

Luo, W., Grupp, I. L., Harrer, J., Ponniah, S., Grupp, G., Duffy, J. J., Doetschman, T., & Kranias, E. G. (1994). Targeted ablation of the phospholamban gene is associated with markedly enhanced myocardial contractility and loss of beta-agonist stimulation. *Circulation Research*, *75*(3), 401–409. https://doi.org/10.1161/01.RES.75.3.401

Lupfer, C., Malik, A., & Kanneganti, T.-D. (2015). Inflammasome control of viral infection. *Current Opinion in Virology*, *12*, 38–46. https://doi.org/10.1016/j.coviro.2015.02.007

Lynes, E. M., Bui, M., Yap, M. C., Benson, M. D., Schneider, B., Ellgaard, L., Berthiaume, L. G., & Simmen, T. (2012). Palmitoylated TMX and calnexin target to the mitochondria-associated membrane. *The EMBO Journal*, *31*(2), 457–470. https://doi.org/10.1038/emboj.2011.384

Lynes, E. M., Raturi, A., Shenkman, M., Ortiz Sandoval, C., Yap, M. C., Wu, J., Janowicz, A., Myhill, N., Benson, M. D., Campbell, R. E., Berthiaume, L. G., Lederkremer, G. Z., & Simmen, T. (2013). Palmitoylation is the Switch that Assigns Calnexin to Quality Control or ER Calcium Signaling. *Journal of Cell Science*. https://doi.org/10.1242/jcs.125856

Lytton, J., Westlin, M., Burk, S. E., Shull, G. E., & MacLennan, D. H. (1992). Functional comparisons between isoforms of the sarcoplasmic or endoplasmic reticulum family of calcium pumps. *Journal of Biological Chemistry*, *267*(20), 14483–14489. https://doi.org/10.1016/S0021-9258(19)49738-X

Lytton, J., Zarain-Herzberg, A., Periasamy, M., & MacLennan, D. H. (1989). Molecular Cloning of the Mammalian Smooth Muscle Sarco(endo)plasmic Reticulum Ca2+-ATPase. *Journal of Biological Chemistry*, *264*(12), 7059–7065. https://doi.org/10.1016/S0021-9258(18)83540-2

MacLennan, D. H., & Kranias, E. G. (2003). Phospholamban: a crucial regulator of cardiac contractility. *Nature Reviews Molecular Cell Biology*, *4*(7), 566–577. https://doi.org/10.1038/nrm1151

Madan, V., Castelló, A., & Carrasco, L. (2008). Viroporins from RNA viruses induce caspase-dependent apoptosis. *Cellular Microbiology*, *10*(2), 437–451. https://doi.org/10.1111/j.1462-5822.2007.01057.x

Matsuo, Y., Akiyama, N., Nakamura, H., Yodoi, J., Noda, M., & Kizaka-Kondoh, S. (2001). Identification of a Novel Thioredoxin-related Transmembrane Protein. *Journal of Biological Chemistry*, *276*(13), 10032–10038. https://doi.org/10.1074/jbc.M011037200

Matsuo, Y., Masutani, H., Son, A., Kizaka-Kondoh, S., & Yodoi, J. (2009). Physical and Functional Interaction of Transmembrane Thioredoxin-related Protein with Major Histocompatibility Complex Class I Heavy Chain: Redox-based Protein Quality Control and Its Potential Relevance to Immune Responses. *Molecular Biology of the Cell*, *20*, 4552–4562. https://doi.org/10.1091/mbc.E09

Matsuo, Y., Nishinaka, Y., Suzuki, S., Kojima, M., Kizaka-Kondoh, S., Kondo, N., Son, A., Sakakura-Nishiyama, J., Yamaguchi, Y., Masutani, H., Ishii, Y., & Yodoi, J. (2004). TMX, a human transmembrane oxidoreductase of the thioredoxin family: the possible role in disulfide-linked protein folding in the endoplasmic reticulum. *Archives of Biochemistry and Biophysics*, *423*(1), 81–87. https://doi.org/10.1016/j.abb.2003.11.003

Mazur-Panasiuk, N., Rabalski, L., Gromowski, T., Nowicki, G., Kowalski, M., Wydmanski, W., Szulc, P., Kosinski, M., Gackowska, K., Drweska-Matelska, N., Grabowski, J., Piotrowska-Mietelska, A., Szewczyk, B., Bienkowska-Szewczyk, K., Swadzba, J., Labaj, P., Grzybek, M., & Pyrc, K. (2021). Expansion of a SARS-CoV-2 Delta variant with an 872 nt deletion encompassing ORF7a, ORF7b and ORF8, Poland, July to August 2021. *Eurosurveillance*, *26*(39). https://doi.org/10.2807/1560-7917.ES.2021.26.39.2100902

McCormick, A. L., Smith, V. L., Chow, D., & Mocarski, E. S. (2003). Disruption of Mitochondrial Networks by the Human Cytomegalovirus *UL37* Gene Product Viral Mitochondrion-Localized Inhibitor of Apoptosis. *Journal of Virology*, *77*(1), 631–641. https://doi.org/10.1128/JVI.77.1.631-641.2003

McNally, B. A., Somasundaram, A., Jairaman, A., Yamashita, M., & Prakriya, M. (2013). The C- and N-terminal STIM1 binding sites on Orai1 are required for both trapping and gating CRAC

channels. *The Journal of Physiology*, *591*(11), 2833–2850. https://doi.org/10.1113/jphysiol.2012.250456

Meis, L., & Vianna, A. L. (1979). Energy Interconversion by the Ca2+-Dependent ATPase of the Sarcoplasmic Reticulum. *Annual Review of Biochemistry*, *48*(1), 275–292. https://doi.org/10.1146/annurev.bi.48.070179.001423

Mekahli, D., Bultynck, G., Parys, J. B., de Smedt, H., & Missiaen, L. (2011). Endoplasmic-Reticulum Calcium Depletion and Disease. *Cold Spring Harbor Perspectives in Biology*, *3*(6), a004317–a004317. https://doi.org/10.1101/cshperspect.a004317

Mercier, E., Holtkamp, W., Rodnina, M. v., & Wintermeyer, W. (2017). Signal recognition particle binds to translating ribosomes before emergence of a signal anchor sequence. *Nucleic Acids Research*, *45*(20), 11858–11866. https://doi.org/10.1093/nar/gkx888

Meyer, D. I., Krause, E., & Dobberstein, B. (1982). Secretory protein translocation across membranes—the role of the 'docking protein.' *Nature*, *297*(5868), 647–650. https://doi.org/10.1038/297647a0

Michalak, M., Milner, R. E., Burns, K., & Opas, M. (1992). Calreticulin. *Biochemical Journal*, *285*(3), 681–692. https://doi.org/10.1042/bj2850681

Michalak, M., Robert Parker, J. M., & Opas, M. (2002). Ca2+ signaling and calcium binding chaperones of the endoplasmic reticulum. *Cell Calcium*, *32*(5–6), 269–278. https://doi.org/10.1016/S0143416002001884

Missiroli, S., Patergnani, S., Caroccia, N., Pedriali, G., Perrone, M., Previati, M., Wieckowski, M. R., & Giorgi, C. (2018). Mitochondria-associated membranes (MAMs) and inflammation. In *Cell Death and Disease* (Vol. 9, Issue 3). Nature Publishing Group. https://doi.org/10.1038/s41419-017-0027-2

Miyoshi, N., Oubrahim, H., Chock, P. B., & Stadtman, E. R. (2006). Age-dependent cell death and the role of ATP in hydrogen peroxide-induced apoptosis and necrosis. *Proceedings of the National Academy of Sciences*, *103*(6), 1727–1731. https://doi.org/10.1073/pnas.0510346103

Monaco, G., Decrock, E., Akl, H., Ponsaerts, R., Vervliet, T., Luyten, T., de Maeyer, M., Missiaen, L., Distelhorst, C. W., de Smedt, H., Parys, J. B., Leybaert, L., & Bultynck, G. (2012). Selective regulation of IP3-receptor-mediated Ca2+ signaling and apoptosis by the BH4 domain of Bcl-2 versus Bcl-Xl. *Cell Death & Differentiation*, *19*(2), 295–309. https://doi.org/10.1038/cdd.2011.97

Mothes, W., Prehn, S., & Rapoport, T. A. (1994). Systematic probing of the environment of a translocating secretory protein during translocation through the ER membrane. *The EMBO Journal*, *13*(17), 3973–3982. https://doi.org/10.1002/j.1460-2075.1994.tb06713.x

Mozzi, A., Oldani, M., Forcella, M. E., Vantaggiato, C., Cappelletti, G., Pontremoli, C., Valenti, F., Forni, D., Biasin, M., Sironi, M., Fusi, P., & Cagliani, R. (2022). SARS-CoV-2 ORF3c impairs mitochondrial respiratory metabolism, oxidative stress and autophagic flow. *BioRxiv*. https://doi.org/10.1101/2022.10.04.510754

Myhill, N., Lynes, E. M., Nanji, J. A., Blagoveshchenskaya, A. D., Fei, H., Carmine Simmen, K., Cooper, T. J., Thomas, G., & Simmen, T. (2008). The Subcellular Distribution of Calnexin Is Mediated by PACS-2. *Molecular Biology of the Cell*, *19*(7), 2777–2788. https://doi.org/10.1091/mbc.e07-10-0995

Namba, T. (2019). BAP31 regulates mitochondrial function via interaction with Tom40 within ER-mitochondria contact sites. *Science Advances*, *5*(6). https://doi.org/10.1126/sciadv.aaw1386

Naqvi, A. A. T., Fatima, K., Mohammad, T., Fatima, U., Singh, I. K., Singh, A., Atif, S. M., Hariprasad, G., Hasan, G. M., & Hassan, Md. I. (2020). Insights into SARS-CoV-2 genome, structure, evolution, pathogenesis and therapies: Structural genomics approach. *Biochimica et Biophysica Acta (BBA) - Molecular Basis of Disease*, *1866*(10), 165878. https://doi.org/10.1016/j.bbadis.2020.165878

Nieva, J. L., Madan, V., & Carrasco, L. (2012). Viroporins: Structure and biological functions. In *Nature Reviews Microbiology* (Vol. 10, Issue 8, pp. 563–574). https://doi.org/10.1038/nrmicro2820

Nikolaev, Y., & Pervushin, K. (2009). Rethinking Leucine Zipper – a ubiquitous signal transduction motif. *Nature Precedings*. https://doi.org/10.1038/npre.2009.3271.1

O'Keefe, S., Zong, G., Duah, K. B., Andrews, L. E., Shi, W. Q., & High, S. (2021). An alternative pathway for membrane protein biogenesis at the endoplasmic reticulum. *Communications Biology*, *4*(1), 828. https://doi.org/10.1038/s42003-021-02363-z

Olesen, C., Picard, M., Winther, A.-M. L., Gyrup, C., Morth, J. P., Oxvig, C., Møller, J. V., & Nissen, P. (2007). The structural basis of calcium transport by the calcium pump. *Nature*, *450*(7172), 1036–1042. https://doi.org/10.1038/nature06418

Olichon, A., Emorine, L. J., Descoins, E., Pelloquin, L., Brichese, L., Gas, N., Guillou, E., Delettre, C., Valette, A., Hamel, C. P., Ducommun, B., Lenaers, G., & Belenguer, P. (2002). The human dynamin-related protein OPA1 is anchored to the mitochondrial inner membrane facing the inter-membrane space. *FEBS Letters*, *523*(1–3), 171–176. https://doi.org/10.1016/S0014-5793(02)02985-X

Oliver, J. D., van der Wal, F. J., Bulleid, N. J., & High, S. (1997). Interaction of the Thiol-Dependent Reductase ERp57 with Nascent Glycoproteins. *Science*, *275*(5296), 86–88. https://doi.org/10.1126/science.275.5296.86

Orrenius, S., Gogvadze, V., & Zhivotovsky, B. (2007). Mitochondrial Oxidative Stress: Implications for Cell Death. *Annual Review of Pharmacology and Toxicology*, *47*(1), 143–183. https://doi.org/10.1146/annurev.pharmtox.47.120505.105122

Osellame, L. D., Singh, A. P., Stroud, D. A., Palmer, C. S., Stojanovski, D., Ramachandran, R., & Ryan, M. T. (2016). Cooperative and independent roles of Drp1 adaptors Mff and MiD49/51 in mitochondrial fission. *Journal of Cell Science*. https://doi.org/10.1242/jcs.185165

Paillusson, S., Gomez-Suaga, P., Stoica, R., Little, D., Gissen, P., Devine, M. J., Noble, W., Hanger, D. P., & Miller, C. C. J. (2017). α-Synuclein binds to the ER–mitochondria tethering protein VAPB to disrupt Ca2+ homeostasis and mitochondrial ATP production. *Acta Neuropathologica*, *134*(1), 129–149. https://doi.org/10.1007/s00401-017-1704-z

Pal, A., Fontanilla, D., Gopalakrishnan, A., Chae, Y.-K., Markley, J. L., & Ruoho, A. E. (2012). The sigma-1 receptor protects against cellular oxidative stress and activates antioxidant response elements. *European Journal of Pharmacology*, *682*(1–3), 12–20. https://doi.org/10.1016/j.ejphar.2012.01.030

Palmgren, M. G., & Nissen, P. (2011). P-Type ATPases. *Annual Review of Biophysics*, *40*(1), 243–266. https://doi.org/10.1146/annurev.biophys.093008.131331

Patten, D. A., Wong, J., Khacho, M., Soubannier, V., Mailloux, R. J., Pilon-Larose, K., MacLaurin, J. G., Park, D. S., McBride, H. M., Trinkle-Mulcahy, L., Harper, M., Germain, M., & Slack, R. S. (2014). OPA1-dependent cristae modulation is essential for cellular adaptation to metabolic demand. *The EMBO Journal*, *33*(22), 2676–2691. https://doi.org/10.15252/embj.201488349

Paumard, P., Vaillier, J., Coulary, B., Schaeffer, J., Soubannier, V., Mueller, D. M., Brèthes, D., di Rago, J.-P., & Velours, J. (2002). The ATP synthase is involved in generating mitochondrial cristae morphology. *The EMBO Journal*, *21*(3), 221–230. https://doi.org/10.1093/emboj/21.3.221

Pekosz, A., Schaecher, S. R., Diamond, M. S., Fremont, D. H., Sims, A. C., & Baric, R. S. (2006). Structure, Expression, and Intracellular Localization of the SARS-CoV Accessory Proteins 7a and 7b. In *The Nidoviruses, Advances in Experimental Medicine and Biology* (Vol. 581, pp. 115–120). https://doi.org/10.1007/978-0-387-33012-9_20

Periasamy, M., & Kalyanasundaram, A. (2007). SERCA pump isoforms: Their role in calcium transport and disease. *Muscle & Nerve*, *35*(4), 430–442. https://doi.org/10.1002/mus.20745

Pisoni, G. B., Ruddock, L. W., Bulleid, N., & Molinari, M. (2015). Division of labor among oxidoreductases: TMX1 preferentially acts on transmembrane polypeptides. *Molecular Biology of the Cell*, *26*(19), 3390–3400. https://doi.org/10.1091/mbc.E15-05-0321

Pliss, A., Kuzmin, A. N., Prasad, P. N., & Mahajan, S. D. (2022). Mitochondrial Dysfunction: A Prelude to Neuropathogenesis of SARS-CoV-2. *ACS Chemical Neuroscience*, *13*(3), 308–312. https://doi.org/10.1021/acschemneuro.1c00675

Prakriya, M., Feske, S., Gwack, Y., Srikanth, S., Rao, A., & Hogan, P. G. (2006). Orai1 is an essential pore subunit of the CRAC channel. *Nature*, *443*(7108), 230–233. https://doi.org/10.1038/nature05122

Putney, J. W. (1986). A model for receptor-regulated calcium entry. *Cell Calcium*, *7*(1), 1–12. https://doi.org/10.1016/0143-4160(86)90026-6

Qian, W., Choi, S., Gibson, G. A., Watkins, S. C., Bakkenist, C. J., & van Houten, B. (2012). Mitochondrial hyperfusion induced by loss of the fission protein Drp1 causes ATM-dependent G2/M arrest and aneuploidy through DNA replication stress. *Journal of Cell Science*, *125*(23), 5745–5757. https://doi.org/10.1242/jcs.109769

Qin, F., Siwik, D. A., Lancel, S., Zhang, J., Kuster, G. M., Luptak, I., Wang, L., Tong, X., Kang, Y. J., Cohen, R. A., & Colucci, W. S. (2013). Hydrogen Peroxide–Mediated SERCA Cysteine 674 Oxidation Contributes to Impaired Cardiac Myocyte Relaxation in Senescent Mouse Heart. *Journal of the American Heart Association*, *2*(4). https://doi.org/10.1161/JAHA.113.000184

Rajagopalan, S., Xu, Y., & Brenner, M. B. (1994). Retention of Unassembled Components of Integral Membrane Proteins by Calnexin. *Science*, *263*(5145), 387–390. https://doi.org/10.1126/science.8278814

Ramachandran, K., Maity, S., Muthukumar, A. R., Kandala, S., Tomar, D., Abd El-Aziz, T. M., Allen, C., Sun, Y., Venkatesan, M., Madaris, T. R., Chiem, K., Truitt, R., Vishnu, N., Aune, G., Anderson, A., Martinez-Sobrido, L., Yang, W., Stockand, J. D., Singh, B. B., … Madesh, M. (2022). SARS-CoV-2 infection enhances mitochondrial PTP complex activity to perturb cardiac energetics. *IScience*, *25*(1), 103722. https://doi.org/10.1016/j.isci.2021.103722

Rapoport, T. A. (2007). Protein translocation across the eukaryotic endoplasmic reticulum and bacterial plasma membranes. *Nature*, *450*(7170), 663–669. https://doi.org/10.1038/nature06384

Rasmussen, A. L., Diamond, D. L., McDermott, J. E., Gao, X., Metz, T. O., Matzke, M. M., Carter, V. S., Belisle, S. E., Korth, M. J., Waters, K. M., Smith, R. D., & Katze, M. G. (2011). Systems Virology Identifies a Mitochondrial Fatty Acid Oxidation Enzyme, Dodecenoyl Coenzyme A Delta Isomerase, Required for Hepatitis C Virus Replication and Likely

Pathogenesis. *Journal of Virology*, *85*(22), 11646–11654. https://doi.org/10.1128/JVI.05605-11

Raturi, A., Gutiérrez, T., Ortiz-Sandoval, C., Ruangkittisakul, A., Herrera-Cruz, M. S., Rockley, J. P., Gesson, K., Ourdev, D., Lou, P. H., Lucchinetti, E., Tahbaz, N., Zaugg, M., Baksh, S., Ballanyi, K., & Simmen, T. (2016). TMX1 determines cancer cell metabolism as a thiolbased modulator of ER-mitochondria Ca2+ flux. *Journal of Cell Biology*, *214*(4), 433–444. https://doi.org/10.1083/jcb.201512077

Ravindran, M. S., Bagchi, P., Cunningham, C. N., & Tsai, B. (2016). Opportunistic intruders: how viruses orchestrate ER functions to infect cells. *Nature Reviews Microbiology*, *14*(7), 407–420. https://doi.org/10.1038/nrmicro.2016.60

Redondo, N., Zaldívar-López, S., Garrido, J. J., & Montoya, M. (2021). SARS-CoV-2 Accessory Proteins in Viral Pathogenesis: Knowns and Unknowns. In *Frontiers in Immunology* (Vol. 12). Frontiers Media S.A. https://doi.org/10.3389/fimmu.2021.708264

Ren, Y., Shu, T., Wu, D., Mu, J., Wang, C., Huang, M., Han, Y., Zhang, X.-Y., Zhou, W., Qiu, Y., & Zhou, X. (2020). The ORF3a protein of SARS-CoV-2 induces apoptosis in cells. *Cellular & Molecular Immunology*, *17*(8), 881–883. https://doi.org/10.1038/s41423-020-0485-9

Riedl, S. J., Li, W., Chao, Y., Schwarzenbacher, R., & Shi, Y. (2005). Structure of the apoptotic protease-activating factor 1 bound to ADP. *Nature*, *434*(7035), 926–933. https://doi.org/10.1038/nature03465

Rizzuto, R., Pinton, P., Carrington, W., Fay, F. S., Fogarty, K. E., Lifshitz, L. M., Tuft, R. A., & Pozzan, T. (1998). Close Contacts with the Endoplasmic Reticulum as Determinants of Mitochondrial Ca $^{2+}$ Responses. *Science*, *280*(5370), 1763–1766. https://doi.org/10.1126/science.280.5370.1763

Roderick, H. L., Lechleiter, J. D., & Camacho, P. (2000). Cytosolic Phosphorylation of Calnexin Controls Intracellular Ca2+ Oscillations via an Interaction with Serca2b. *Journal of Cell Biology*, *149*(6), 1235–1248. https://doi.org/10.1083/jcb.149.6.1235

Rodrigues, T. S., de Sá, K. S. G., Ishimoto, A. Y., Becerra, A., Oliveira, S., Almeida, L., Gonçalves, A. v., Perucello, D. B., Andrade, W. A., Castro, R., Veras, F. P., Toller-Kawahisa, J. E., Nascimento, D. C., de Lima, M. H. F., Silva, C. M. S., Caetite, D. B., Martins, R. B., Castro, I. A., Pontelli, M. C., … Zamboni, D. S. (2020). Inflammasomes are activated in response to SARS-cov-2 infection and are associated with COVID-19 severity in patients. *Journal of Experimental Medicine*, *218*(3). https://doi.org/10.1084/JEM.20201707

Roingeard, P., Eymieux, S., Burlaud-Gaillard, J., Hourioux, C., Patient, R., & Blanchard, E. (2022). The double-membrane vesicle (DMV): a virus-induced organelle dedicated to the replication of SARS-CoV-2 and other positive-sense single-stranded RNA viruses. *Cellular and Molecular Life Sciences*, *79*(8), 425. https://doi.org/10.1007/s00018-022-04469-x

Romero-Garcia, S., & Prado-Garcia, H. (2019). Mitochondrial calcium: Transport and modulation of cellular processes in homeostasis and cancer (Review). In *International Journal of Oncology* (Vol. 54, Issue 4, pp. 1155–1167). Spandidos Publications. https://doi.org/10.3892/ijo.2019.4696

Roos, J., DiGregorio, P. J., Yeromin, A. v., Ohlsen, K., Lioudyno, M., Zhang, S., Safrina, O., Kozak, J. A., Wagner, S. L., Cahalan, M. D., Veliçelebi, G., & Stauderman, K. A. (2005). STIM1, an essential and conserved component of store-operated Ca2+ channel function. *Journal of Cell Biology*, *169*(3), 435–445. https://doi.org/10.1083/jcb.200502019

Russell, W. C., Graham, F. L., Smiley, J., & Nairn, R. (1977). Characteristics of a Human Cell Line Transformed by DNA from Human Adenovirus Type 5. *Journal of General Virology*, *36*(1), 59–72. https://doi.org/10.1099/0022-1317-36-1-59

Saito, Y. (1999). Calreticulin functions in vitro as a molecular chaperone for both glycosylated and non-glycosylated proteins. *The EMBO Journal*, *18*(23), 6718–6729. https://doi.org/10.1093/emboj/18.23.6718

Sala-Vila, A., Navarro-Lérida, I., Sánchez-Alvarez, M., Bosch, M., Calvo, C., López, J. A., Calvo, E., Ferguson, C., Giacomello, M., Serafini, A., Scorrano, L., Enriquez, J. A., Balsinde, J., Parton, R. G., Vázquez, J., Pol, A., & del Pozo, M. A. (2016). Interplay between hepatic mitochondria-associated membranes, lipid metabolism and caveolin-1 in mice. *Scientific Reports*, *6*(1), 27351. https://doi.org/10.1038/srep27351

Samavarchi-Tehrani, P., Abdouni, H., Knight, J. D., Astori, A., Samson, R., Lin, Z.-Y., Kim, D.-K., Knapp, J. J., St-Germain, J., Go, C. D., Larsen, B., Wong, C. J., Cassonnet, P., Demeret, C., Jacob, Y., Roth, F. P., Raught, B., & Gingras, A.-C. (2020). A SARS-CoV-2 – host proximity interactome. *BioRxiv*. https://doi.org/10.1101/2020.09.03.282103

Samavati, L., & Uhal, B. D. (2020). ACE2, Much More Than Just a Receptor for SARS-COV-2. *Frontiers in Cellular and Infection Microbiology*, *10*. https://doi.org/10.3389/fcimb.2020.00317

Sano, R., Annunziata, I., Patterson, A., Moshiach, S., Gomero, E., Opferman, J., Forte, M., & d'Azzo, A. (2009). GM1-Ganglioside Accumulation at the Mitochondria-Associated ER Membranes Links ER Stress to Ca2+-Dependent Mitochondrial Apoptosis. *Molecular Cell*, *36*(3), 500–511. https://doi.org/10.1016/j.molcel.2009.10.021

Santana, L. F., Kranias, E. G., & Lederer, W. J. (1997). Calcium Sparks and Excitation-Contraction Coupling in Phospholamban-Deficient Mouse Ventricular Myocytes. *The Journal of Physiology*, *503*(1), 21–29. https://doi.org/10.1111/j.1469-7793.1997.021bi.x

Schaecher, S. R., Diamond, M. S., & Pekosz, A. (2008). The Transmembrane Domain of the Severe Acute Respiratory Syndrome Coronavirus ORF7b Protein Is Necessary and Sufficient for Its Retention in the Golgi Complex. *Journal of Virology*, *82*(19), 9477–9491. https://doi.org/10.1128/jvi.00784-08

Schaecher, S. R., Mackenzie, J. M., & Pekosz, A. (2007). The ORF7b Protein of Severe Acute Respiratory Syndrome Coronavirus (SARS-CoV) Is Expressed in Virus-Infected Cells and Incorporated into SARS-CoV Particles. *Journal of Virology*, *81*(2), 718–731. https://doi.org/10.1128/jvi.01691-06

Schwarz, D. S., & Blower, M. D. (2016). The endoplasmic reticulum: structure, function and response to cellular signaling. *Cellular and Molecular Life Sciences*, *73*(1), 79–94. https://doi.org/10.1007/s00018-015-2052-6

Seth, R. B., Sun, L., Ea, C.-K., & Chen, Z. J. (2005). Identification and Characterization of MAVS, a Mitochondrial Antiviral Signaling Protein that Activates NF-κB and IRF3. *Cell*, *122*(5), 669–682. https://doi.org/10.1016/j.cell.2005.08.012

Shang, C., Liu, Z., Zhu, Y., Lu, J., Ge, C., Zhang, C., Li, N., Jin, N., Li, Y., Tian, M., & Li, X. (2022). SARS-CoV-2 Causes Mitochondrial Dysfunction and Mitophagy Impairment. *Frontiers in Microbiology*, *12*. https://doi.org/10.3389/fmicb.2021.780768

Shindiapina, P., & Barlowe, C. (2010). Requirements for Transitional Endoplasmic Reticulum Site Structure and Function in Saccharomyces cerevisiae. *Molecular Biology of the Cell*, *21*(9), 1530–1545. https://doi.org/10.1091/mbc.e09-07-0605

Shoshan-Barmatz, V., de Pinto, V., Zweckstetter, M., Raviv, Z., Keinan, N., & Arbel, N. (2010). VDAC, a multi-functional mitochondrial protein regulating cell life and death. *Molecular Aspects of Medicine*, *31*(3), 227–285. https://doi.org/10.1016/j.mam.2010.03.002

Silvas, J. A., Vasquez, D. M., Park, J.-G., Chiem, K., Allué-Guardia, A., Garcia-Vilanova, A., Platt, R. N., Miorin, L., Kehrer, T., Cupic, A., Gonzalez-Reiche, A. S., Bakel, H. van, García-Sastre, A., Anderson, T., Torrelles, J. B., Ye, C., & Martinez-Sobrido, L. (2021). Contribution of SARS-CoV-2 Accessory Proteins to Viral Pathogenicity in K18 Human ACE2 Transgenic Mice. *Journal of Virology*, *95*(17). https://doi.org/10.1128/jvi.00402-21

Simmen, T., Aslan, J. E., Blagoveshchenskaya, A. D., Thomas, L., Wan, L., Xiang, Y., Feliciangeli, S. F., Hung, C.-H., Crump, C. M., & Thomas, G. (2005). PACS-2 controls endoplasmic reticulum–mitochondria communication and Bid-mediated apoptosis. *The EMBO Journal*, *24*(4), 717–729. https://doi.org/10.1038/sj.emboj.7600559

Simmerman, H. K. B., Kobayashi, Y. M., Autry, J. M., & Jones, L. R. (1996). A Leucine Zipper Stabilizes the Pentameric Membrane Domain of Phospholamban and Forms a Coiled-coil Pore Structure. *Journal of Biological Chemistry*, *271*(10), 5941–5946. https://doi.org/10.1074/jbc.271.10.5941

Simmerman, H. K., Collins, J. H., Theibert, J. L., Wegener, A. D., & Jones, L. R. (1986). Sequence analysis of phospholamban. Identification of phosphorylation sites and two major structural domains. *The Journal of Biological Chemistry*, *261*(28), 13333–13341.

Smeazzetto, S., Armanious, G. P., Moncelli, M. R., Bak, J. J., Lemieux, M. J., Young, H. S., & Tadini-Buoninsegni, F. (2017). Conformational memory in the association of the transmembrane protein phospholamban with the sarcoplasmic reticulum calcium pump SERCA. *Journal of Biological Chemistry*, *292*(52), 21330–21339. https://doi.org/10.1074/jbc.M117.794453

Smith, J. A. (2021). STING, the Endoplasmic Reticulum, and Mitochondria: Is Three a Crowd or a Conversation? *Frontiers in Immunology*, *11*. https://doi.org/10.3389/fimmu.2020.611347

Steenbergen, R., Nanowski, T. S., Beigneux, A., Kulinski, A., Young, S. G., & Vance, J. E. (2005). Disruption of the Phosphatidylserine Decarboxylase Gene in Mice Causes Embryonic Lethality and Mitochondrial Defects. *Journal of Biological Chemistry*, *280*(48), 40032–40040. https://doi.org/10.1074/jbc.M506510200

Stoica, R., de Vos, K. J., Paillusson, S., Mueller, S., Sancho, R. M., Lau, K.-F., Vizcay-Barrena, G., Lin, W.-L., Xu, Y.-F., Lewis, J., Dickson, D. W., Petrucelli, L., Mitchell, J. C., Shaw, C. E., & Miller, C. C. J. (2014). ER–mitochondria associations are regulated by the VAPB–PTPIP51 interaction and are disrupted by ALS/FTD-associated TDP-43. *Nature Communications*, *5*(1), 3996. https://doi.org/10.1038/ncomms4996

Stoica, R., Paillusson, S., Gomez-Suaga, P., Mitchell, J. C., Lau, D. H., Gray, E. H., Sancho, R. M., Vizcay-Barrena, G., de Vos, K. J., Shaw, C. E., Hanger, D. P., Noble, W., & Miller, C. C. (2016). ALS/FTD-associated FUS activates GSK-3β to disrupt the VAPB–PTPIP51 interaction and ER–mitochondria associations. *EMBO Reports*, *17*(9), 1326–1342. https://doi.org/10.15252/embr.201541726

Stone, S. J., & Vance, J. E. (2000a). Phosphatidylserine Synthase-1 and -2 Are Localized to Mitochondria-associated Membranes. *Journal of Biological Chemistry*, *275*(44), 34534–34540. https://doi.org/10.1074/jbc.M002865200

Stone, S. J., & Vance, J. E. (2000b). Phosphatidylserine Synthase-1 and -2 Are Localized to Mitochondria-associated Membranes. *Journal of Biological Chemistry*, *275*(44), 34534–34540. https://doi.org/10.1074/jbc.M002865200

Stukalov, A., Girault, V., Grass, V., Karayel, O., Bergant, V., Urban, C., Haas, D. A., Huang, Y., Oubraham, L., Wang, A., Hamad, M. S., Piras, A., Hansen, F. M., Tanzer, M. C., Paron, I., Zinzula, L., Engleitner, T., Reinecke, M., Lavacca, T. M., … Pichlmair, A. (2021). Multilevel proteomics reveals host perturbations by SARS-CoV-2 and SARS-CoV. *Nature*, *594*(7862), 246–252. https://doi.org/10.1038/s41586-021-03493-4

Sureda, A., Alizadeh, J., Nabavi, S. F., Berindan-Neagoe, I., Cismaru, C. A., Jeandet, P., Łos, M. J., Clementi, E., Nabavi, S. M., & Ghavami, S. (2020). Endoplasmic reticulum as a potential therapeutic target for covid-19 infection management? *European Journal of Pharmacology*, *882*, 173288. https://doi.org/10.1016/j.ejphar.2020.173288

Szabadkai, G., Bianchi, K., Várnai, P., de Stefani, D., Wieckowski, M. R., Cavagna, D., Nagy, A. I., Balla, T., & Rizzuto, R. (2006). Chaperone-mediated coupling of endoplasmic reticulum and mitochondrial Ca2+ channels. *Journal of Cell Biology*, *175*(6), 901–911. https://doi.org/10.1083/jcb.200608073

Szado, T., Vanderheyden, V., Parys, J. B., de Smedt, H., Rietdorf, K., Kotelevets, L., Chastre, E., Khan, F., Landegren, U., Söderberg, O., Bootman, M. D., & Roderick, H. L. (2008). Phosphorylation of inositol 1,4,5-trisphosphate receptors by protein kinase B/Akt inhibits Ca^{2+} release and apoptosis. *Proceedings of the National Academy of Sciences*, *105*(7), 2427–2432. https://doi.org/10.1073/pnas.0711324105

Takizawa, T. (2004). Cleavage of Calnexin Caused by Apoptotic Stimuli: Implication for the Regulation of Apoptosis. *Journal of Biochemistry*, *136*(3), 399–405. https://doi.org/10.1093/jb/mvh133

Thompson, M. D., Mei, Y., Weisbrod, R. M., Silver, M., Shukla, P. C., Bolotina, V. M., Cohen, R. A., & Tong, X. (2014). Glutathione Adducts on Sarcoplasmic/Endoplasmic Reticulum Ca2+ ATPase Cys-674 Regulate Endothelial Cell Calcium Stores and Angiogenic Function as Well as Promote Ischemic Blood Flow Recovery. *Journal of Biological Chemistry*, *289*(29), 19907–19916. https://doi.org/10.1074/jbc.M114.554451

Tiku, V., Tan, M.-W., & Dikic, I. (2020). Mitochondrial Functions in Infection and Immunity. *Trends in Cell Biology*, *30*(4), 263–275. https://doi.org/10.1016/j.tcb.2020.01.006

Toft-Bertelsen, T. L., Jeppesen, M. G., Tzortzini, E., Xue, K., Giller, K., Becker, S., Mujezinovic, A., Bentzen, B. H., B. Andreas, L., Kolocouris, A., Kledal, T. N., & Rosenkilde, M. M. (2021). Amantadine has potential for the treatment of COVID-19 because it inhibits known and novel ion channels encoded by SARS-CoV-2. *Communications Biology*, *4*(1). https://doi.org/10.1038/s42003-021-02866-9

Toldo, S., Bussani, R., Nuzzi, V., Bonaventura, A., Mauro, A. G., Cannatà, A., Pillappa, R., Sinagra, G., Nana-Sinkam, P., Sime, P., & Abbate, A. (2021). Inflammasome formation in the lungs of patients with fatal COVID-19. *Inflammation Research*, *70*(1), 7–10. https://doi.org/10.1007/s00011-020-01413-2

Tong, X., Hou, X., Jourd'heuil, D., Weisbrod, R. M., & Cohen, R. A. (2010). Upregulation of Nox4 by TGFβ1 Oxidizes SERCA and Inhibits NO in Arterial Smooth Muscle of the Prediabetic Zucker Rat. *Circulation Research*, *107*(8), 975–983. https://doi.org/10.1161/CIRCRESAHA.110.221242

Toyoshima, C., Nakasako, M., Nomura, H., & Ogawa, H. (2000). Crystal structure of the calcium pump of sarcoplasmic reticulum at 2.6 Å resolution. *Nature*, *405*(6787), 647–655. https://doi.org/10.1038/35015017

Traaseth, N., Elfering, S., Solien, J., Haynes, V., & Giulivi, C. (2004). Role of calcium signaling in the activation of mitochondrial nitric oxide synthase and citric acid cycle. *Biochimica et*

Biophysica Acta (BBA) - Bioenergetics, *1658*(1–2), 64–71. https://doi.org/10.1016/j.bbabio.2004.04.015

Triantafilou, K., Kar, S., van Kuppeveld, F. J. M., & Triantafilou, M. (2013). Rhinovirus-induced calcium flux triggers NLRP3 and NLRC5 activation in bronchial cells. *American Journal of Respiratory Cell and Molecular Biology*, *49*(6), 923–934. https://doi.org/10.1165/rcmb.2013-0032OC

Ushioda, R., Miyamoto, A., Inoue, M., Watanabe, S., Okumura, M., Maegawa, K., Uegaki, K., Fujii, S., Fukuda, Y., Umitsu, M., Takagi, J., Inaba, K., Mikoshiba, K., & Nagata, K. (2016). Redox-assisted regulation of Ca $^{2+}$ homeostasis in the endoplasmic reticulum by disulfide reductase ERdj5. *Proceedings of the National Academy of Sciences*, *113*(41). https://doi.org/10.1073/pnas.1605818113

van Klompenburg, W. (1997). Anionic phospholipids are determinants of membrane protein topology. *The EMBO Journal*, *16*(14), 4261–4266. https://doi.org/10.1093/emboj/16.14.4261

Vance, J. E. (1990). Phospholipid synthesis in a membrane fraction associated with mitochondria. *Journal of Biological Chemistry*, *265*(13), 7248–7256. https://doi.org/10.1016/S0021-9258(19)39106-9

Vandecaetsbeek, I., Trekels, M., de Maeyer, M., Ceulemans, H., Lescrinier, E., Raeymaekers, L., Wuytack, F., & Vangheluwe, P. (2009). Structural basis for the high Ca $^{2+}$ affinity of the ubiquitous SERCA2b Ca $^{2+}$ pump. *Proceedings of the National Academy of Sciences*, *106*(44), 18533–18538. https://doi.org/10.1073/pnas.0906797106

Vangheluwe, P., Raeymaekers, L., Dode, L., & Wuytack, F. (2005). Modulating sarco(endo)plasmic reticulum Ca2+ ATPase 2 (SERCA2) activity: Cell biological implications. *Cell Calcium*, *38*(3–4), 291–302. https://doi.org/10.1016/j.ceca.2005.06.033

Vardhana, S. A., & Wolchok, J. D. (2020). The many faces of the anti-COVID immune response. *Journal of Experimental Medicine*, *217*(6). https://doi.org/10.1084/jem.20200678

Vassilakos, A., Michalak, M., Lehrman, M. A., & Williams, D. B. (1998). Oligosaccharide Binding Characteristics of the Molecular Chaperones Calnexin and Calreticulin. *Biochemistry*, *37*(10), 3480–3490. https://doi.org/10.1021/bi972465g

Vastag, L., Koyuncu, E., Grady, S. L., Shenk, T. E., & Rabinowitz, J. D. (2011). Divergent Effects of Human Cytomegalovirus and Herpes Simplex Virus-1 on Cellular Metabolism. *PLoS Pathogens*, *7*(7), e1002124. https://doi.org/10.1371/journal.ppat.1002124

Verboomen, H., Wuytack, F., de Smedt, H., Himpens, B., & Casteels, R. (1992). Functional difference between SERCA2a and SERCA2b Ca2+ pumps and their modulation by phospholamban. *Biochemical Journal*, *286*(2), 591–595. https://doi.org/10.1042/bj2860591

Verstraelen, T. E., van Lint, F. H. M., Bosman, L. P., de Brouwer, R., Proost, V. M., Abeln, B. G. S., Taha, K., Zwinderman, A. H., Dickhoff, C., Oomen, T., Schoonderwoerd, B. A., Kimman, G. P., Houweling, A. C., Gimeno-Blanes, J. R., Asselbergs, F. W., van der Zwaag, P. A., de Boer, R. A., van den Berg, M. P., van Tintelen, J. P., & Wilde, A. A. M. (2021). Prediction of ventricular arrhythmia in phospholamban p.Arg14del mutation carriers–reaching the frontiers of individual risk prediction. *European Heart Journal*, *42*(29), 2842–2850. https://doi.org/10.1093/eurheartj/ehab294

V'kovski, P., Kratzel, A., Steiner, S., Stalder, H., & Thiel, V. (2021). Coronavirus biology and replication: implications for SARS-CoV-2. *Nature Reviews Microbiology*, *19*(3), 155–170. https://doi.org/10.1038/s41579-020-00468-6

Voelker, D. R. (1993). The ATP-dependent translocation of phosphatidylserine to the mitochondria is a process that is restricted to the autologous organelle. *Journal of Biological Chemistry*, *268*(10), 7069–7074. https://doi.org/10.1016/S0021-9258(18)53146-X

Voeltz, G. K., Rolls, M. M., & Rapoport, T. A. (2002). Structural organization of the endoplasmic reticulum. *EMBO Reports*, *3*(10), 944–950. https://doi.org/10.1093/embo-reports/kvf202

von Heijne, G. (1986). The distribution of positively charged residues in bacterial inner membrane proteins correlates with the trans-membrane topology. *The EMBO Journal*, *5*(11), 3021–3027. https://doi.org/10.1002/j.1460-2075.1986.tb04601.x

von Heijne, G. (1989). Control of topology and mode of assembly of a polytopic membrane protein by positively charged residues. *Nature*, *341*(6241), 456–458. https://doi.org/10.1038/341456a0

Wada, I., Rindress, D., Cameron, P. H., Ou, W. J., Doherty, J. J., Louvard, D., Bell, A. W., Dignard, D., Thomas, D. Y., & Bergeron, J. J. (1991). SSR alpha and associated calnexin are major calcium binding proteins of the endoplasmic reticulum membrane. *The Journal of Biological Chemistry*, *266*(29), 19599–19610.

Walter, P., Ibrahimi, I., & Blobel, G. (1981). Translocation of proteins across the endoplasmic reticulum. I. Signal recognition protein (SRP) binds to in-vitro-assembled polysomes synthesizing secretory protein. *Journal of Cell Biology*, *91*(2), 545–550. https://doi.org/10.1083/jcb.91.2.545

Walter, P., & Ron, D. (2011). The Unfolded Protein Response: From Stress Pathway to Homeostatic Regulation. *Science*, *334*(6059), 1081–1086. https://doi.org/10.1126/science.1209038

Wang, K., Yan, R., Cooper, K. F., & Strich, R. (2015). Cyclin C mediates stress-induced mitochondrial fission and apoptosis. *Molecular Biology of the Cell*, *26*(6), 1030–1043. https://doi.org/10.1091/mbc.E14-08-1315

Wang, M., & Kaufman, R. J. (2016). Protein misfolding in the endoplasmic reticulum as a conduit to human disease. *Nature*, *529*(7586), 326–335. https://doi.org/10.1038/nature17041

Wang, N., Wang, C., Zhao, H., He, Y., Lan, B., Sun, L., & Gao, Y. (2021). The MAMs Structure and Its Role in Cell Death. *Cells*, *10*(3), 657. https://doi.org/10.3390/cells10030657

Wang, R., Zhu, Y., Lin, X., Ren, C., Zhao, J., Wang, F., Gao, X., Xiao, R., Zhao, L., Chen, H., Jin, M., Ma, W., & Zhou, H. (2019). Influenza M2 protein regulates MAVS-mediated signaling pathway through interacting with MAVS and increasing ROS production. *Autophagy*, *15*(7), 1163–1181. https://doi.org/10.1080/15548627.2019.1580089

Wang, X., Jiang, W., Yan, Y., Gong, T., Han, J., Tian, Z., & Zhou, R. (2014). RNA viruses promote activation of the NLRP3 inflammasome through a RIP1-RIP3-DRP1 signaling pathway. *Nature Immunology*, *15*(12), 1126–1133. https://doi.org/10.1038/ni.3015

Ware, F. E., Vassilakos, A., Peterson, P. A., Jackson, M. R., Lehrman, M. A., & Williams, D. B. (1995). The Molecular Chaperone Calnexin Binds Glc1Man9GlcNAc2 Oligosaccharide as an Initial Step in Recognizing Unfolded Glycoproteins. *Journal of Biological Chemistry*, *270*(9), 4697–4704. https://doi.org/10.1074/jbc.270.9.4697

Watkins, L. C., DeGrado, W. F., & Voth, G. A. (2020). Influenza A M2 Inhibitor Binding Understood through Mechanisms of Excess Proton Stabilization and Channel Dynamics. *Journal of the American Chemical Society*, *142*(41), 17425–17433. https://doi.org/10.1021/jacs.0c06419

Wieckowski, M. R., Giorgi, C., Lebiedzinska, M., Duszynski, J., & Pinton, P. (2009). Isolation of mitochondria-associated membranes and mitochondria from animal tissues and cells. *Nature Protocols*, *4*(11), 1582–1590. https://doi.org/10.1038/nprot.2009.151

Williamson, C. D., & Colberg-Poley, A. M. (2010). Intracellular Sorting Signals for Sequential Trafficking of Human Cytomegalovirus UL37 Proteins to the Endoplasmic Reticulum and Mitochondria. *Journal of Virology*, *84*(13), 6400–6409. https://doi.org/10.1128/JVI.00556-10

Williamson, C. D., Zhang, A., & Colberg-Poley, A. M. (2011). The Human Cytomegalovirus Protein UL37 Exon 1 Associates with Internal Lipid Rafts. *Journal of Virology*, *85*(5), 2100–2111. https://doi.org/10.1128/jvi.01830-10

Wu, F., Zhao, S., Yu, B., Chen, Y. M., Wang, W., Song, Z. G., Hu, Y., Tao, Z. W., Tian, J. H., Pei, Y. Y., Yuan, M. L., Zhang, Y. L., Dai, F. H., Liu, Y., Wang, Q. M., Zheng, J. J., Xu, L., Holmes, E. C., & Zhang, Y. Z. (2020). A new coronavirus associated with human respiratory disease in China. *Nature*, *579*(7798), 265–269. https://doi.org/10.1038/s41586-020-2008-3

Wu, J., Prole, D. L., Shen, Y., Lin, Z., Gnanasekaran, A., Liu, Y., Chen, L., Zhou, H., Chen, S. R. W., Usachev, Y. M., Taylor, C. W., & Campbell, R. E. (2014). Red fluorescent genetically encoded Ca2+ indicators for use in mitochondria and endoplasmic reticulum. *Biochemical Journal*, *464*(1), 13–22. https://doi.org/10.1042/BJ20140931

Wuytack, F., Raeymaekers, L., & Missiaen, L. (2002). Molecular physiology of the SERCA and SPCA pumps. *Cell Calcium*, *32*(5–6), 279–305. https://doi.org/10.1016/S0143416002001847

Yang, J. C., & Cortopassi, G. A. (1998). Induction of the Mitochondrial Permeability Transition Causes Release of the Apoptogenic Factor Cytochrome c. *Free Radical Biology and Medicine*, *24*(4), 624–631. https://doi.org/10.1016/S0891-5849(97)00367-5

Yang, M., Li, C., Yang, S., Xiao, Y., Xiong, X., Chen, W., Zhao, H., Zhang, Q., Han, Y., & Sun, L. (2020). Mitochondria-Associated ER Membranes – The Origin Site of Autophagy. *Frontiers in Cell and Developmental Biology*, *8*. https://doi.org/10.3389/fcell.2020.00595

Yang, R., Zhao, Q., Rao, J., Zeng, F., Yuan, S., Ji, M., Sun, X., Li, J., Yang, J., Cui, J., Jin, Z., Liu, L., & Liu, Z. (2021). SARS-CoV-2 Accessory Protein ORF7b Mediates Tumor Necrosis Factor-α-Induced Apoptosis in Cells. *Frontiers in Microbiology*, *12*. https://doi.org/10.3389/fmicb.2021.654709

Yang, Y., Tang, X., Hao, F., Ma, Z., Wang, Y., Wang, L., & Gao, Y. (2018). Bavachin Induces Apoptosis through Mitochondrial Regulated ER Stress Pathway in HepG2 Cells. *Biological and Pharmaceutical Bulletin*, *41*(2), 198–207. https://doi.org/10.1248/bpb.b17-00672

Yasumura, Y., & Kawakita, Y. (1963). The research for the SV40 by means of tissue culture technique. *Nippon Rinsho*, *21*, 1201–1219.

Yoshimoto, F. K. (2020). The Proteins of Severe Acute Respiratory Syndrome Coronavirus-2 (SARS CoV-2 or n-COV19), the Cause of COVID-19. *The Protein Journal*, *39*(3), 198–216. https://doi.org/10.1007/s10930-020-09901-4

Zamarin, D., García-Sastre, A., Xiao, X., Wang, R., & Palese, P. (2005). Influenza Virus PB1-F2 Protein Induces Cell Death through Mitochondrial ANT3 and VDAC1. *PLoS Pathogens*, *1*(1), e4. https://doi.org/10.1371/journal.ppat.0010004

Zapun, A., Darby, N. J., Tessier, D. C., Michalak, M., Bergeron, J. J. M., & Thomas, D. Y. (1998). Enhanced Catalysis of Ribonuclease B Folding by the Interaction of Calnexin or Calreticulin with ERp57. *Journal of Biological Chemistry*, *273*(11), 6009–6012. https://doi.org/10.1074/jbc.273.11.6009

Zborowski, J., Dygas, A., & Wojtczak, L. (1983). Phosphatidylserine decarboxylase is located on the external side of the inner mitochondrial membrane. *FEBS Letters*, *157*(1), 179–182. https://doi.org/10.1016/0014-5793(83)81141-7

Zhang, J., Ejikemeuwa, A., Gerzanich, V., Nasr, M., Tang, Q., Simard, J. M., & Zhao, R. Y. (2022). Understanding the Role of SARS-CoV-2 ORF3a in Viral Pathogenesis and COVID-19. *Frontiers in Microbiology*, *13*. https://doi.org/10.3389/fmicb.2022.854567

Zhang, J., Feng, H., Zhao, J., Feldman, E. R., Chen, S.-Y., Yuan, W., Huang, C., Akbari, O., Tibbetts, S. A., & Feng, P. (2016). IκB Kinase ε Is an NFATc1 Kinase that Inhibits T Cell Immune Response. *Cell Reports*, *16*(2), 405–418. https://doi.org/10.1016/j.celrep.2016.05.083

Zhang, J., Li, Q., Cruz Cosme, R. S., Gerzanich, V., Tang, Q., Simard, J. M., & Zhao, R. Y. (2022). Genome-Wide Characterization of SARS-CoV-2 Cytopathogenic Proteins in the Search of Antiviral Targets. *MBio*, *13*(1). https://doi.org/10.1128/mbio.00169-22

Zhang, X. C., & Zhang, H. (2019). P-type ATPases use a domain-association mechanism to couple ATP hydrolysis to conformational change. *Biophysics Reports*, *5*(4), 167–175. https://doi.org/10.1007/s41048-019-0087-1

Zhang, X., Gibhardt, C. S., Will, T., Stanisz, H., Körbel, C., Mitkovski, M., Stejerean, I., Cappello, S., Pacheu-Grau, D., Dudek, J., Tahbaz, N., Mina, L., Simmen, T., Laschke, M. W., Menger, M. D., Schön, M. P., Helms, V., Niemeyer, B. A., Rehling, P., … Bogeski, I. (2019). Redox signals at the ER –mitochondria interface control melanoma progression. *The EMBO Journal*, *38*(15). https://doi.org/10.15252/embj.2018100871

Zhang, Y., Chen, Y., Li, Y., Huang, F., Luo, B., Yuan, Y., Xia, B., Ma, X., Yang, T., Yu, F., Liu, J., Liu, B., Song, Z., Chen, J., Yan, S., Wu, L., Pan, T., Zhang, X., Li, R., … Zhang, H. (2021). The ORF8 protein of SARS-CoV-2 mediates immune evasion through down-regulating MHC-I. *Proceedings of the National Academy of Sciences*, *118*(23). https://doi.org/10.1073/pnas.2024202118

Zhao, H., Li, T., Wang, K., Zhao, F., Chen, J., Xu, G., Zhao, J., Li, T., Chen, L., Li, L., Xia, Q., Zhou, T., Li, H.-Y., Li, A.-L., Finkel, T., Zhang, X.-M., & Pan, X. (2019). AMPK-mediated activation of MCU stimulates mitochondrial Ca2+ entry to promote mitotic progression. *Nature Cell Biology*, *21*(4), 476–486. https://doi.org/10.1038/s41556-019-0296-3

Zhao, R., Jiang, S., Zhang, L., & Yu, Z. (2019). Mitochondrial electron transport chain, ROS generation and uncoupling (Review). *International Journal of Molecular Medicine*. https://doi.org/10.3892/ijmm.2019.4188

Zheng, D., Liwinski, T., & Elinav, E. (2020). Inflammasome activation and regulation: toward a better understanding of complex mechanisms. *Cell Discovery*, *6*(1), 36. https://doi.org/10.1038/s41421-020-0167-x

Zhou, R., Yazdi, A. S., Menu, P., & Tschopp, J. (2011). A role for mitochondria in NLRP3 inflammasome activation. *Nature*, *469*(7329), 221–225. https://doi.org/10.1038/nature09663

Zhou, Y., Liu, Y., Gupta, S., Paramo, M. I., Hou, Y., Mao, C., Luo, Y., Judd, J., Wierbowski, S., Bertolotti, M., Nerkar, M., Jehi, L., Drayman, N., Nicolaescu, V., Gula, H., Tay, S., Randall, G., Wang, P., Lis, J. T., … Yu, H. (2022). A comprehensive SARS-CoV-2–human protein–protein interactome reveals COVID-19 pathobiology and potential host therapeutic targets. *Nature Biotechnology*. https://doi.org/10.1038/s41587-022-01474-0

Zou, H., Li, Y., Liu, X., & Wang, X. (1999). An APAF-1·Cytochrome c Multimeric Complex Is a Functional Apoptosome That Activates Procaspase-9. *Journal of Biological Chemistry*, *274*(17), 11549–11556. https://doi.org/10.1074/jbc.274.17.11549